The Institute of Paper Chemistry

Appleton, Wisconsin

Doctor's Dissertation

An Investigation of the Hot Surface Drying of Glass Fiber Beds

W. F. Cowan

June, 1961
Reprint October, 1990

AN INVESTIGATION OF THE HOT SURFACE DRYING OF GLASS FIBER BEDS

A thesis submitted by

W. F. Cowan

B.Eng. 1954, McGill University, Montreal, Canada
M.S. 1957, Lawrence College

in partial fulfillment of the requirements
of The Institute of Paper Chemistry
for the degree of Doctor of Philosophy
from Lawrence College,
Appleton, Wisconsin

June, 1961

TABLE OF CONTENTS

INTRODUCTION

The drying operation represents a necessary and costly stage in the production of paper. A proper understanding of this operation is therefore important to the paper industry. Although an abundant supply of empirical information is available, fundamental comprehension of the drying mechanism has achieved neither depth nor clarity. This doctoral thesis aims at improving fundamental understanding.

Drying is the process whereby liquid is removed from a system by evaporation. This thesis is concerned with the evaporation of water from a porous system. The drying of paper is merely a particular category in this broader classification.

For purposes of analysis, the total drying operation can be broken down into three phenomenological considerations: The introduction or transfer of heat into the porous system, the transfer or movement of heat and mass (liquid and gaseous water) within the porous system, and the removal or mass transfer of water vapor from the system. Obviously, all three phenomena are coincidentally associated with any drying operation. The first and last are primarily dependent on the mode of drying employed, i.e., air drying, hot surface drying, etc. They are referred to throughout this thesis as the boundary conditions of drying. The second or middle factor, although affected by the boundary conditions, is characteristic of the porous system being dried.

Drying studies are commonly characterized by considering the rate of drying as a function of the moisture content of the material being dried. The general form of this curve (see Fig. 1) has been found to apply,

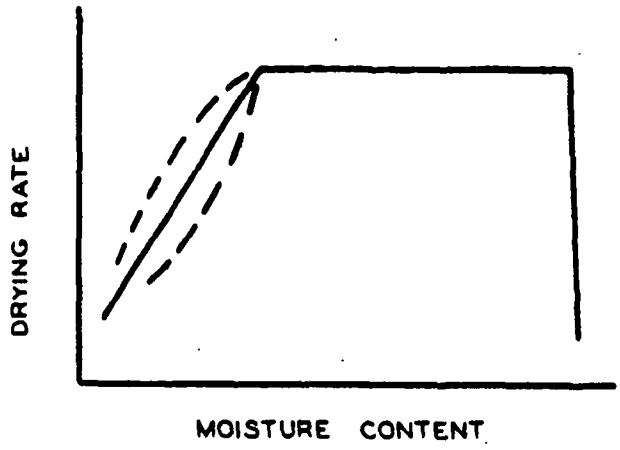

Figure 1. Characteristic Drying Curve

presumably without exception, to all types of porous materials without regard for the particular drying conditions employed. This typical or characteristic drying curve has resulted in the nomenclature which refers to a short heating up period leading to a constant rate drying period which continues to a critical moisture content at which point a falling rate drying period is inaugurated.

The bulk of the literature on drying deals with the effect of boundary conditions on drying rate. A review of this literature is presented by Higgins (1) and later supplemented by Dreshfield (2). These early investigations largely fail to yield more than narrow empirical knowledge because consideration has been given only to the boundary conditions of drying and not to the important transfer processes which occur within the system being dried.

The shape of the characteristic drying curve discussed previously has been shown to apply to such varied systems as the air drying of pulp beds (3), clay beds (4), sand beds (5), and textiles (6); the hot surface

drying of pulp mats (7) and beds of glass beads (8); the radiant heat drying of textiles, glass fibers, and asbestos fibers (9); and the machine drying of paper (10). The characteristic shape of this drying curve is, therefore, not determined by the boundary conditions of drying. Since it is typical of all porous materials, it must be determined by the interactions occurring within and peculiar to the porous system being dried.

The importance of investigating the heat and mass transfer within the porous system is thus evident.

Sherwood (11) advances the most widely accepted qualitative explanation accounting for the characteristic drying curve. He suggests that in the constant rate period of drying the evaporation of water occurs at the surface of the material in a manner similar to evaporation from a free water surface. The resistance to internal movement of water is small compared with the resistance to removal of vapor from the surface, and so the surface is easily replenished. This results in what Sherwood calls "saturated surface drying." The falling rate period begins when, because of depletion of water in the interior, the resistance to internal liquid movement becomes significant. The early stage of this period is characterized by "unsaturated surface drying." Later in the falling rate period the plane of evaporation retreats into the interior of the material. Here the resistance to internal liquid movement becomes large compared to the total resistance to the removal of vapor.

Sherwood's hypothesis clearly involves movement of liquid water from the interior of the porous system to a plane of evaporation at or toward a surface. This movement has been clearly demonstrated by dye migration

studies (2, 17). The mechanism governing such migration has received considerable attention.

During the drying process the liquid water within the porous medium is distributed in such a way that a moisture gradient exists from some point or points within the material toward the plane or planes of evaporation. This has been qualitatively shown by Higgins (1) in the air drying of paper and by McCready (7) for the hot surface drying of pulp mats. Recent investigations by Dreshfield (2) and by Ulmanen (12) clearly demonstrate these gradients for hot surface drying of pulp beds.

Early investigators considered that liquid movement occurred as a result of diffusion under the influence of the liquid concentration or moisture gradient. Fick's diffusion law was variously manipulated to describe liquid movement during the constant rate period of drying.

The investigations of Ceaglske and Hougen (5) and Barkas and Hallan (13) demolished this diffusion concept of liquid movement. Their experiments strongly supported the contention that capillary forces are the primary driving force for liquid flow during drying. The validity of this concept is now generally acknowledged.

Basic capillary theory indicates that a pressure difference exists across a curved interface between two fluid phases. The magnitude of this pressure difference is a function of the interfacial tension and the principal radii of curvature in accordance with

$$\Delta P = \gamma[1/r_1 + 1/r_2] \qquad (1)$$

where ΔP is the pressure difference across the curved interface, γ is the interfacial tension, and r_1 and r_2 are the principal radii of curvature. For a fluid contained in a uniform capillary of radius r, Equation (1) becomes .

$$\Delta P = 2\gamma \cos \phi / r \qquad (2)$$

where ϕ is the contact angle between fluid and capillary wall. From this relationship it is apparent that, in an interconnected capillary system, water will exist in smaller pores ~~at the expense, if necessary,~~ of larger pores. Immediately prior to a projected drying operation the liquid water is evenly distributed throughout the porous material. All air-water interfaces will then have the same curvature and the system is said to be at capillary equilibrium. Subsequent to the start of the drying operation, water at the plane of evaporation will be depleted; and air-water interfaces at the plane of evaporation will tend to a smaller radius of curvature. Thus, a capillary pressure difference will be established between interior water and water at the plane of evaporation. This acts as a driving force to replenish the water at the plane of evaporation. The tendency of the system to establish capillary equilibrium is, thus, responsible for the liquid movement during the drying operation.

Up to this point the drying phenomenon has been examined quite generally. The boundary conditions of drying influence, but do not determine, the interactions involved within the porous material being dried. Thus, an investigation of these interactions under certain boundary conditions should yield understanding which is limited in scope only by the nature of the porous material and not by the particular set of boundary conditions

utilized. For reasons which will be presented later, hot surface drying was selected as the mode of drying for the investigation to be described. This defines a drying system in which heat is introduced into a material from one side via a hot impermeable surface while the water vapor produced can escape only from the opposite open face. The discussion will now be directed toward this particular mode of drying.

The most extensive investigations of the hot surface drying operation are embodied in the work of Dreshfield (2) and Ulmanen (12). Using a beta-ray transmission technique developed by Dreshfield, they were able to obtain moisture distribution and other data for the drying of pulp mats. These will now be discussed in relation to the heat and mass transfer within the pulp mats during the drying operation.

The over-all drying rate curve for these studies reflect in essence the characteristic drying curve representative of porous materials. However, Ulmanen's work suggests (see Fig. 2) that the constant rate period actually involves not a constant but a slowly changing rate. From the point of view of drying mechanism this is an important observation and will be fully discussed at a later stage.

Figure 2. Drying Rate Curve from Ulmanen's Study

Dreshfield, by comparing moisture distribution with dye migration measurements, was able to give a qualitative picture of the mass transfer occurring within thin pulp mats during a hot surface drying operation. These data are presented in Fig. 3 and represent general conditions existing within the sheet during the constant rate period and first part of the falling rate period.

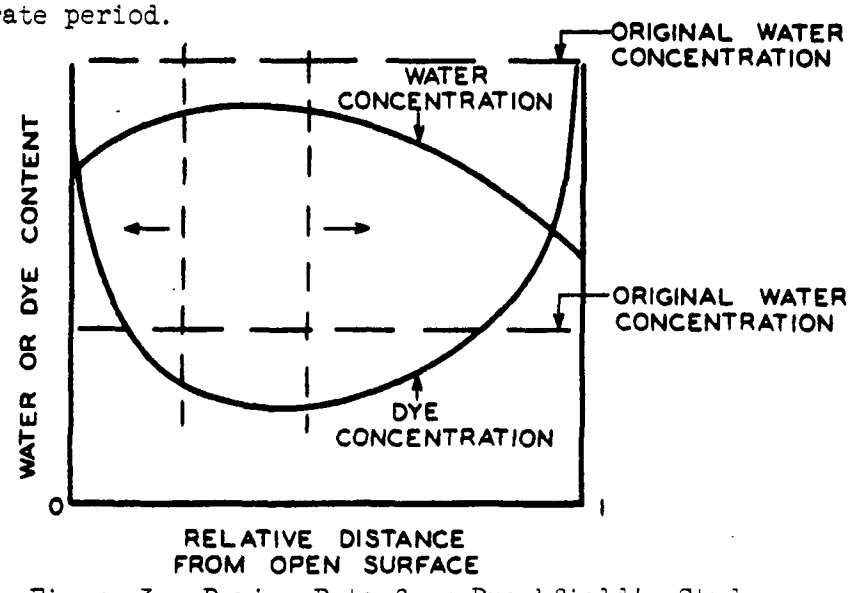

Figure 3. Drying Data from Dreshfield's Study

These results led to the following observations by Dreshfield:

> ... the maximum moisture content was found in a zone 20-30% of the distance from the cold to the hot surface. In this same region, a zone of minimum dye content existed. There appeared to be no movement of dye and therefore no movement of liquid water across this zone. Liquid water, which was initially between this zone and the hot surface moved toward the hot surface; liquid water which was between this zone and the cold surface moved toward the cold surface. Liquid water movement was in the direction of decreasing moisture content and was predominantly toward the hot surface of the sheet.
>
> Water vapor could leave the sheet only at the air interface. Therefore, the liquid water moving to the hot surface must have been vaporized there, and this vapor must have moved back through the sheet in order to escape from the open surface. The sharp concentration of dye right at the hot-surface interface indicates that most of the vaporization occurred right at the interface.

> A sharp concentration of dye was also found at the air interface of the sheet. This indicates that a significant amount of vaporization occurred there ... The heat required for vaporization at the air interface as well as the sensible heat transferred to the air must have been propagated through the sheet from the hot surface.

To explain his findings, Dreshfield presented a description of the mechanism and phenomena involved in hot surface drying:

> At the start of the drying run, there is a short period during which the sheet is coming to the constant-rate drying rate and temperature distribution. During the constant-rate period heat is being added to the sheet at the hot surface and vaporization of water occurs there. This vapor has a partial pressure greater than the equilibrium vapor pressure of the rest of the sheet, and there is a net internal condensation as the vapor passes through the sheet and enters the air stream over the open surface. The heat transferred to the sheet by the condensing vapor is moved in the direction of decreasing temperature by conduction. At the open surface, a small fraction of the heat is transferred to the air by convection; the remainder causes net evaporation.
>
> The vaporization at the two surfaces depletes the liquid water content of the sheet at these places. The process occurs too rapidly for capillary suction equilibrium to be maintained, so moisture gradients toward the surfaces are established. These cause movement of liquid water to the surfaces. The rate of drying is determined by a complex balance of heat and mass transfer, the terms of which cannot be determined.

Dreshfield goes on to suggest that the constant rate period ends when the zone at the hot surface becomes too dry to maintain the initial evaporation rate. This results in a decrease in the heat transfer rate and, hence, in the over-all drying rate. Liquid water continues to flow from the central region to the surfaces until the moisture content is reduced to the point where the contained water exists in a multitude of discrete pockets. Continued drying occurs by a process of evaporation at these pockets and the diffusion of vapor to the open face.

Ulmanen's work represents an extension of Dreshfield's investigation to include thicker pulp mats. His findings support Dreshfield's conclusions. However, additional information in the form of temperature distribution and thickness measurements of pulp mats as a function of drying time were obtained. This allowed his data to be analyzed from the viewpoint of heat transfer to the mat. This analysis by Han and Ulmanen (14) assumed that heat transferred across the hot surface is dissipated as latent heat of vaporization and as sensible heat absorbed by the fiber and the water. They neglected radiative or convective heat loss to the air. This analysis together with Ulmanen's data allowed the calculation of apparent thermal conductivity as a function of the moisture content of the pulp mat. This relation is shown in Fig. 4.

Quoting from Han and Ulmanen:

> In the high moisture region ... the apparent conductivity is of the order of magnitude as, but somewhat larger than, that of water ... A possible reason for this difference is that the transfer of heat across the hot surface may not be entirely by conduction. Some convection may also be present.
>
> In the intermediate range of moisture, $\underline{k}$ drops sharply. This may be attributed to the entrance of air into the sheet ... Finally in the very low moisture range, the conductivity approaches a fixed value [which is shown to be of the order of magnitude of the thermal conductivity of dry pulp mats].

This introductory discussion has aimed at presenting a unified development of concepts which are important to an understanding of the significance of the research work shortly to be described. It has stressed the importance of the heat and mass transfer within the porous material as defining the drying mechanism. The hot surface drying operation has been examined from this viewpoint in the light of available information. The next section

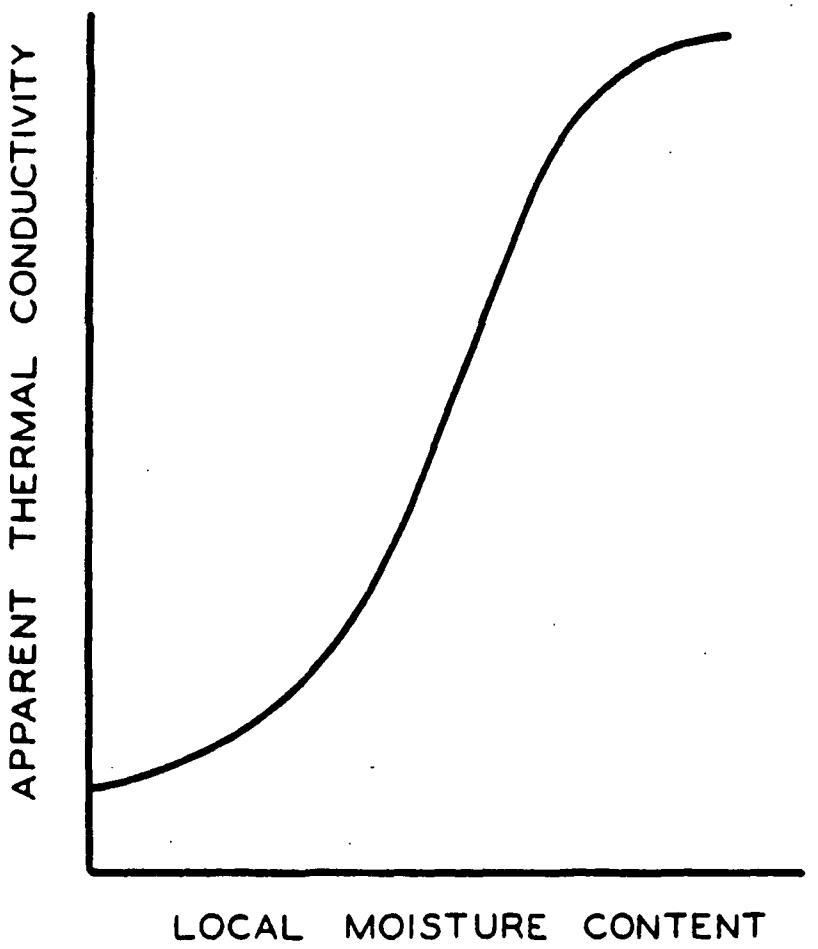

Figure 4. Apparent Thermal Conductivity
(Study of Han and Ulmanen)

outlines in an orderly fashion the approach that has been taken to develop a research program capable of elucidating the interactions within a porous material during a drying operation.

DEVELOPMENT OF EXPERIMENTAL APPROACH

The internal pore network of a porous material is obviously an important factor in characterizing heat and mass transfer within the material during drying. The elucidation of the relation between this internal structure and its manifestation in terms of heat and mass transfer within a porous media during a drying operation will greatly enhance our comprehension of the over-all drying process. Such is the basic premise upon which this thesis program builds.

Since the internal structure of porous media is to be an important aspect of this thesis, a certain background should be established. Porous media are characterized by a more or less even distribution of void spaces or pores which contribute manifestly to the total geometric volume of the material. The percentage of this total geometric volume which is constituted by void space is termed the porosity. Pores in a porous system can be interconnected or nonconnected. The porous media of interest to this discussion contain totally interconnected pore structures. The size or effective diameter of a pore can vary over wide limits. In fact, these limits can be only intuitively defined. In terms of macroscopic transfer phenomena, very large voids which are graphically described as "caverns" are too large to be considered pores; voids of molecular dimensions are too small. The porous materials which have been studied in relation to drying characteristics embrace a range of pore sizes from a few millimicrons up to several hundred microns.

The characterization of the internal pore structure is necessary if its relation to drying characteristics is to be studied. However, the

internal void network of a porous material is extremely complex. To completely characterize it would require a geometric description of all parts of the network. Such an approach has not as yet been found possible. A more feasible approach involves an empirical investigation via capillary pressure measurements. This technique yields a pore-size distribution which in essence divides the pore volume into fractions which act like uniform capillaries of particular diameters. Although the analysis derived from capillary pressure measurement is strictly empirical, for a particular range of pore sizes, it does effectively distinguish between different porous media. This is shown in Fig. 5 based on data compiled by Parker (15).

A detailed description of the capillary pressure technique is included elsewhere in this thesis and is not essential to the discussion at this point. It is only necessary to indicate that such a technique gives an empirical definition of pore structure which has proved useful in permeability studies (15). Thus, it is accepted as the most promising method of evaluating the internal structure in relation to the goals of this thesis.

The boundary conditions of drying are presumably unimportant to a study of the internal heat and mass transfer processes within a porous mat during drying. However, certain drying conditions must obviously be established. Since the moisture and temperature gradients within the porous mat during the drying operation are the observable criteria for heat and mass transfer, these are the items which must be measured. Therefore, drying conditions must be selected which will produce precisely measurable gradients.

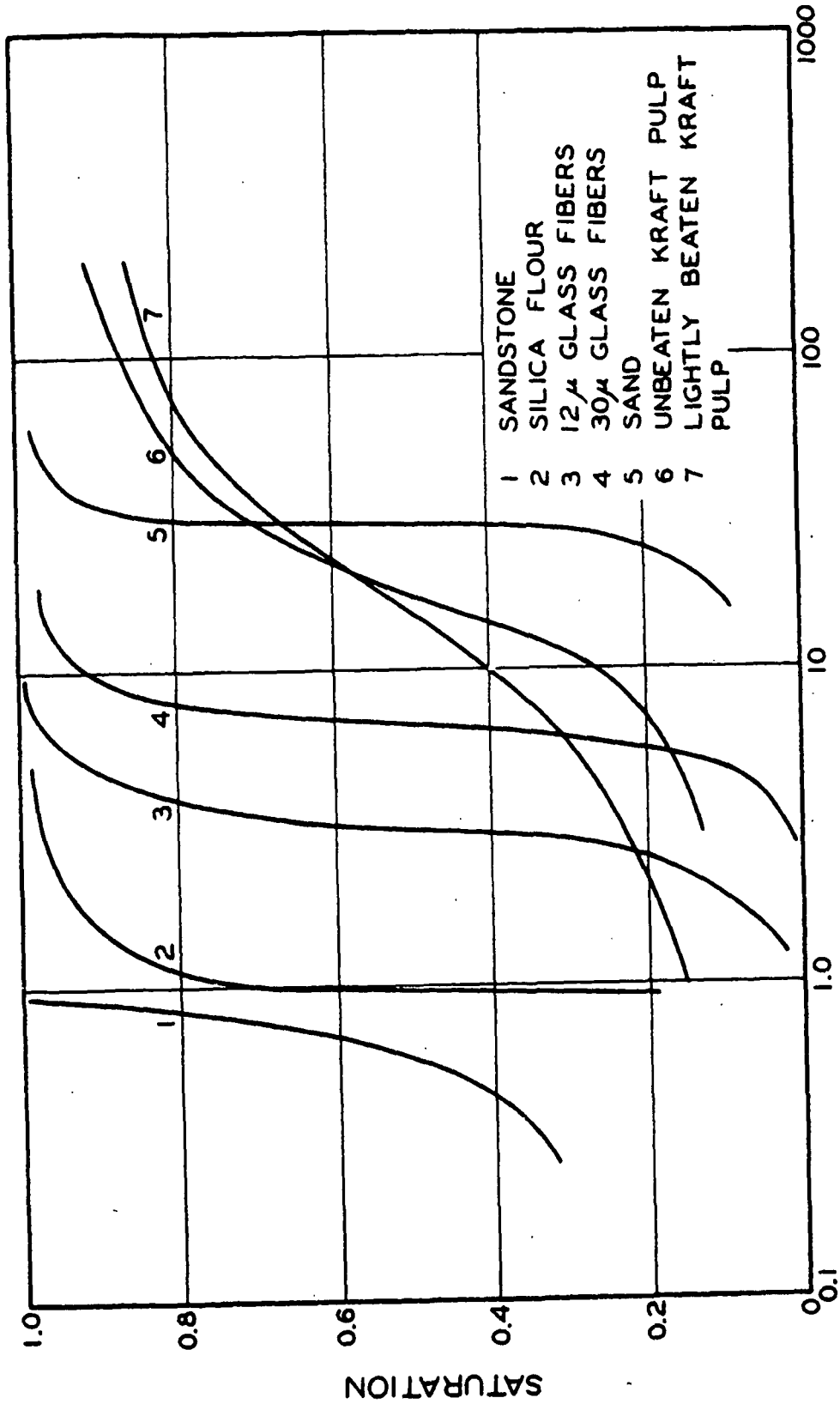

Figure 5. Pore Size Distribution by Capillary Pressure Measurement

Hot surface drying as conducted by Dreshfield (2) produces gradients which can be satisfactorily measured. The most comprehensive information available on internal transfer processes are represented by Dreshfield (2) and Ulmanen (12), who both studied hot surface drying of pulp mats. The equipment and techniques developed by Dreshfield were available to this study. For these reasons, hot surface drying was established as the mode of drying for this thesis work. The actual details of apparatus are discussed in a later section.

A research project which is aimed at developing knowledge concerning the drying of paper should carefully consider whether or not it should restrict itself to a study of pulp mats. This may seem paradoxical. However, the problems being investigated in this work are not amenable to solution by a direct study of a pulp system.

This thesis includes internal structure in a study of the internal heat and mass transfer during a hot surface drying operation. During drying, pulp fibers tend to shrink, twist, and collapse. This produces marked changes in the internal structure of a bed composed of such fibers. To characterize such a continually changing structure is difficult; to relate such a characterization to transfer processes within the bed during the drying operation is truly formidable. Water contained in a pulp bed may exist in interfiber voids, inside the fiber lumen, or in a physically adsorbed condition. The different response to drying conditions of these three forms of water complicates the analysis of liquid movement within a pulp bed.

There is little doubt that at this time these complications preclude a satisfactory analysis of the desired nature by studying pulp beds. A simpler system is necessary.

Glass fibers are geometrically uniform and well defined. They are noncompressible, nonporous, nonhygroscopic, and chemically inactive. They have a zero contact angle with water. Glass fibers form porous beds, and all water contained within the bed is interfiber, capillary-held water. The pore size distribution of these beds falls within narrow limits. A light compressive load on the bed ensures dimensional stability during drying. All these factors contribute to an idealized fibrous bed and promote the use of glass fibers for the proposed study.

Our present knowledge of the paper drying process suggests that attention be directed to the internal heat and mass transfer which occurs in the wet paper web during drying. However, the complex nature of the paper network dictates that initial study of these phenomena utilize simpler systems. This thesis employs a porous bed of glass fibers. The internal pore structure is characterized by capillary pressure measurements. Moisture and temperature gradients are measured within this glass fiber system during a hot surface drying operation using techniques developed by Dreshfield (2). These data allow an analysis of the relation between pore structure and heat and mass transfer within the pore system during hot surface drying. From this more comprehensive understanding of a simple system, future work can build toward a knowledge of the similar but more complex system, paper.

DISCUSSION OF EXPERIMENTAL TECHNIQUES

PREPARATION OF GLASS FIBERS

To obtain the most satisfactory test beds from the standpoint of characterizable internal geometry, the glass fibers employed should be as uniform as possible in diameter and as free as possible from fine debris. The weight of glass fibers present in each of the two laminates of the laminated test beds used for the hot surface drying experiments must be accurately known. The process of delamination and weighing after the bed has been completely dried is unsatisfactory because a clean-cut delamination is not possible. Thus, an accurate prediction of laminate weight from a knowledge of the amount of original fiber utilized is necessary. The fiber preparation procedure was developed to satisfactorily approach the above conditions.

The glass fibers being used in this study were obtained through the services of Mr. Labino of Johns-Manville Fiber Glass, Inc. These fibers were received in the form of glass wool; that is, fibers of extreme length. Proper fiber dispersion in a water slurry prior to bed formation is made possible only by reducing the fiber length to about 1/8-1/4 inch. Starch or some other type of organic material is used as a binder in the fiber manufacturing process and remains present as a surface coating on the fibers. The fiber preparation thus involves decontamination and fiber-length reduction of the glass wool.

The glass wool as received is cut in a random fashion using a guillotine paper cutter. This initial or primary cut product is stuffed

into beakers and heated in a muffle furnace at 950°F. for about eight hours. The effectiveness of this decontaminating treatment was evaluated by testing starch-contaminated fibers with an iodine solution before and after heating. The deep blue coloration produced by the starch-iodine complex, present prior to heating, was entirely absent after the heating period.

Approximately four-gram lots of this primary-cut, decontaminated fiber are disintegrated in tap water for 1000 counts in a British Disintegrator and then formed into sheets on a British Sheet Mold. These sheets are cut into approximately 1/8-inch strips using a guillotine cutter, and these strips are in turn cut to produce approximately 1/8-inch squares. Such a procedure guarantees an acceptable maximum fiber length.

However, this multiple cutting and disintegration procedure produces a certain amount of debris. In order to reduce the amount of this debris to a minimum, four-gram samples of the 1/8-inch squares of fiber agglomerates are disintegrated for 200 counts in a British Disintegrator and then placed in one compartment of a Bauer-McNett Classifier. A 150-mesh screen is located at the overflow from the compartment. Water is flowed through the compartment for five minutes after which the slurry remaining in the compartment is collected in a bucket. Most of the original debris is presumed to be washed through the 150-mesh screen. The slurry in the bucket is transferred to the British Sheet Mold and formed into sheets. These glass fiber sheets are oven dried and stored in air-tight polyethylene bags. This represents the stock supply of fiber suitable for use in glass fiber bed formation.

The diameter of the fibers used in this study was given by the manufacturer as 5.8 μ. Microscopic examination of the prepared fiber indicated a weighted average fiber diameter of 5.29 μ. The measurements were made by Jack Hankey of the Fiber Microscopy Group at The Institute of Paper Chemistry at a magnification of 970X under oil immersion. The range of fiber diameters contributing to this average is quite narrow as can be judged from Table I.

TABLE I

FIBER DIAMETER DISTRIBUTION

Fiber Diameter, μ	Number of Fibers
4.5	4
5.0	50
5.5	38
6.0	5
6.5	3
Arithmetic average	5.26 μ
Surface weighted average	5.29 μ

The value of 5.3 (5.29) μ is considered the most reliable estimate of the average fiber diameter since the manufacturer's measurements have at least the disadvantage of applying to a starch coated fiber.

The density of the glass fibers was measured pycnometrically, and an average of three separate determinations gave a result of 2.59 g./cm.^{3} with a precision of better than one per cent. Certain problems are encountered in this type of density determination which are peculiar to small particle systems. Appendix III gives the details of the method developed to overcome these difficulties.

FORMATION OF GLASS FIBER BEDS

The ideal fiber bed for this study can be described as one which is composed of multiple layers of uniform diameter fibers, each layer containing fibers randomly oriented in the two-dimensional plane of the layer. Such a bed should result from the filtration of a perfectly dispersed fiber slurry. Hence, the initial concern is to obtain such a slurry.

Glass fibers from the prepared stock supply are weighed and then added in approximately 3-gram lots to about 3 1/2 liters of purified water in 4-liter suction flasks. The consistency is thus about 0.1%.

Tap water is passed through a fine grade Fulflo filter and then a commercial water softening, ion-exchange unit to obtain the purified water.

The fiber in each suction flask is dispersed by vigorous stirring with a stirring rod. The flasks are then hooked up to a laboratory aspirator and the slurries deaerated for a suitable period (at least three to four hours).

The filtration system utilized for bed formation is depicted in Fig. 6. The filtration septum or screen (A) consists of a perforated frame supporting a 150-mesh screen clamped tightly over a 35-mesh backing screen.

Prior to assembly, this septum must be thoroughly cleaned in order for it to deliver a uniform flow across the full cross section. It is scrubbed with detergent, rinsed thoroughly with water, immersed for a short interval in acetone, and finally dried by subjecting it to a 105°C. oven atmosphere for a brief period.

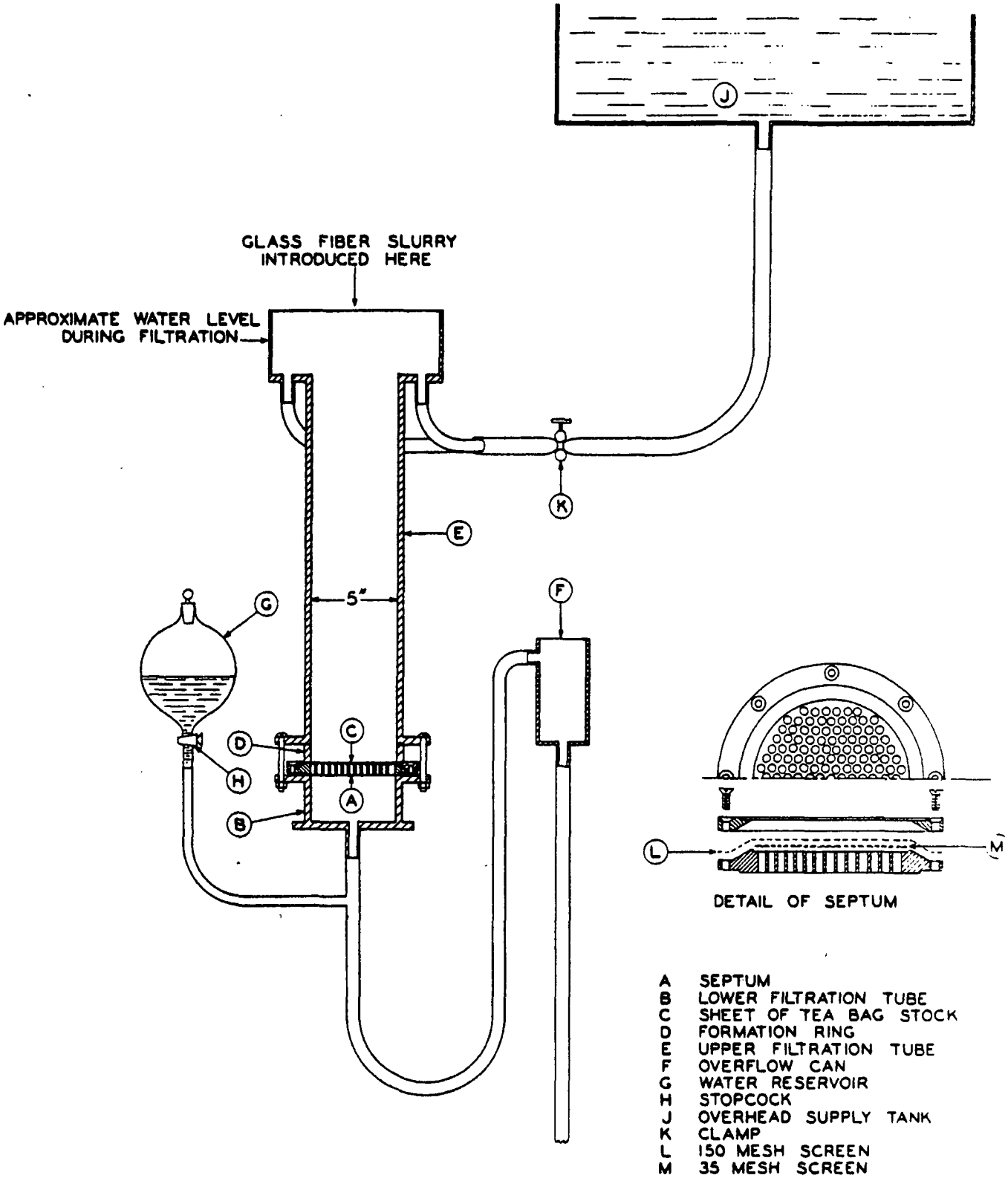

Figure 6. Filtration Apparatus

The septum (A) is positioned over an O-ring supported on the lower filtration tube (B). A dental dam gasket is placed on the upper face of the septum in readiness for the formation ring. A sheet of tea bag stock (C) is then laid over the septum and gasket and trapped in position by the formation ring (D). The presence of this sheet reduces fiber loss through the screen and allows the final glass fiber bed to be readily dissociated from the septum.

The upper filtration tube (E) is placed in position on the formation ring which is separated from it by a rubber O-ring. The upper and lower filtration tubes are bolted together, thereby clamping the whole assembly and producing a water-tight filtration column.

The flow-controlling overflow can (F) is adjusted to a level approximating the top of the upper filtration tube. Purified water is then introduced into the system from the reservoir (G). The water level is slowly raised until the septum and the sheet of tea bag stock have been uniformly wet and all air has been purged from the assembly. When the water level is a few inches above the septum, the filtration unit is isolated from the reservoir by closing stopcock (H).

Rubber hose connections are made to link the filtration tube with an overhead supply tank (J). This tank is filled with purified water. Screw-type clamp (K) acts as a needle valve controlling flow out of the tank. By adjusting this clamp and the level of the overflow can a steady flow of water through the filtration tube is maintained.

The drying study requires that a radioactive source and a fine-wire thermocouple be located at any desired level within the fiber bed. This

was initially accomplished by separately preparing two laminates and sandwiching the source and thermocouple between them. However, accumulated data demonstrated that this preparation introduced a discontinuity at the plane of lamination which resulted in significant error.

A satisfactory alternative method involves forming one laminate, placing the source and thermocouple in position, and then depositing the top laminate by means of a second filtration. This procedure is described below.

The deaerated, dispersed glass fiber slurry is poured slowly and carefully from the suction flask into the top bowl of the filtration tube. The fiber suspension is diluted and carried down to the septum by the flow of pure water. Good dispersion is maintained by gentle agitation with a long-handled perforated piston.

Prior to the introduction of this procedure, the fiber slurry was poured into the overhead supply tank where an agitator secured continual mixing. However, excessive flocculation occurred while the fiber slurry was travelling in the hose connecting the supply tank with the filtration tube. Thus, the new procedure described was introduced as a means of eliminating this defect.

The slurry in the filtration tube during the filtration operation was observed to be well dispersed with only a few small fiber bundles present. These apparently do not affect the desired random orientation in the fiber bed.

When all the glass fibers of the bottom laminate have been accepted into the bed, the control clamp (K) is closed, halting the flow of water. The overflow can is lowered so that the water level in the filtration tube reaches the upper face of the fiber bed. The bolts are released and the upper filtration tube is removed. This leaves the water-saturated fiber laminate contained in the formation ring (D) sitting on the septum (A) which is supported on the lower filtration tube (B).

A fine-wire thermocouple[1] is carefully laid on the exposed fiber surface of the lower laminate forming a loop, with the thermocouple junction near the center of the bed. The leads are brought out close together over the formation ring.

Next, the three or four radioactive glass fibers[2] are carefully placed side by side near the center of the bed.

A perforated piston is placed in position over the lower laminate and the upper filtration tube is replaced and rebolted, thus restoring the filtration column of Fig. 6. The presence of the fine thermocouple wires between the formation ring and the upper filtration tube does not hinder the rubber "O" ring in producing an effective seal. The overflow can (F) is slowly raised causing the water level to rise above the fiber laminate. The presence of the perforated piston discourages any tendency for fibers to be back washed out of the fiber bed. In addition, the thermocouple and radioactive source are maintained in position. The hose

---

[1] A discussion of the preparation of these thermocouples is given in Appendix I.

[2] For a discussion of the preparation of the radioactive source refer to Appendix II.

connection with the overhead supply tank is re-established, and water is slowly added until the filtration tube is filled and flow through the bed has been initiated. The perforated piston is carefully removed by lifting it out of the column. The flow of water minimizes any disturbance resulting from the removal of the piston.

The fiber slurry representing the top laminate is added in a manner identical to that already described for the lower laminate. In this way a complete bed is formed with the radioactive source and the fine wire thermocouple located at any desired level.

PREPARATION OF FIBER BED FOR TESTING

The drying study requires that the glass fiber bed be transferred from the formation ring and septum to a test ring. It was found possible to utilize the same test beds for both the drying and capillary suction studies. Consequently, all fiber beds used in the over-all study were prepared in the following manner, with reference to Fig. 7.

Perforated piston (C), (Fig. 7:I) is slid into the formation ring (D) until it nestles on the fiber bed. The piston flange (E) rests on top of the formation ring. By tightening set screw (F), the piston and flange are locked in position. The septum and supporting assembly can then be lifted free of the lower filtration tube and inverted. (See Fig. 7:II.) From this position the septum can be lifted off and the tea bag stock peeled from the fiber bed while the bed remains supported by the perforated piston.

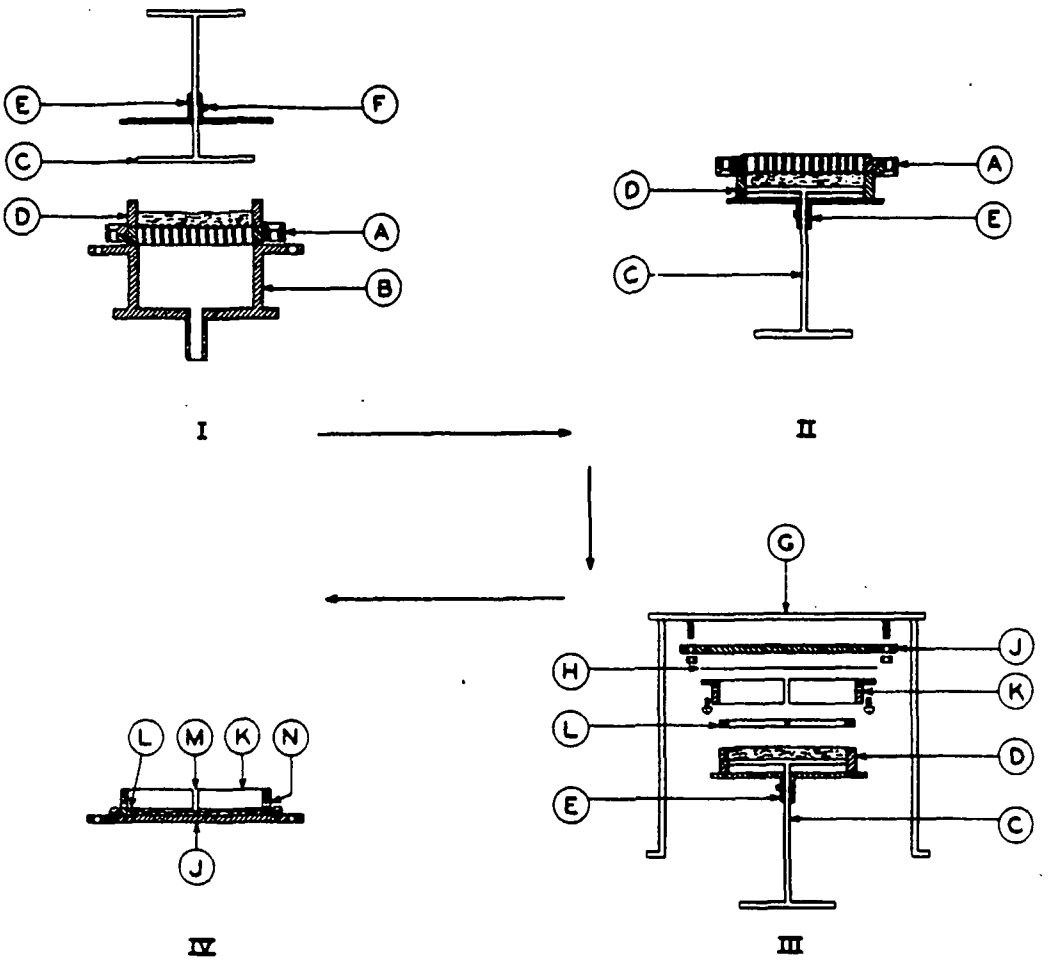

A SEPTUM
B LOWER FILTRATION TUBE
C PERFORATED PISTON
D FORMATION RING
E PISTON FLANGE
F SET SCREW
G MAIN STAND
H ALUMINUM FOIL
J BASE PLATE
K RING HOUSING
L TEST RING
M SLOT IN RING HOUSING
N DRILL HOLES IN HOUSING

Figure 7. Transfer Apparatus

An assembly consisting of base plate (J) to which is screwed ring housing (K) securing in position perforated aluminum foil (H) is bolted to the main stand (G) of the transfer apparatus. The Plexiglas test ring (L) is slid into the ring housing and followed by the piston and bed assembly represented by (C), (E), and (D). This is accomplished in such a manner that the groove in the test ring and the thermocouple leads from the bed line up with the slot (M) in the ring housing. The piston flange (E) bolts to the ring housing and thus locks the test ring and formation ring in position. The set screw is released and the piston is advanced until the fiber bed has been displaced from the formation ring to the test ring. The multiple assembly is then unbolted, removed from the main stand, and inverted. Figure 7:IV describes the situation which occurs when the piston assembly and formation ring are removed.

This assembly is placed in an oven at 105°C. in order to dry the fiber bed. The dry bed is then compressed into the test ring. The ring housing is removed from the assembly. The aluminum foil sheet is trimmed, scotch taped to the sides of the plexiglas ring, and additionally secured by an elastic band. The thermocouple leads are taped into the groove in the test ring, care being taken that no contact between leads occurs. The bed is then ready to undergo the necessary testing involved in the drying experiments and later in the capillary pressure measurements.

DRYING STUDY

The apparatus involved in producing and controlling the hot surface drying environment is shown in Fig. 8 and is essentially that of Dreshfield (2) as improved by Ulmanen (12).

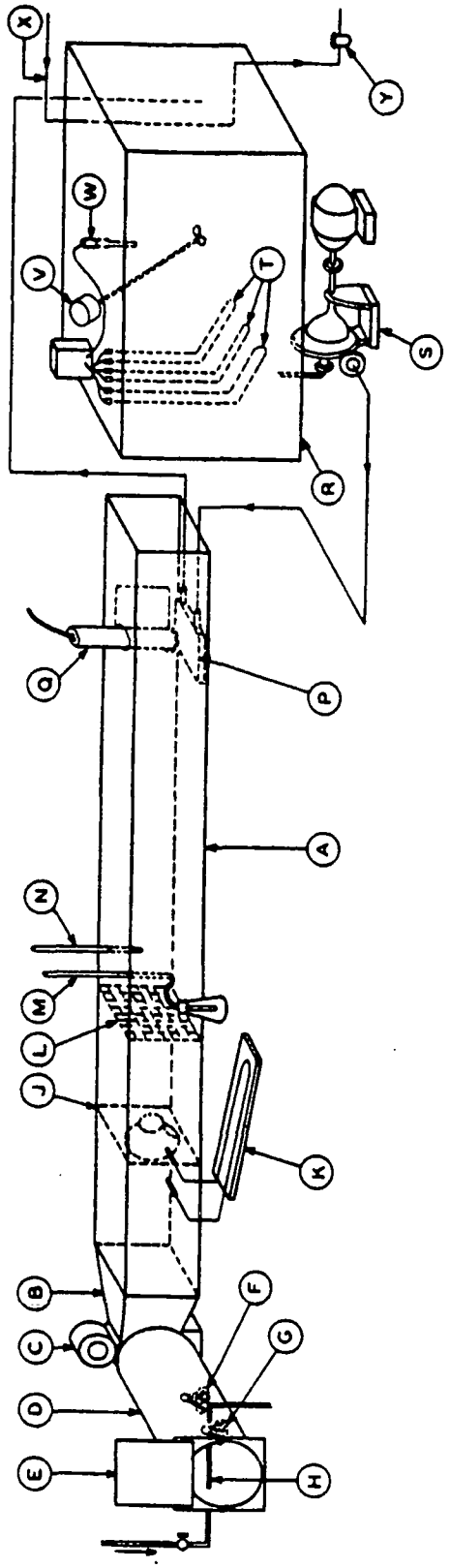

Figure 8. Drying Apparatus

The hot surface (P) against which the glass fiber bed is clamped is located towards the end inside of a 9 by 9 inch cross section drying tunnel. Fan (B) driven by motor (C) draws air through intake manifold (D) and delivers it through the drying tunnel. The temperature of the air is controlled by cone heaters (G) and (F) located in the intake manifold. One of these heaters is connected through a rheostat in order to provide control adjustment. The moisture content of the air is controlled by injecting steam into the air flow by means of a perforated steam line (H). The air flow rate is estimated by a calibrated inclined water manometer (K) which records the pressure drop across the flow nozzle (J). The purpose of this measurement is primarily to assure constancy of the flow rate over an extended experimental period; and, thus, the calibration is reliable to only about 5%. A 14-mesh screen (L) helps to even the air flow from the nozzle. Wet and dry bulb thermometers (M) and (N) give the required measure of air moisture content and temperature.

The hot plate (P) consists of a 1/8-inch aluminum top plate covering a hollow chamber through which hot water is circulated at the rate of about 15 g.p.m. The hot water system consists of an insulated tank (R) of about 9-cu. ft. capacity in which water temperature is controlled by the combination of heater (T) thermostat (W) and mixer (V). Steam line (X) discharging through trap (Y) is used for the initial heating-up period. Pump (S) delivers the hot water from the tank and circulates it through the hot plate and back to the tank.

Figure 9 gives a more detailed picture of the hot plate and clamping assembly as well as illustrating the technique for measuring the temperature within the bed during the drying operation.

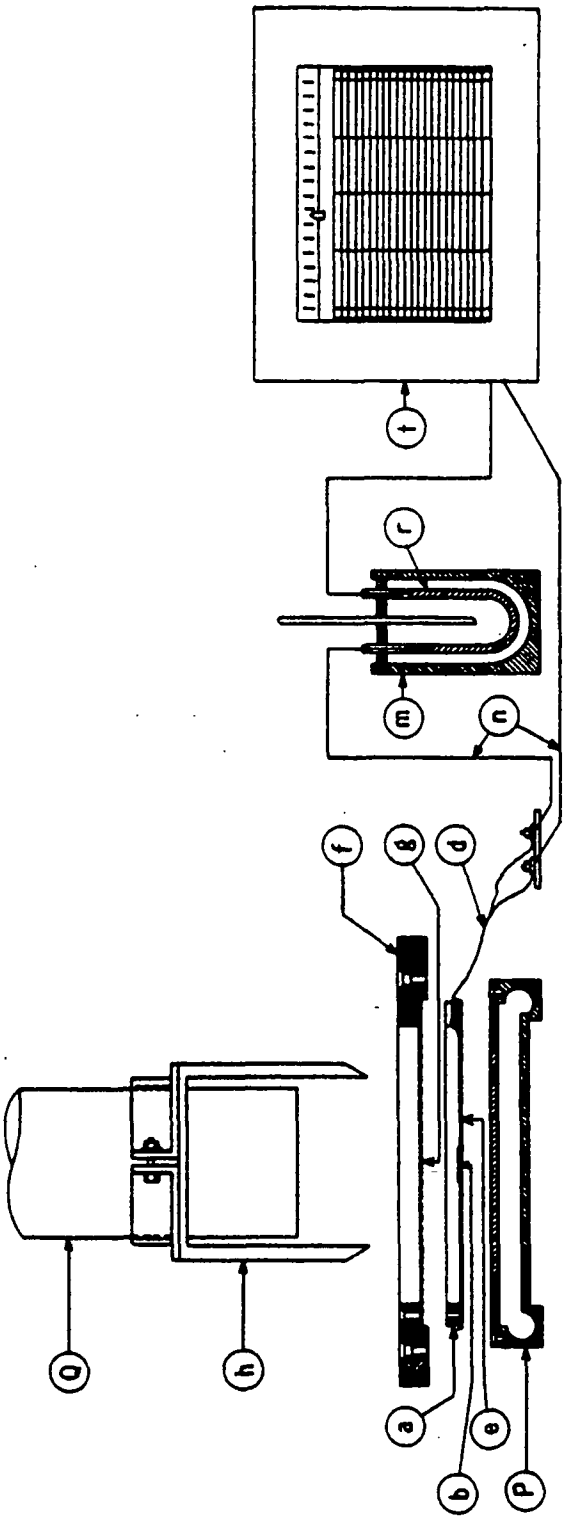

Figure 9. Clamping Assembly and Temperature Measuring Circuit

Radioactive source (b) and fine-wire thermocouple (d) are shown located in position in the fiber bed contained within the plexiglas ring (a) and supported by the aluminum foil (e). The plexiglas ring is attached to a screen assembly by three screws. This assembly consists of an aluminum frame (f) over which is stretched and clamped a 50-mesh aluminum wire screen (g). The scintillation head (Q) is clamped to a device (h) which when lowered contacts both the frame and screen of the screen assembly. Two T-bar wedge clamps establish favorable contact between the fiber bed and hot plate as well as lightly compressing the fiber bed into the test ring.

The fine-wire thermocouple leads are clamped to junctions from which larger diameter leads (n) of the same materials (chromel and alumel) continue the circuit. This circuit includes a Minneapolis-Honeywell recording potentiometer (t) and a cold junction consisting of a Dewar flask containing crushed ice and purified water in which the chromel-alumel cold junction is created by the mercury containing U-tube (r).

The method employed in this study for measuring the moisture content of the fiber as a function of drying time was developed by Dreshfield. Detailed background information concerning this technique is presented in his thesis (2). However, some of these aspects should be included here for the convenience of this development.

Certain radioactive isotopes including Sr^{90} and Tl^{204} suffer spontaneous beta disintegration of the nucleus. This signifies that emission is restricted to beta radiation, no alpha or gamma radiation being present. The disintegration rate is predictable according to the mathematical concept

of radioactive decay. The half-lives of the two isotopes Sr^{90} and Tl^{204} are sufficiently long that over the period of the experimental program their emission rate can be assumed constant.

A distinguishing characteristic of beta radiation is the continuous distribution in energy of the emitted electrons. This makes mathematical quantification of the absorption of the beta radiation by matter largely empirical. The range or ability of the beta radiation to penetrate is dependent upon the maximum energy of the beta emission. It is possible to generalize that for low molecular weight materials (which include glass, water, and aluminum), the amount of absorption is dependent upon the mass per unit area and that secondary emission and backscattering are relatively inconsequential.

In a drying operation, the total mass per unit area (basis weight) of the porous material decreases as water is evaporated and departs from the system. This decrease can be detected by placing the porous material between a source of beta radiation and a suitable detector. By empirical calibration, the change in the beta radiation received at the detector (counting rate) due to changes in the basis weight of water during drying can be accurately related to the moisture content of the porous material.

By locating the radioactive source at different positions within the porous material being dried, the moisture distribution within the material during drying can be calculated. This is the basic concept behind the technique so successfully developed by Dreshfield.

Beta radiation is detectable by a number of methods. The scintillation detector is utilized in this study and so will be briefly considered.

Certain crystals have the property of emitting a photon of light when struck by a beta particle of sufficient energy. The stilbene crystal used in this work detects incident beta radiation with an energy of 200 kev. or more. When this crystal is linked with a photomultiplier tube and an electronic counting circuit, the number of beta particles received at the crystal can be counted.

A particular source emits beta radiation equally in all directions. That portion of the radiation which strikes the scintillation crystal is thus very dependent upon the geometrical relationship between source and detector. This dictates the need for maintaining constancy of this relationship.

The mathematical certitude of the rate of emission of a radioactive isotope is in reality dependent upon the number of emissions considered. Since nuclear disintegrations have a perfectly random distribution in time, it follows that the uncertainty in predicting the emission rate can be determined from the Poisson distribution. For such a distribution the standard deviation is related to the number of events considered by:

$$s_t = \sqrt{N} \qquad (3)$$

where s_t is the standard deviation, and N is the number of events considered. The indication is, thus, that 10,000 counts recorded at the electronic counter predict a counting rate with a reliability of 1%.

With this background established, the actual apparatus and general considerations involved in measuring moisture content can be described. The apparatus is shown in Fig. 10.

detector counting rate is a function of the voltage applied to the tube which is controlled at the autoscaler. It is desirable to set this "high voltage" control at a position which corresponds to the middle of the plateau of the characteristic counting rate-voltage curve. This setting was experimentally selected as 1450 volts.

The autoscaler is controlled through a voltage regulator (3). The time required for 10,000 counts to be collected at the autoscaler has been shown to be a statistically accurate measure of the counting rate. An electric clock (4) with a full sweep second hand is connected so that it starts automatically when the autoscaler counting mechanism is activated. The autoscaler operating in the automatic position stops the clock when 10,000 counts have been collected. Thus, the clock reading in hundredths of a second gives the desired measure of the counting rate.

The following steps represent the procedure adopted for obtaining the hot surface drying data needed.

Each bed tested was separately calibrated prior to drying. The empirical nature of the absorption vs. the basis weight relationship for beta radiation, depending as it does on source strength and source-detector geometry, makes construction of a master calibration curve applicable to all beds difficult. In effect, it is easier simply to calibrate each bed separately.

The calibration procedure consists of measuring the beta-ray transmission as a function of the moisture content of the fiber bed. For purposes of this study, the beta-ray transmission is defined as the

beta-ray counting rate at a particular moisture content divided by the counting rate for the dry bed. Thus, the transmission of the dry test bed is 100.0%.

An aluminum screen assembly (F of Fig. 9) is screwed to the plexiglas ring containing the test bed. This unit represents the test assembly. This assembly is mounted as shown in Fig. 9 for the drying experiments. Similarly for calibration work the same mounting is used except that the hot plate is of course unheated. In this manner, calibration conditions are geometrically identical to drying conditions.

An aluminum cover plate was machined to snugly cover the exposed area of aluminum wire screen (g of Fig. 9). With this in place, a moist fiber bed is effectively sealed against evaporation losses. By weighing the test assembly (with cover plate) for dry bed conditions, a weight measurement of the test assembly with a moist bed makes calculable the weight of water in the bed. In resumé, the test assembly with cover plate in position is weighed as a measure of the amount of water in the bed. The test assembly, without cover plate, is mounted in the test position in the drying apparatus, and the beta-ray counting rate is recorded. The ratio of this value to the counting rate for the dry bed assembly is the transmission value. A calibration curve plotting beta-ray transmission against weight of water above the source can thus be constructed. Details of this calculation are presented later.

A fiber bed as prepared for this study contains approximately 600% by weight of water when completely saturated. The drying experiments call for an initial bed moisture content of around 250%. This value represents

about the upper limit for effective measurement using the strontium source. However, 250% by weight of water simply cannot be added to the dry bed and expected to distribute itself uniformly. The degree of nonuniformity of distribution is related to the pore distribution of the bed. A narrow pore distribution gives greater nonuniformity, while a broad range of pore sizes allows a more even moisture distribution to occur. The narrow pore distribution of the test beds thus aggravates the problem.

Therefore, the bed must be completely saturated, and then the moisture content reduced in such a manner as to maintain uniform distribution at decreasing levels of moisture content.

The initial problem is, therefore, to effect complete water saturation of the bed. Capillary considerations show that it is impossible to completely replace one fluid phase by a second fluid phase using flow displacement only. When water is caused to flow through an initially dry fiber bed, discrete air pockets will remain trapped in the bed as a consequence of the capillary nature of the bed and the existence of interfacial tension forces. The amount of air so trapped is some function of the nature of the pore structure as well as the flow conditions established. An effective way to remove this residual air is to cause it to be dissolved in the saturating water.

The following procedure based on the above reasoning was used to saturate the glass fiber beds. Boiling water is poured through the test assembly (minus cover plate) supported on a wire screen and perforated brass plate. A regular pattern of 1/64-inch diameter holes were drilled, prior to assembly, in the sheet of aluminum foil which represents the bottom of the test bed.

Thus, an open channel is available for pouring water through the bed while the presence of the top screen of the test assembly prevents disruption of the fiber bed. The hot water is allowed time to cool and dissolve the residual air. The system is then flushed out with normal temperature water.

The next problem is to lower the moisture content from saturation (600%) to about 250% for drying studies and various lower levels for calibration purposes. This only becomes a problem when the stipulation is made that at any particular level of moisture content the water be uniformly distributed throughout the bed. The chief reason for requiring a uniform moisture distribution is a result of the calibration method as it applies to the case where the beta source is located at some point within the fiber bed. The moisture content above the beta source is determined on the basis of the total weight of water in the bed. In other words, if the distribution is not uniform, the moisture content above the beta source is not necessarily equal to the over-all moisture content. This gives a calibration error which will reflect seriously on the accuracy of the drying measurements. A method of desaturation which first comes to mind is to dry the bed to the desired moisture level. Of course, it is recognized that any drying procedure will establish a moisture gradient within the bed. However, if the drying is conducted at a sufficiently slow rate, this gradient presumably should become negligible.

Such an assumption is based on ordinary rate concepts. It neglects structural effects of the fiber bed. Experimental data soon suggested that this assumption is not valid. The moisture gradient established by slow air drying definitely yielded a significant departure from the desired uniformity of moisture distribution. Another method of desaturation had to be found.

When water is drawn from a saturated bed through the application of a negative pressure, the quantity of water remaining in the bed is that which is at capillary equilibrium with the applied pressure. It is a basic concept that water at capillary equilibrium within a uniform porous network must be uniformly distributed. This concept offers an escape from the horns of the aforementioned dilemma.

The saturated fiber bed is placed in the capillary suction apparatus in a manner similar to the description given shortly on pages 44 and 45. However, it is only necessary to place the bed in position and use the weighted perforated brass plate to maintain adequate contact. No clamping is required. The mercury reservoir is lowered slowly until the moisture content of the bed has been reduced to a desired level. A short period is allowed for equilibrium to be closely approached. By using a flat spatula, the bed can be removed from the porous plate without significant fiber loss.

During the calibration procedure this bed is tested, returned to the apparatus, and a further increment of water removed. In this manner, various levels of uniform moisture content down to about 25% by weight can be calibrated.

For the drying study the procedure is to achieve a moisture content slightly above the desired initial moisture content. Two or three adjustments interspersed with check weighings readily achieve this goal. The bed is then slowly air dried to the desired initial moisture content of 250%. This final air drying introduces no measurable gradation error.

The hot surface drying experiments have as their goal the description of moisture and temperature conditions within a glass fiber bed of constant porosity, pore distribution, and basis weight at any time during a drying operation using fixed drying conditions.

The internal geometry of the fiber bed can be fixed by utilizing a constant weight of fiber which when compressed into the test ring will yield a structure that is not affected by the surface tension forces active during drying. This condition is suitably achieved by forming test beds containing approximately 12 grams of dry fiber.

The initial weight of water in the bed (immediately prior to a drying operation) was controlled at 30.00 $\pm$ 0.2 g.

Drying conditions are established by controlling the hot water circulating temperature (i.e., the hot surface temperature) and the temperature, humidity, and flow rate of the circulating air. The absolute values chosen for these drying conditions are the same as those selected by Ulmanen. This was done in order that the data of this study would be more realistically compared with Ulmanen's data. These conditions are:

Hot water circulating temperature = 90.0°C. $\pm$ 0.1°C.

Air flow rate = 135 $\pm$ 5 c.f.m.

Air temperature = 100.0°F. $\pm$ 0.5°F. dry bulb
78.0°F. $\pm$ 0.5°F. wet bulb

The drying run was conducted as follows: The drying environment was established at the desired control conditions. The fiber bed was desaturated, as previously described, to the desired initial moisture content of 250%

(30 g.). The fine wire thermocouple leads from the bed were secured at the temperature measuring junction (see Fig. 9), and the recording potentiometer was turned on. The bed assembly was then quickly placed in position on the hot plate, a stop watch started, the top cover plate removed, and the clamping device lowered and clamped into position. This operation took about ten seconds to accomplish.

The time for 10^4 counts to be received at the beta-ray detector was recorded as a function of drying time as ascertained by the stopwatch reading. Readings at approximately three-minute intervals produced an adequate description of the drying process.

The temperature at the thermocouple junction within the bed was automatically recorded on a strip chart at the recording potentiometer.

The treatment of raw data is discussed in a later section.

CAPILLARY PRESSURE STUDY

The capillary pressure[1] apparatus designed and built for this study is essentially the same as the smaller apparatus employed by Parker (15). The following description of assembly and operation makes reference to Fig. 11.

The apparatus consists of a lower plexiglas housing (A) attached to a precision bore glass tube (B) filled with mercury and connected to a mercury reservoir (C). This reservoir rests on a traveller (D) which runs

[1] The terms capillary pressure and capillary suction are used interchangeably throughout this thesis.

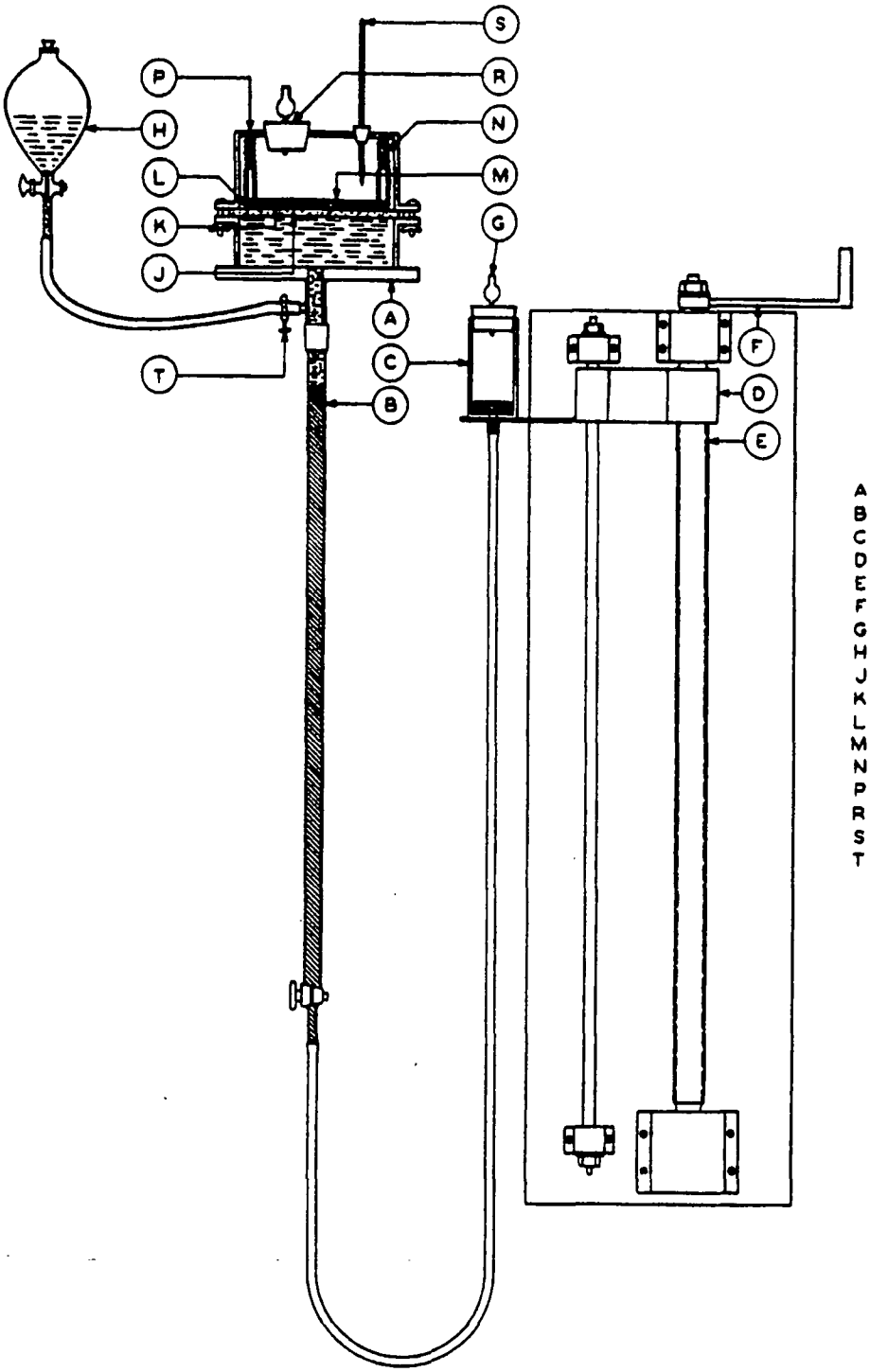

A LOWER HOUSING
B PRECISION BORE TUBE
C MERCURY RESERVOIR
D TRAVELLER
E SCREW
F HANDLE
G DRYING TUBE
H WATER RESERVOIR
J SINTERED GLASS POROUS PLATE
K GLASS FIBER BED
L PLEXIGLASS RING
M PERFORATED BRASS PLATE
N SPRING
P UPPER HOUSING
R ACCESS PLUG WITH DRYING TUBE
S THERMOMETER
T HOSE CLAMP

Figure 11. Capillary Pressure Apparatus

on screw (E) and can thus be adjusted vertically by turning handle (F). Drying tube (G) loosely filled with cotton batting connects the mercury reservoir with the atmosphere.

Lower housing (A) is filled with deaerated, filtered water from water reservoir (H). Water-saturated sintered glass porous plate (J) is placed in position over the lower housing. This is effected in such a manner that all air is purged from beneath the porous plate.

The porous glass plate was obtained from Corning Glass Co. It is 7 1/2 inches inside diameter with approximately one inch of edge fusing and 5 1/2 inches of porous area. The surfaces are machined flat and parallel to a tolerance of 0.002 inch. The thickness is approximately 3/8 inch. The plate was originally cleaned by allowing contact with freshly prepared hot cleaning solution (sulfuric acid-dichromate solution) and then boiled in successive lots of purified water until the last traces of discoloration due to the cleaning solution had disappeared. The plate is water saturated by submerging it in hot purified water in a vacuum desiccator under reduced pressure.

Water-saturated[1] fiber bed (K) is placed on the porous plate with the free fiber face in contact and the aluminum foil-covered opposite face upward. Spring loaded, heavy perforated brass plate (M) and plexiglas ring (L) constrain the fiber bed in the required geometry. The water in the glass fiber bed is now connected by an unbroken water leg with the mercury in the precision bore tube.

---

[1] Saturating procedure is discussed on page 37.

Upper plexiglas housing (P) is then bolted to the lower housing, thus clamping the porous plate and glass fiber bed in position. A large rubber stopper (R) fitted with a drying tube containing water-saturated cotton batting seals an access hole in the top of the upper housing. This prevents evaporation of water from the fiber bed but allows the pressure to remain atmospheric. Thermometer (S) records the temperature in the sealed bed compartment.

The apparatus assembled, the bulk of superfluous water is pipetted from around the fiber bed via the access hole. The water reservoir is then lowered in order to drain the residual free water from the fiber bed and porous plate. Thus, a slight negative pressure actually exists for the zero reading. The hose clamp (T) is closed, and the apparatus is isolated from the water reservoir.

By lowering reservoir (C) a negative pressure is transmitted to the water in the fiber bed. This negative pressure will draw water out of the bed in accordance with the laws of capillarity. The volume of water removed can be evaluated by measuring the displacement of the mercury-water interface in the precision bore tube. The pressure established is evaluated by measuring the elevation of the mercury interfaces (tube and reservoir) with reference to the center of the glass fiber bed taken as a datum. These measurements are obtained through the use of a cathetometer.

In order that a particular capillary pressure be maintained despite movement of the mercury-water interface in the tube the cross-sectional area of the reservoir was made 13.6 (ratio density mercury to water) times the cross-sectional area of the precision bore tube. In this way a fine-wire

indicator attached to the reservoir can be set at a predetermined position; the reservoir is lowered until this wire indicates the level of the mercury-water interface. As long as this match is maintained, the increasing head of water in the tube is exactly compensated by the decreasing head of mercury in the reservoir. Thus, the net capillary pressure remains unchanged.

By calibrating the porous plate prior to testing the glass fiber beds, the water removed from the fiber bed at any particular capillary pressure can be differentiated from the water removed from the porous plate.

Two variables which have a marked effect on capillary pressure measurements are temperature and interfacial tension. The capillary pressure apparatus was located in an isolarium with temperature controlled at 25 $\pm$ 1/2°C. All water associated with this experimental work was of known and satisfactory purity with a surface tension closely approaching that listed for pure water. Surface tension measurements of the water in the apparatus before and after each run assured that this value remained unchanged. Surface tension measurements were made with a De Nouy surface tensiometer.

After completion of a capillary suction run, the residual saturation of the bed, that is, water contained in discrete noncontinuous pockets in the fiber bed, is determined by removing the fiber bed, weighing it, oven drying, and reweighing it. This information completes the required data and allows the degree of saturation of the glass fiber bed to be related to the applied capillary suction. This is the experimental basis from which, as will be discussed later, a pore size distribution function can be determined.

DEVELOPMENT AND CRITICAL ANALYSIS OF DATA

The last section discussed the procedures and techniques that have been developed in order to obtain the desired data. The next section discusses the results as defined by these data. A transition is needed to allow discussion of the accuracy and precision of the data and to clarify its general development. The following section supplies this need.

DRYING STUDY

The calibration procedure relates the water content of the fiber bed with a beta-ray transmission figure. A particular water content is established, as previously described, by the use of a capillary suction technique. Preliminary data were collected to assess the reproducibility of the calibration curve using this technique. Part of this data, presented in Table II, clarifies the required calculations.

TABLE II

CALIBRATION DATA, D-111

(a) Assembly Weight, g.	(b) Beta-Ray Counting Rate, sec./10^4 counts	(c) Weight of Water in Bed, g.	(d) Beta-Ray Transmission, %
1028.80 (dry bed)	1.46	0.00	100.0
1048.25	2.21	19.45	66.1
1060.41	3.31	31.61	44.2

The total weight of the test bed assembly is recorded in column (a). The corresponding beta-ray counting rate is given in column (b). By subtracting the dry bed assembly weight (1028.80) from the weight of the wet

bed assembly, column (c) is obtained. Dividing the dry bed counting rate (1.46) by the counting rate when water is present in the bed gives, by definition, the beta-ray transmission recorded in column (d).

Figure 12 shows the reproducibility of the calibration data. All points are for the same bed. The bed was saturated and calibrated, then resaturated and checked several times. Different symbols indicate test values obtained after resaturation. All subsequent calibration data demonstrated precision comparable to Fig. 12. This is suggested as satisfactory evidence for the reliability of calibration data.

The capillary suction technique is a valuable additional tool for drying studies. It is a theoretically sound manner in which to produce a uniform moisture content of any specified value. Also, it offers a rapid means of obtaining such moisture contents. With this technique, for instance, a complete calibration curve can be established in about two hours. In addition, a bed can be rapidly desaturated to the desired level for a drying experiment. This obviates the need for extended periods of slow air drying even where such a technique is valid.

Some typical drying data are given in Table III to illustrate the necessary calculations.

The original measurements are recorded in columns (a) and (b). The beta-ray transmission calculated from the counting rate data, as previously described, is shown in column (c). The calibration chart is consulted for the values of water content corresponding to the particular transmission figures. These are tabulated in column (d).

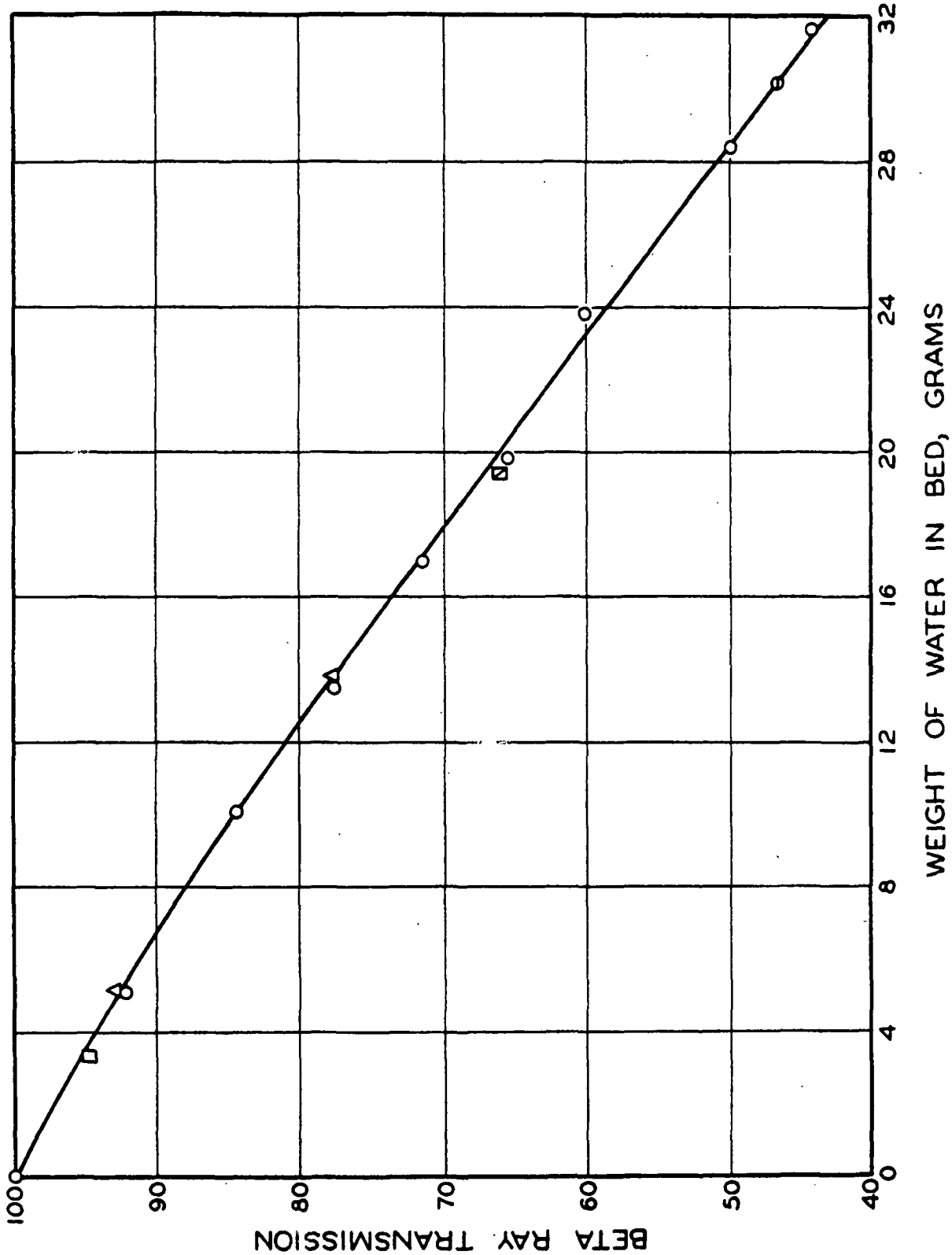

Figure 12. Calibration Curve D-111

TABLE III

DRYING DATA, D-132

(a) Drying Time, min.:sec.	(b) Counting Rate, sec./10^4 counts	(c) Beta-Ray Transmission %	(d) Water Above Source, g.
1:00	1.60	61.9	11.2
7:00	1.51	65.6	10.1
21:00	1.19	83.1	4.9
Final	0.99	100.0	0

The temperature is calculated from a continuous potentiometric record of a thermocouple junction located at the desired point in the bed. This record, in millivolts, is converted to temperature by use of a calibration curve.

The calibration curve was constructed by measuring the millivoltage output from the thermocouple junction located in a temperature-controlled hot water bath. A Bureau of Standards thermometer was used for recording the actual temperature. The calibration curve was found to closely coincide with standard chromel-alumel junction potential-temperature correlations. The basic drying and temperature data obtained in this manner are presented in Fig. 13-16.

The only criterion of accuracy in determining the moisture and temperature distributions within the glass fiber bed during drying is the precision of measurement and the internal consistency of the data. In the drying experiments, sources of error can be classified into two general categories--those which contribute to variation in test results for one particular bed and those which contribute to a between-bed variation.

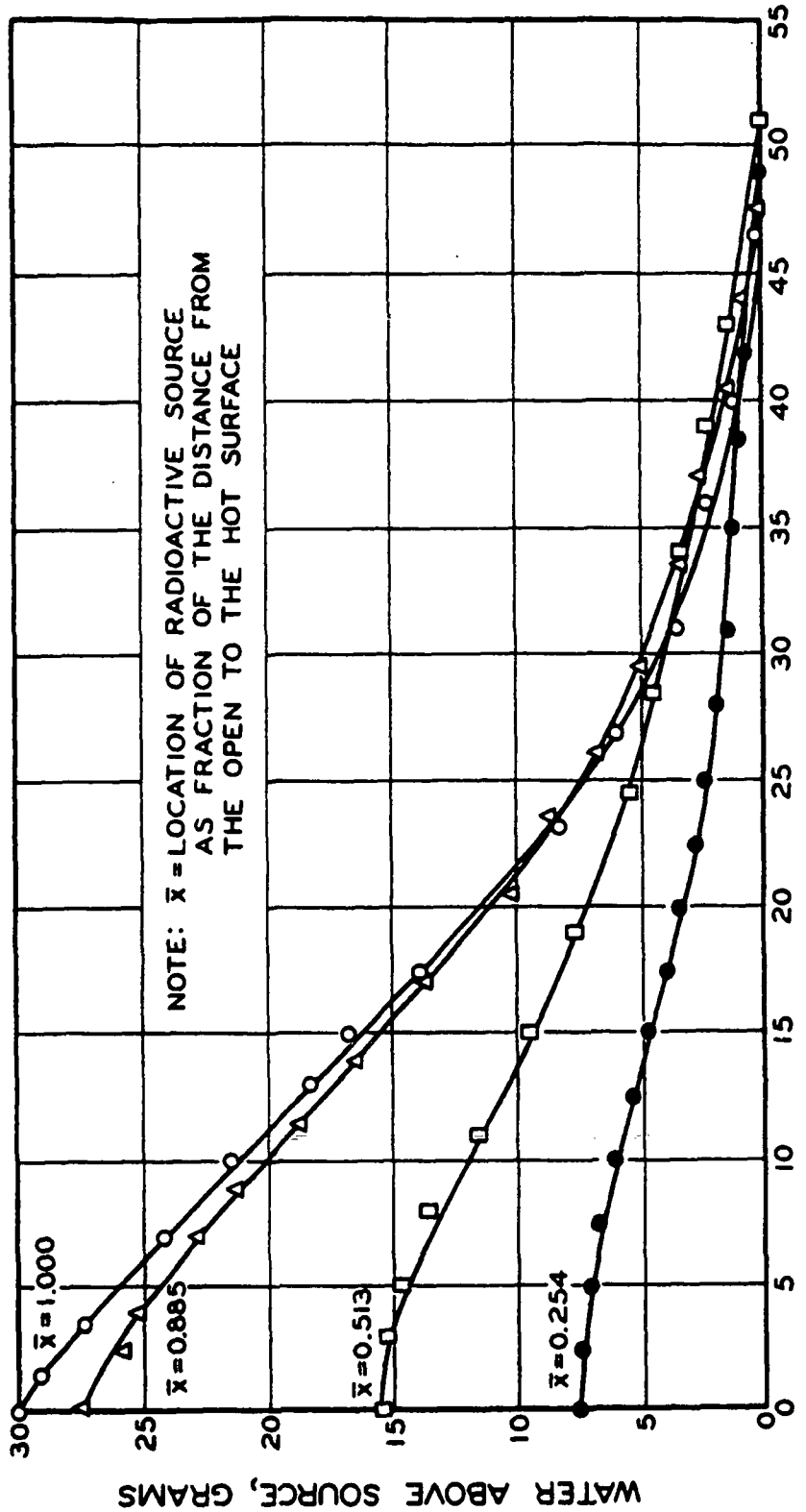

Figure 13. Original Drying Data I

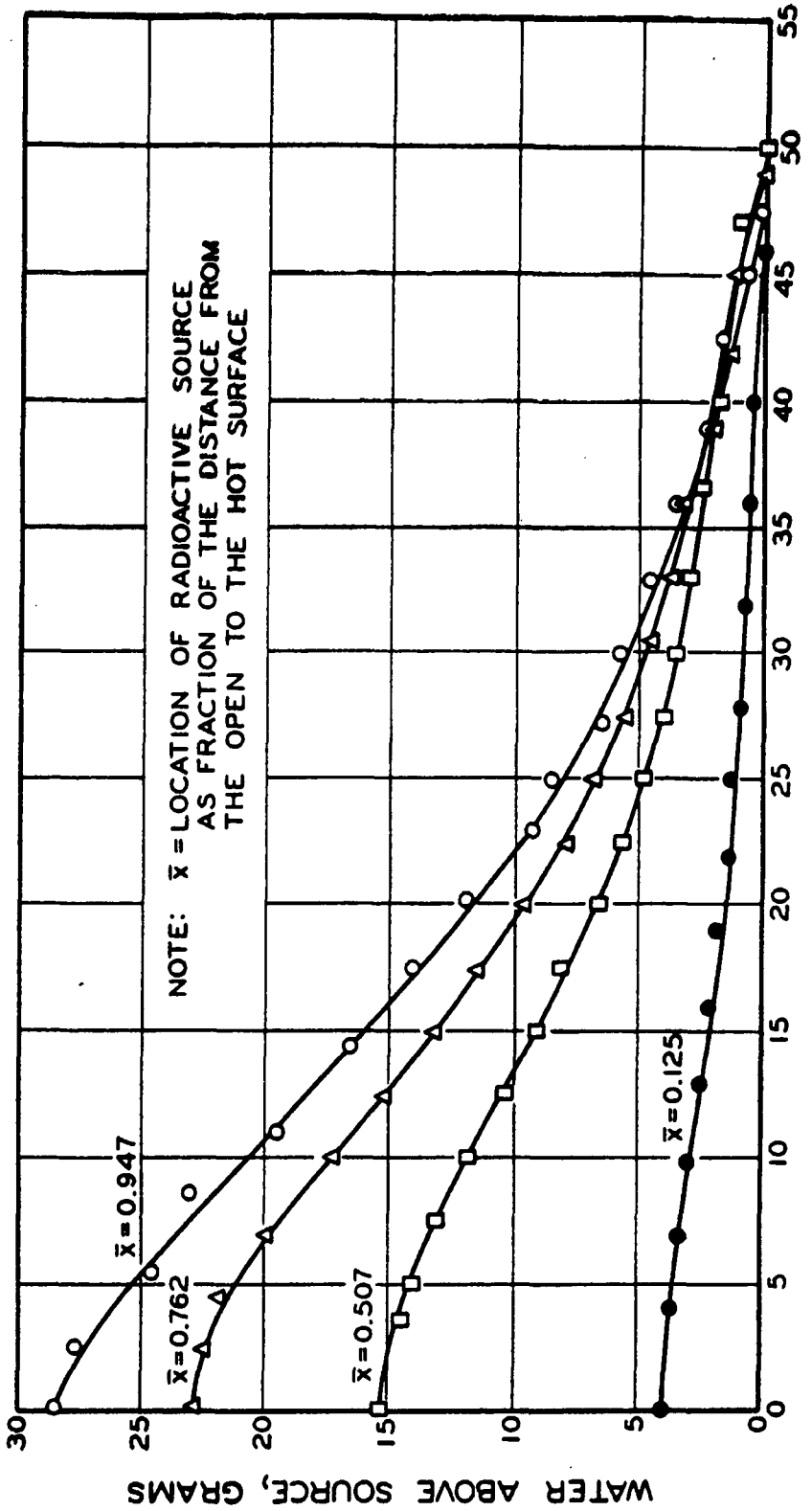

Figure 14. Original Drying Data II

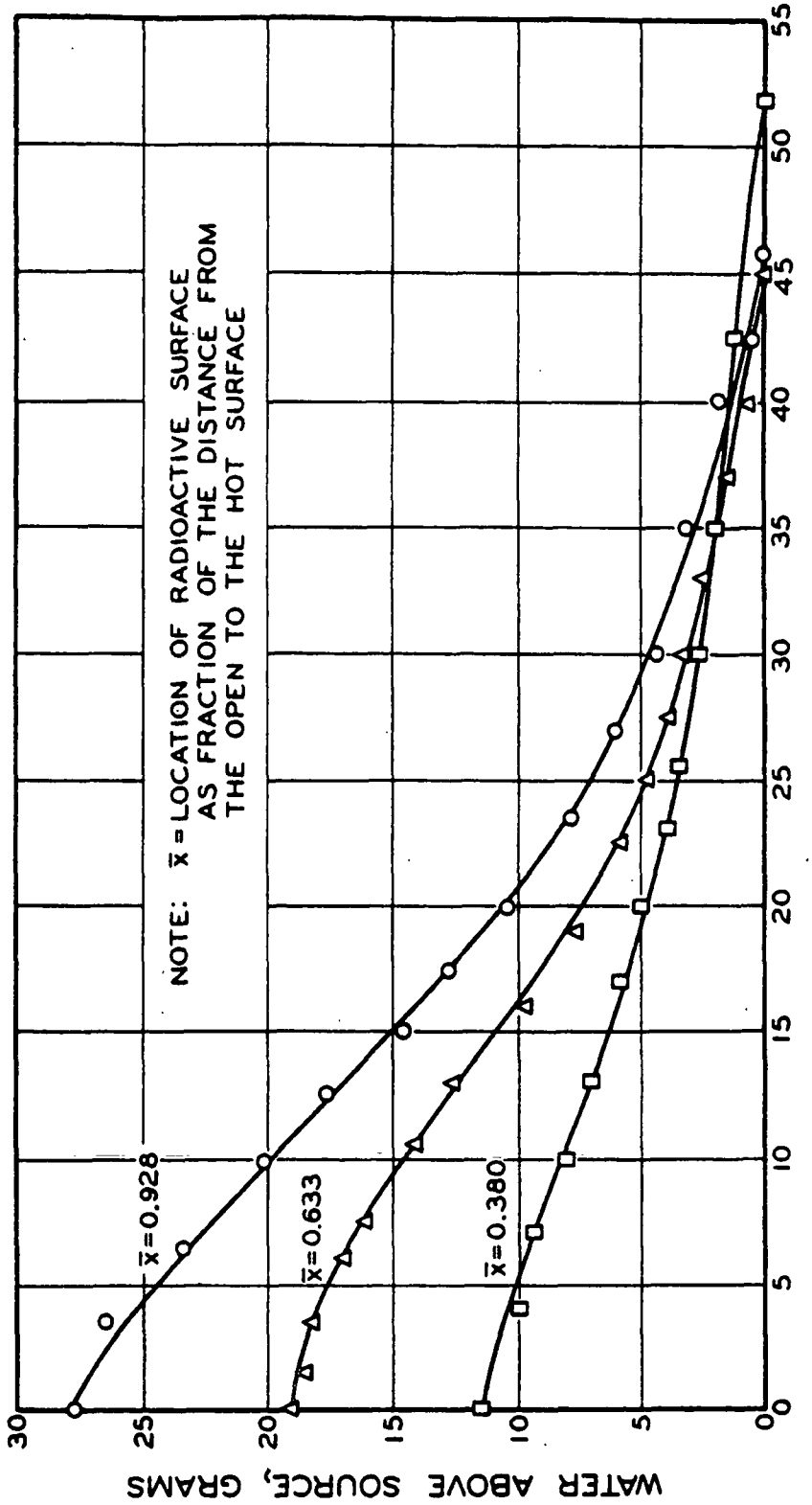

Figure 15. Original Drying Data III

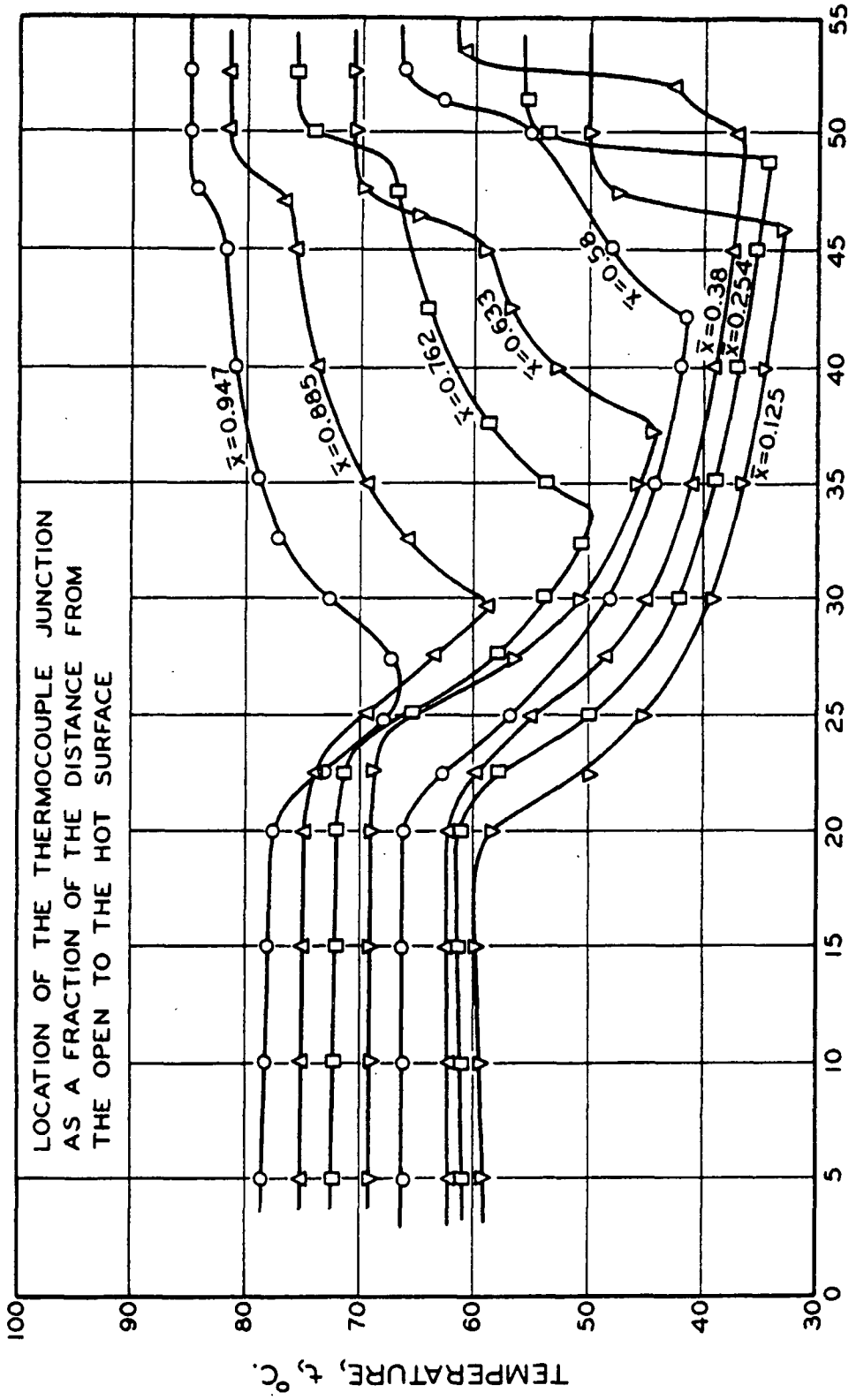

Figure 16. Original Temperature Data

A particular bed, after calibration, can be saturated to the desired level, dried, and then resaturated and redried. Without exception, results from such duplicate or even triplicate tests on one particular bed demonstrated excellent reproducibility. Figure 17 shows the water content above a beta source, located at a position approximately 5/8 of the distance from the hot surface to the open face, as a function of drying time. These data represent two drying runs on the same bed made on different days. Figure 18 represents similar temperature data.

Since this precision was invariably maintained, it suggests that the drying environment (hot surface temperature and air conditions) was adequately controlled; that the initial moisture content was satisfactorily reproduced; and that no important changes occurred in the bed as a result of its past history.

The moisture and temperature distributions are reconstructed from data obtained from different test beds, each bed yielding one point in the desired distribution curves. The accuracy of this reconstruction is naturally dependent upon the assumption that the different beds dry in precisely the same manner. One necessary but not sufficient criterion of precision is that different beds require the same time to dry.

Experience has indicated that the point (C) marked on the temperature curve of Fig. 18 represents the time when liquid water completely disappears from the bed. The total drying time evaluated in this manner can be seen from Fig. 16 to vary for different beds by as much as six minutes in extreme directions. An attempt was made to determine the cause of this variation. The drying variables have already been eliminated as possible

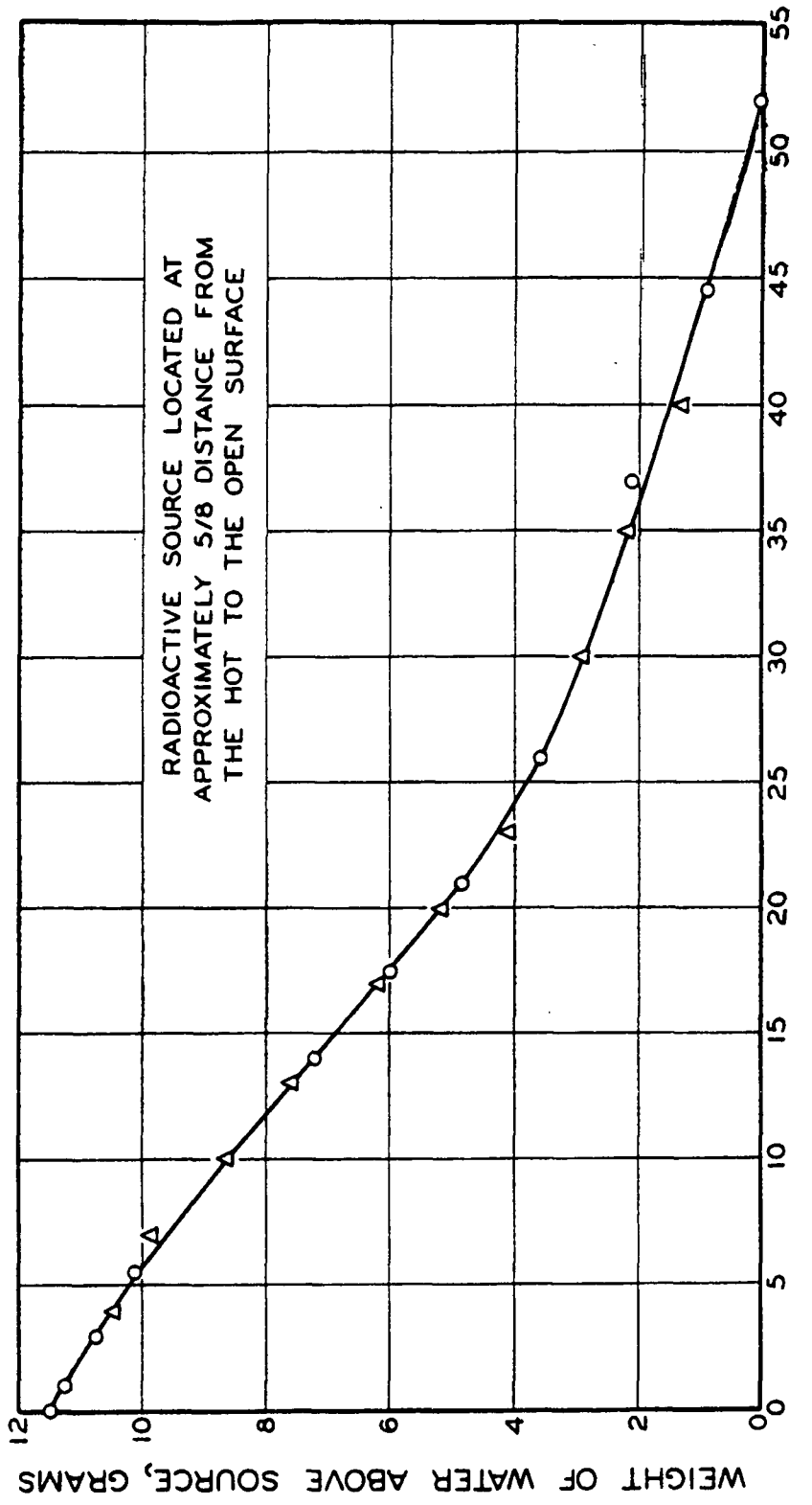

Figure 17. Drying Data D-152

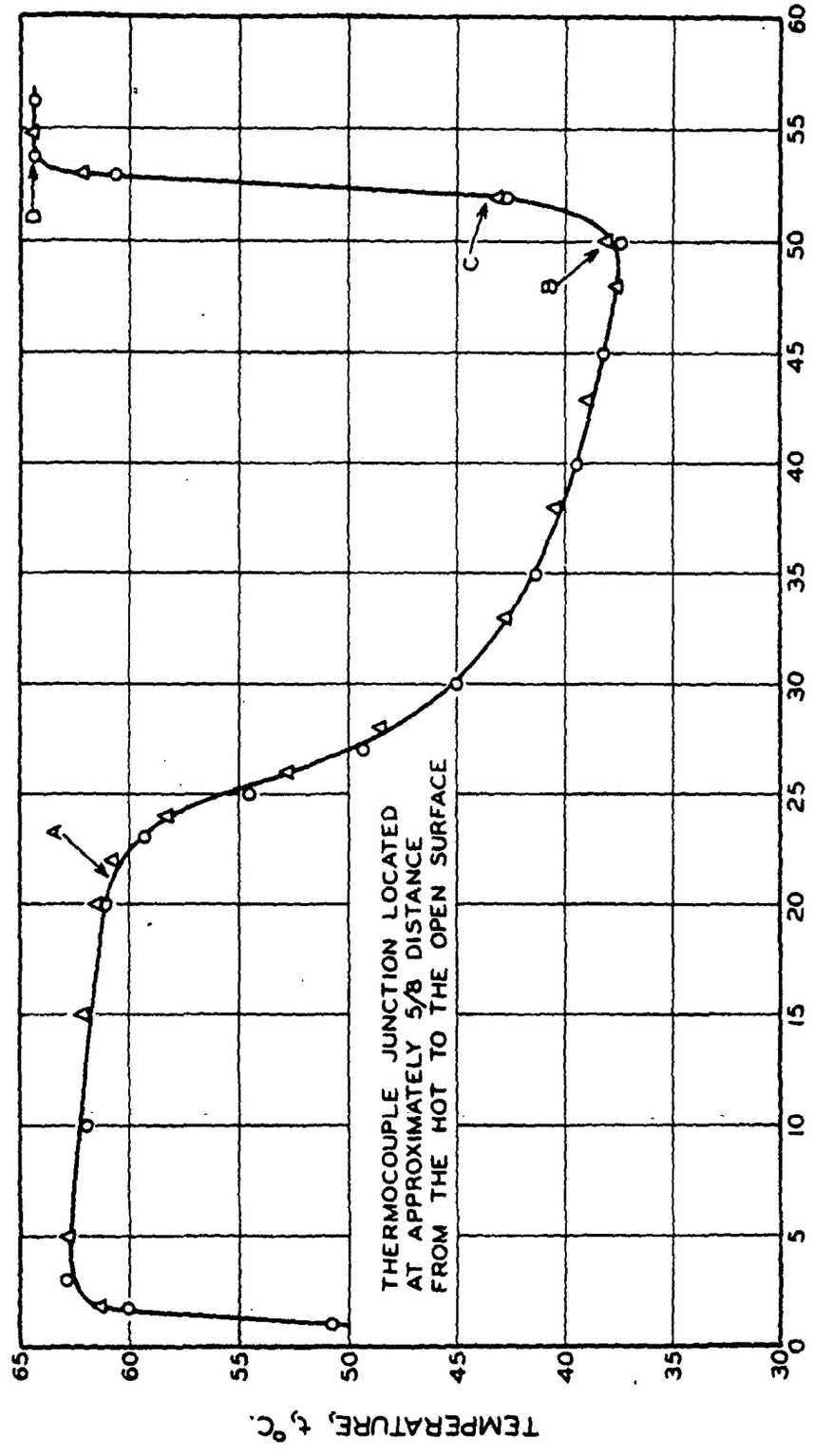

Figure 18. Temperature Data D-132

offenders. Therefore, the variation must be attributed to physical differences between different beds. One such possibility is porosity differences. The small size of the fibers made it impossible, in spite of all precautions, to eliminate fiber loss through the septum. The extent of fiber loss varied somewhat, thus yielding variations in the total weight of dry fiber in different beds. Table IV lists the porosities of a number of beds together with the total time required to dry them. This table includes the maximum porosity variation encountered. It can be seen, first, that while the porosity variation is not insignificant, it is not great. Second, no correlation can be observed between the porosity and the total drying time. For glass fiber beds, pore size distribution is sensitive to porosity variations (15). Thus, it is impossible to attribute the encountered differences in drying time to variations in the average internal geometry of different beds.

TABLE IV

POROSITY VARIATION AND TOTAL DRYING TIME

Porosity	Total Drying Time, min.
0.944	47
0.947	50
0.945	46
0.943	47
0.943	49

Further consideration of the between-bed reproducibility and non-reproducibility is necessary before returning to the question of its cause. The basic drying and temperature data for independent measurements on

different beds with the thermocouple and radioactive source located at essentially the same position in the bed (near the midpoint) are shown in Fig. 19. It can be seen that the drying data are reproducible for about 15 to 20 minutes of drying after which a diversion results in the termination of the curves at the different total drying times. Similarly, the temperature data is reproducible for about 20 minutes of drying after which wide divergencies are apparent.

Experience suggests that point (A) shown in Fig. 18 represents the time when liquid water disappears from the hot surface. The subsequent fall in temperature is rapidly transmitted throughout the bed. In other words, the location of the point (A) should be reproducible. Although the variation in the location of this point does occur, this variation can be seen to be considerably less than that experienced in the value of the total drying time. In addition, no consistent relation between the location of points (A) and (C) for a given bed could be deduced.

The above evidence suggests that a small variation operative over the latter part of the drying period produces the measurable variation in the total time required to dry the beds. This could be caused by small differences in the constitution of the surface of the bed that is in contact with the hot surface during drying. For instance, it was not found possible to totally eliminate fine material from the fiber sample. Variations in the amount or distribution of fines present at the surface could conceivably result in small changes in thermal conductivity at the interface as well as producing small changes in the capillary structure at the interface. At any rate, the possible ways that small structural differences could occur

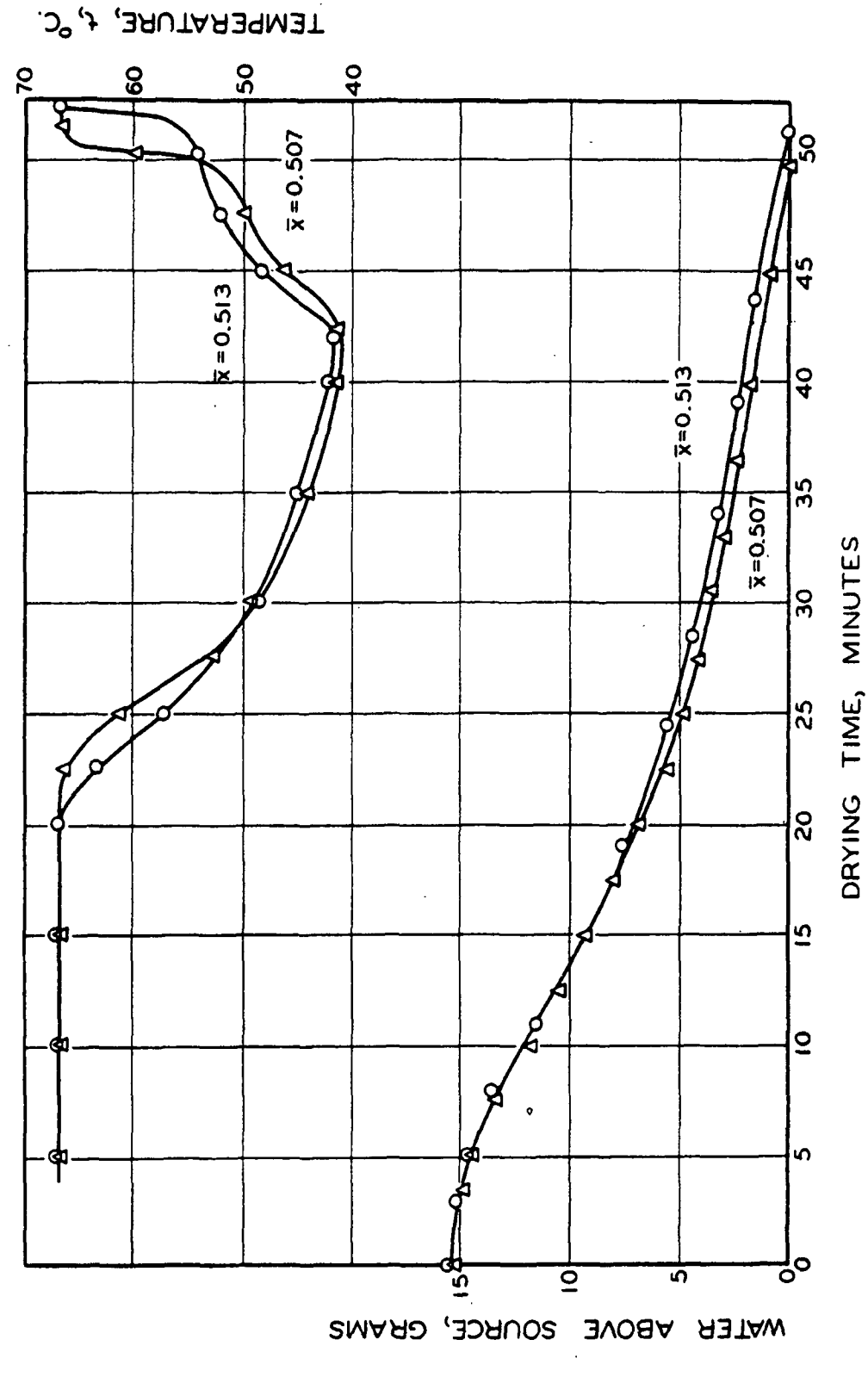

Figure 19. Between-Bed Reproducibility

at the surface must be considered as uncontrollable properties of the glass fiber bed formation.

It is therefore judged that the determination of moisture and temperature distributions from the basic data will be quite precise during the first 15 to 20 minutes of drying. Hence, the primary analysis will be based upon this data for the early drying period.

In order to produce a consistent qualitative picture it was necessary to make a linear adjustment to the data for the later drying period so that all drying curves terminated at the same drying time. These adjustments have been incorporated to produce the family of curves shown in Fig. 20. A comparison of this data with that presented in Fig. 13-15 indicates the extent of the adjustment. It can be seen that the adjustment has been applied only, where necessary, to data obtained for the later drying period.

At any drying time the cumulative water content of the bed can be readily deduced from the data shown in Fig. 20. It is convenient to express the cumulative water content of the bed in terms of cumulative saturation. By definition, the saturation, s, of a porous bed is the fraction of the void space or porosity, e, that is occupied by liquid water. The weight of water in a fully saturated bed can be calculated from the known geometric dimensions of the bed and the known volume of fiber in the bed. Dividing the cumulative water content by this figure converts the system to cumulative saturation. The results of such calculations are presented as a family of curves in Fig. 21.

The derivative or slope of the cumulative saturation function represents the actual saturation at any point in the bed for the drying interval

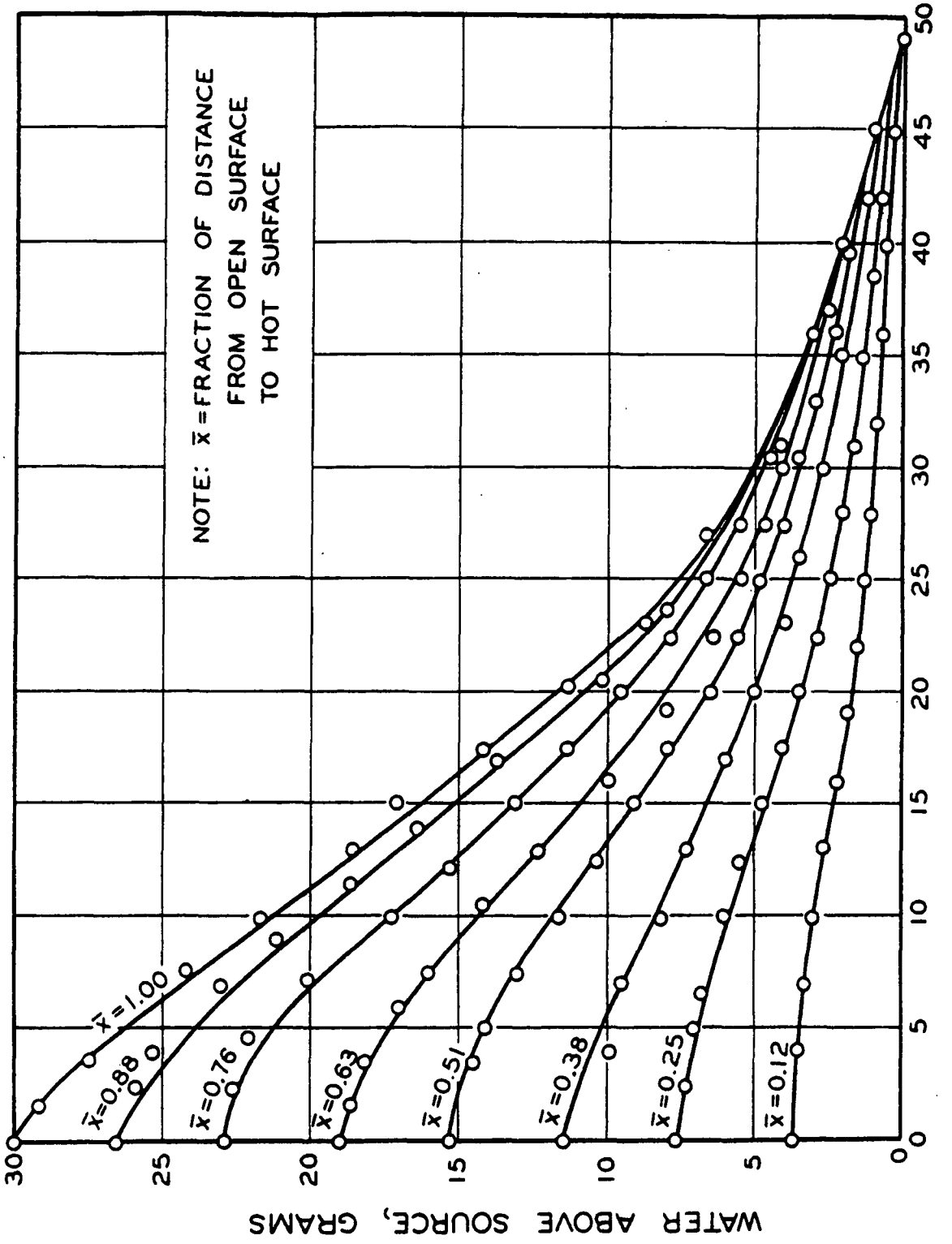

Figure 20. Drying Data

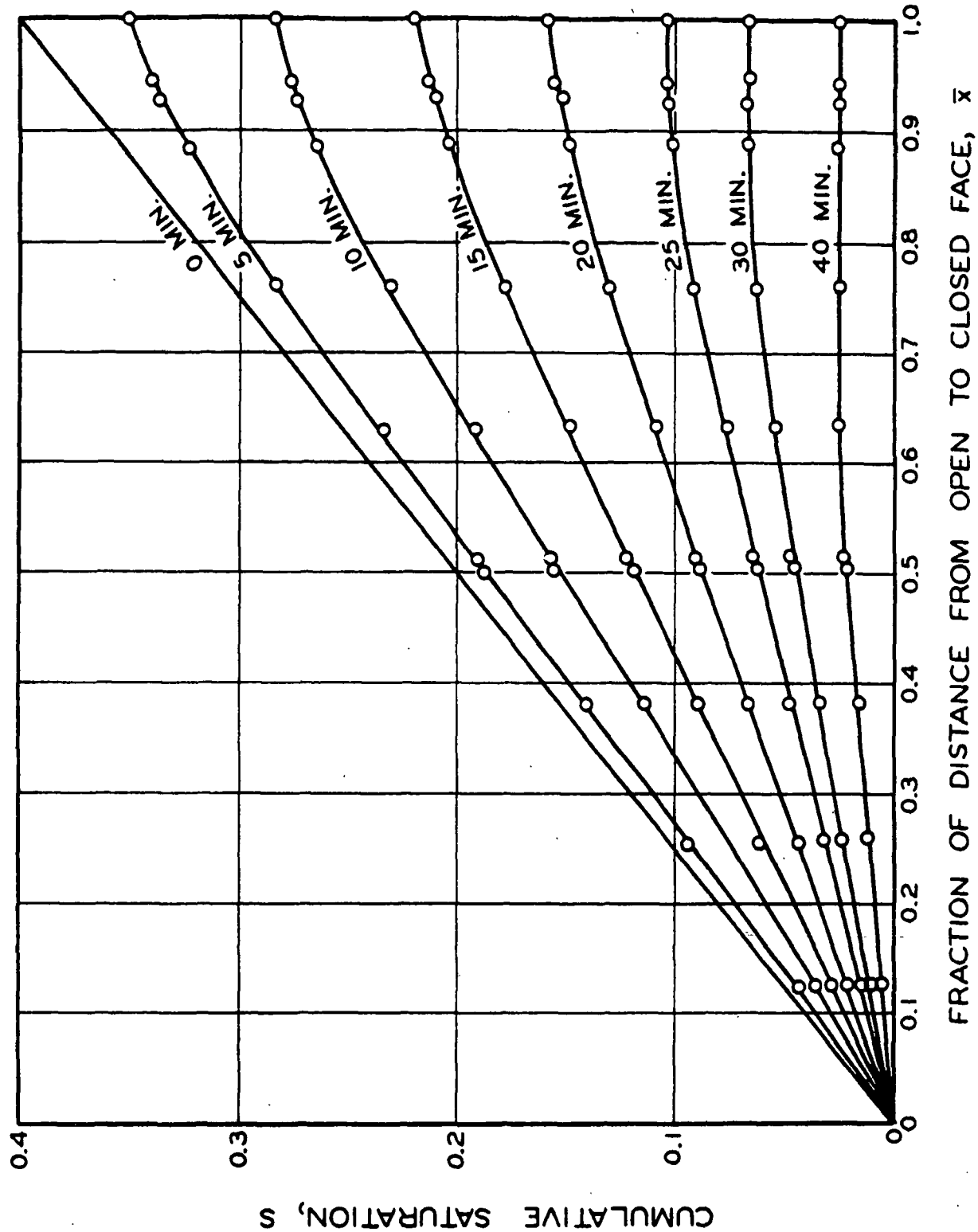

Figure 21. Cumulative Saturation Curves

which the function represents. Thus, by measuring the slopes at several positions along the curves of Fig. 21, the final moisture distribution as a function of drying time and of position in the bed can be constructed. These curves are presented in a later section.

In summary, the basic technique developed by Dreshfield for studying the drying phenomenon has been significantly improved in the direction of obtaining more precise data. The primary difficulty that now faces investigation in this area is to prepare fiber beds which are identical to each other in all characteristics which affect the precise manner in which they dry. This thesis is not able to offer a complete solution to this latter problem. As a result, portions of the data cannot be considered sufficiently precise to allow extensive quantitative analysis. However, in the early stages the description of drying is believed to be quite precise and the over-all description presents a good qualitative picture.

CAPILLARY PRESSURE STUDY

The application of a negative pressure to the water in a saturated pore system will cause the water to be drawn from the system. This will continue until the capillary pressure as defined by Equation (2) (see page 5) exactly opposes the applied negative pressure. At this time all effective pores of radius r or smaller will remain filled with water while pores larger than r will be empty.

The capillary pressure technique described in an earlier section utilizes this concept to evaluate the capillary pressure exerted by the water in the bed at any particular degree of saturation and to convert this to an effective pore distribution.

Figure 22 is used to illustrate the method of calculation involved in developing the data from capillary pressure measurements. The original data for all pertinent capillary pressure work are referred to in Appendix IV.

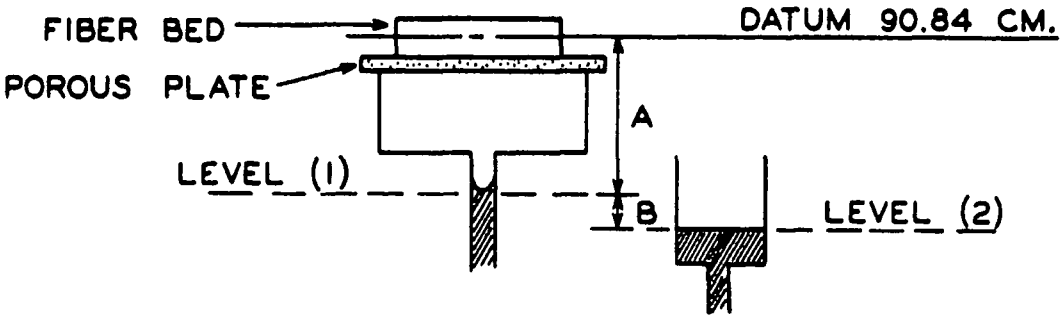

Figure 22. Capillary Pressure Measurements

The basic data, recorded in columns (a) and (b) of Table V, give the elevation by cathetometer reading of the mercury-water interface in the precision bore tube [level (1)] and the mercury level in the reservoir [level (2)].

The negative pressure exerted on the water in the bed is dependent upon the exact elevation of this water. The selection of the datum plane to intersect the center of the bed results in the calculation of an average pressure. For negative pressures of more than 1 cm. of Hg the deviation within the bed from the average value is completely negligible. The elevation of the datum plane (90.84 cm.) is obtained by adding half the known thickness of the bed to the elevation of the top of the porous plate.

The negative pressure exerted on the water in the bed consists of A cm. of water plus B cm. of Hg. These values are recorded in columns (c) and (d). Converting the A value to cm. Hg and adding to B gives the capillary pressure exerted on the water in the bed. This is given in column (e).

TABLE V

DEVELOPMENT OF CAPILLARY PRESSURE DATA, P-106

(a) Level (1), cm.	(b) Level (2), cm.	(c) A, cm. H_2O	(d) B, cm. Hg	(e) Capillary Pressure, cm. Hg	(f) Cumulative Water from Plate & Bed, g.	(g) Cumulative Water from Plate, g.	(h) Saturation
68.30	68.90	-22.54	+0.60	-1.06	-	-	-
67.52	66.31	-23.32	-1.21	-2.95	1.2	0.8	0.99
50.78	49.40	-40.06	-1.38	-4.32	27.1	1.2	0.65
24.67	24.06	-66.17	-0.61	-5.48	66.2	1.6	0.14
20.28	19.12	-70.56	-1.16	-6.35	73.0	1.8	0.05
18.71	16.57	-72.13	-2.14	-7.44	75.4	2.2	0.02
17.65	12.82	-73.19	-4.83	-10.21	77.0	3.0	0.01
16.10	4.15	-74.74	-11.95	-17.44	79.4	5.7	0.01

The precision bore tube was calibrated and found to have a volume of 1.551 cm.^{3} per cm. of length. This compares well with the value of 1.550 calculated from the manufacturer's specification. The successive elevations of the mercury-water interface [column (a)], therefore, give a means of calculating the cumulative amount of water withdrawn from both the fiber bed and the porous plate. These values are tabulated in column (f).

The water that is drawn from the plate as a function of capillary pressure is determined by a separate experiment in which only the plate is included in the apparatus. The results of such a calibration are shown graphically in Fig. 23. At the particular capillary pressures recorded in column (e) the cumulative water removed from the plate can be determined from the calibration curve. These values are presented in column (g). The difference between columns (f) and (g) represents the water withdrawn from the fiber bed.

It is not possible to remove all the water from the fiber bed by the application of a negative pressure. Discrete, isolated pockets of water eventually form in the fiber bed as the continuous water network breaks down. This residual water was found by weight measurement to be 0.92 gram.

From a knowledge of the geometric volume of the glass fiber test bed together with the dry fiber weight and density, the weight of water contained in the completely saturated bed can be calculated. This value is 75.4 grams.

The total cumulative water plus the residual saturation gives a figure of 74.9 grams. However, it can be seen that the zero point for these calculations occurs at a capillary pressure of 1.06 cm. Hg. The difference of

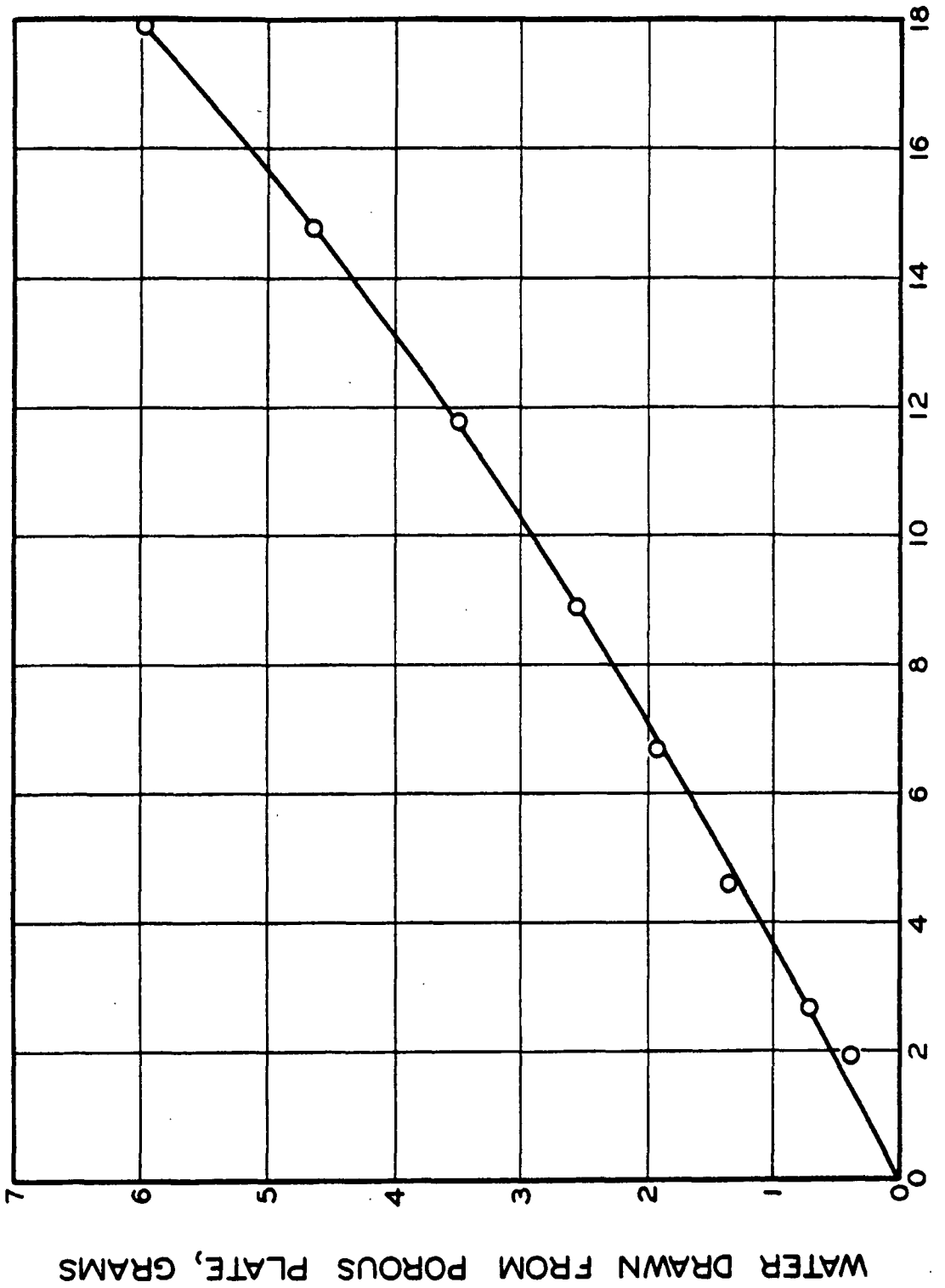

Figure 23. Porous Plate Calibration Curve

0.5 gram between the calculated and theoretical water content at complete saturation is partially due to this initial pressure. The error, in any event, is still less than one per cent.

By adding this error to the cumulative water content of the bed and subtracting this value from 75.4, the water retained in the bed is estimated at various negative pressures. This value divided by 75.4 is, by definition, the degree of saturation of the bed. These values are given in the final column.

The degree of saturation as a function of capillary pressure can be established by plotting the figures of columns (e) and (h). This plot is introduced in a later section. The reproducibility of this capillary pressure curve from separate tests on different beds was excellent.

The application of Equation (2) assumes the presence of circular capillaries. A more realistic view introduces the hydraulic radius,

$$m = \frac{\gamma}{\Delta P}. \qquad (4)$$

For porous media it is common to consider the hydraulic radius as expressing a ratio of porosity to specific surface per unit volume of media. Carman (16) gives evidence to show that Equation (4), while not rigorous, can be successfully applied to capillary rise studies with granular media. Equation (4), therefore, appears to be the most meaningful relation between capillary pressure and effective pore size.

The surface tension of the water used in capillary pressure studies varied only slightly. The average value obtained with a Cenco-De Nouy

interfacial tensiometer (serial no. 240) for water at 25°C. was 75.8 dynes/cm. Applying the ring correction factor of 0.94 gives the actual surface tension of the water as 71.2 dynes/cm.

Using Equation (4) together with the measured value of the surface tension, γ, the saturation-capillary pressure relationship can be transformed into a saturation-effective pore size relationship. This is a representation of the cumulative pore-size distribution of the glass fiber bed and is presented in a later section.

RESULTS AND DISCUSSION

INTRODUCTION

The hot surface drying rate as a function of drying time for the glass fiber bed of this study is presented in Fig. 24. The general conformity to the characteristic drying rate curve, discussed in the introduction to this thesis, is apparent. In addition, the observation of Ulmanen for pulp beds that the so-called constant rate period is in fact a slowly changing rate apparently applies with more emphasis to glass fiber beds. This question of the so-called constant rate period will be clarified later.

Moisture distributions in the glass fiber bed at various drying times are shown in Fig. 25. These distributions are essentially similar to those determined by Ulmanen (see Fig. 26) for thick pulp beds. Notable differences in detail are that (1) the gradient toward the hot surface of the glass fiber bed is substantially greater and toward the open face substantially less than that of the pulp bed; (2) a slight moisture gradient is detectable in the plateau region of moisture content in the central portion of the glass fiber bed whereas no apparent gradient exists in this region of the pulp bed; and (3) after a certain period of drying, liquid water completely disappears from the hot surface-glass fiber bed interface whereas for the pulp bed liquid water persists at the hot surface interface for almost the entire drying period.

The temperatures at various levels in the glass fiber bed as a function of drying time are shown in Fig. 27. It can be seen that no adjustment has been made to the data up to 15-20 minutes of drying. The degree of subsequent adjustment can be judged by comparing Fig. 27 with the basic data

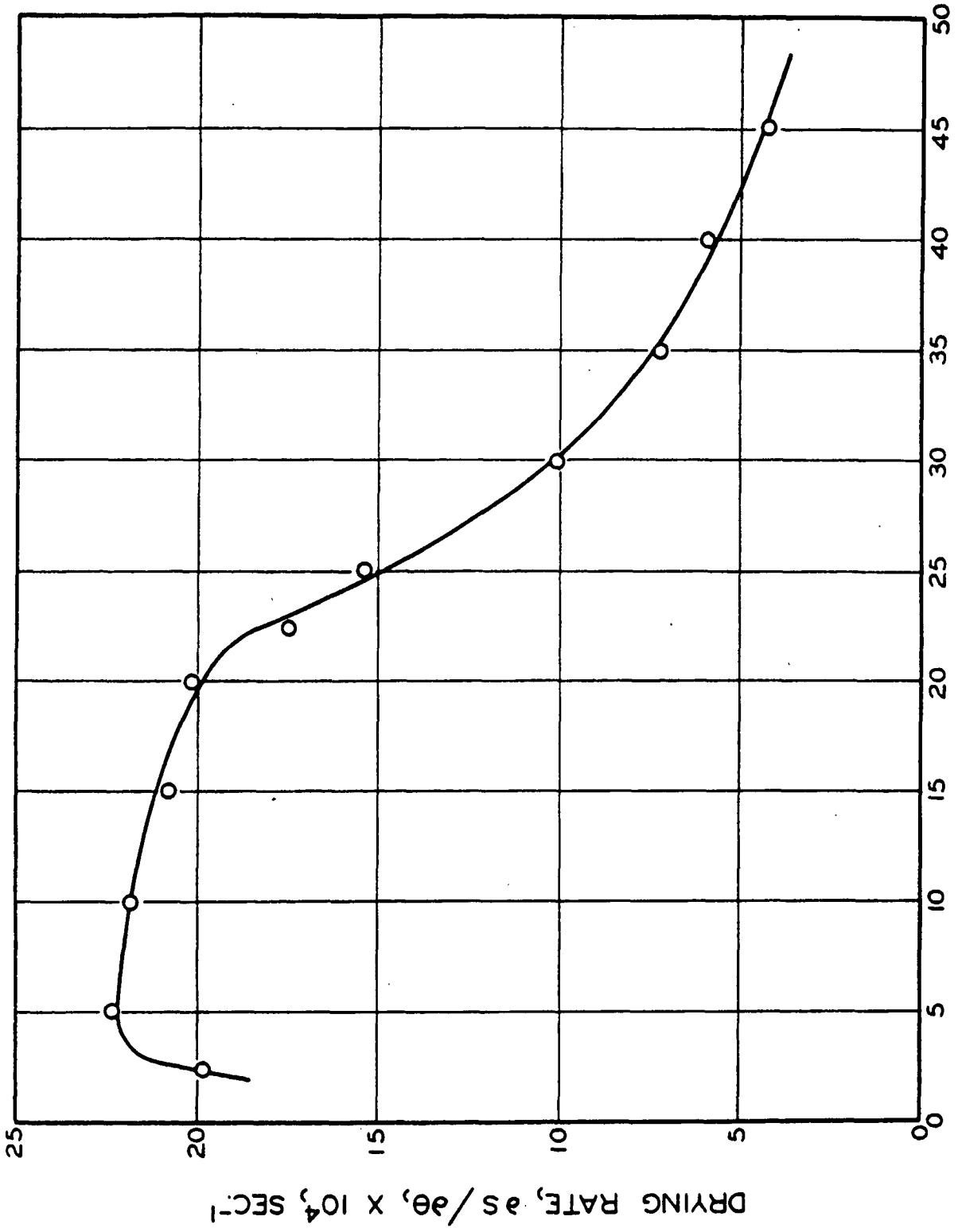

Figure 24. Over-all Drying Rate

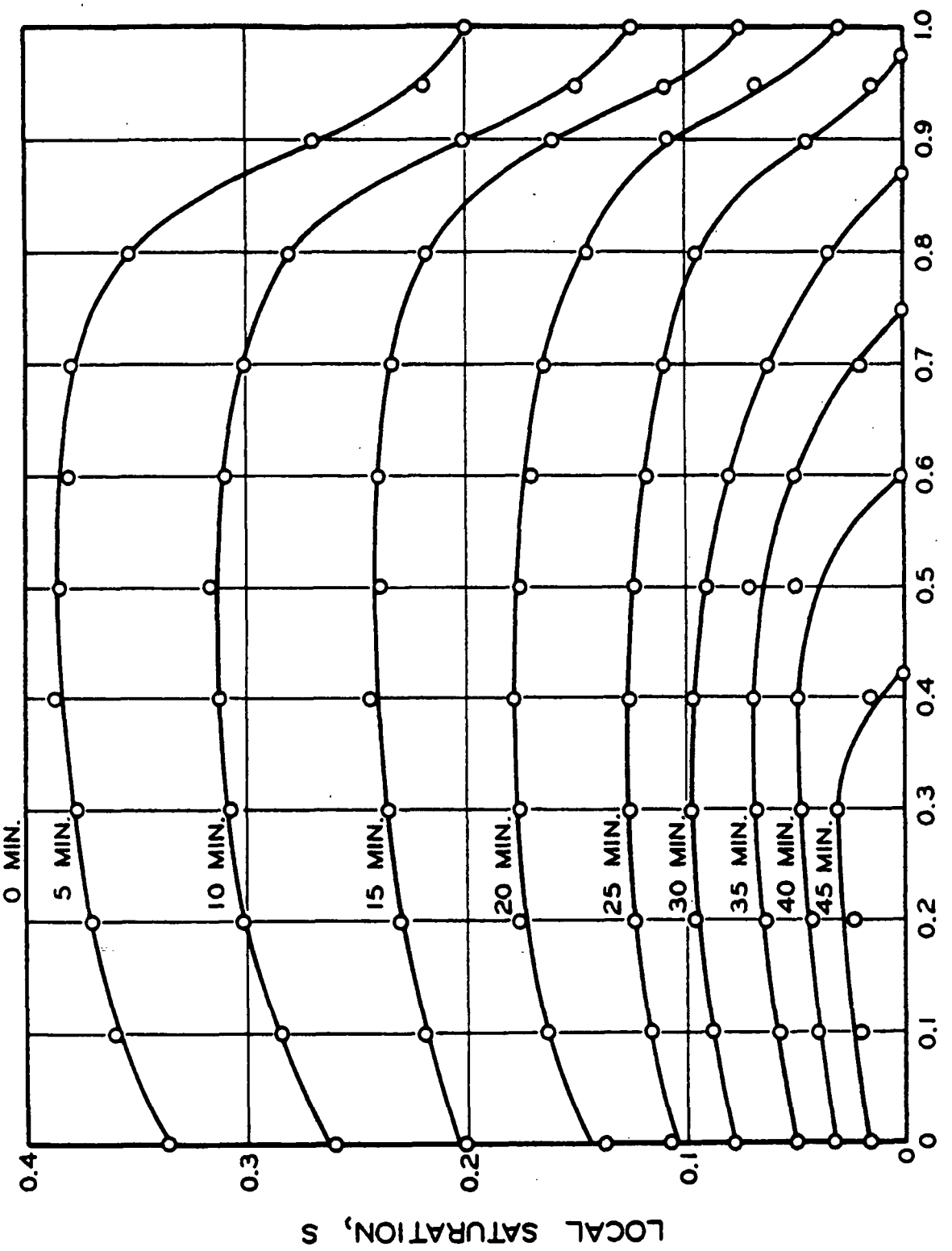

Figure 25. Moisture Distribution Curves

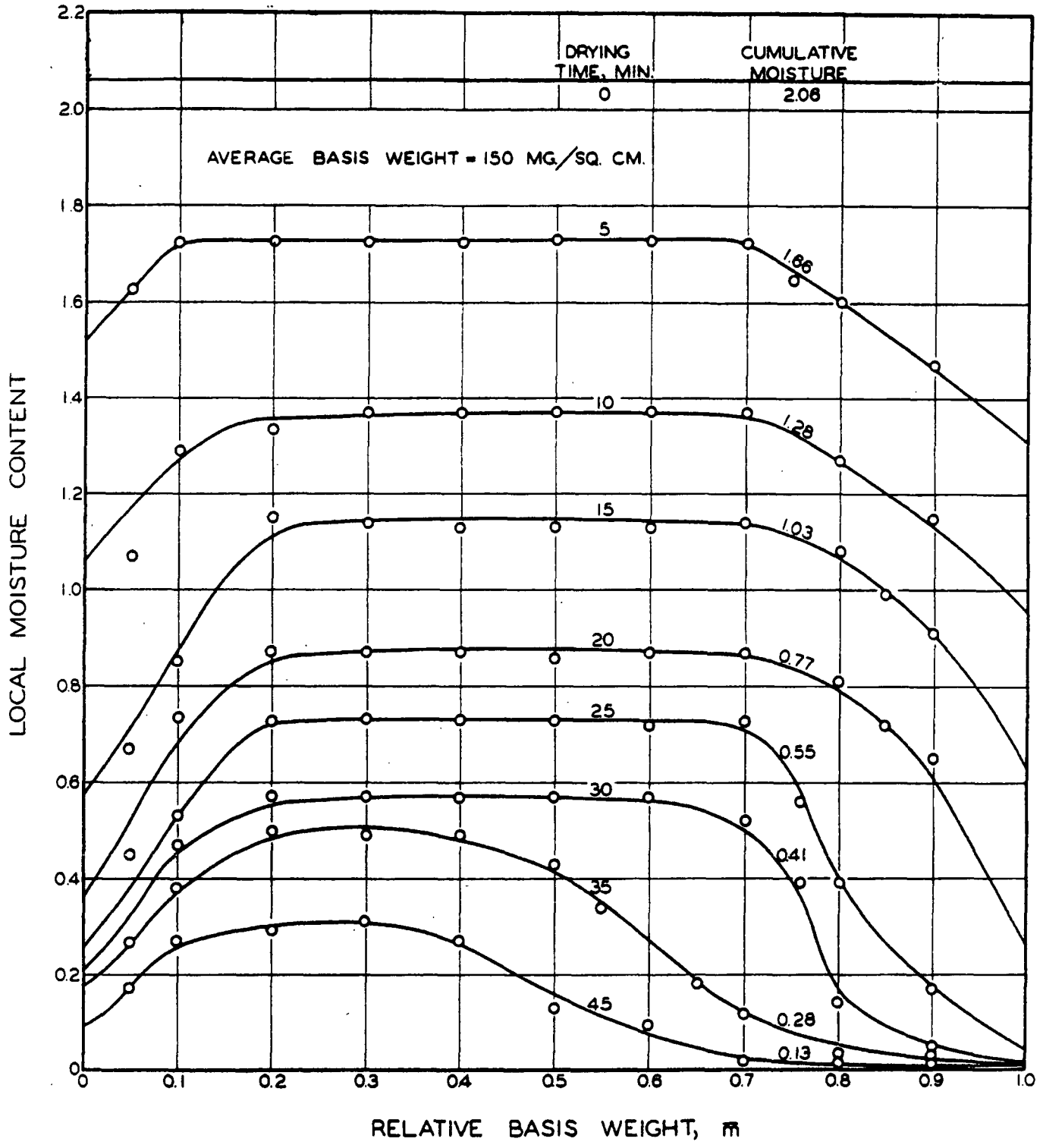

Figure 26. Local Moisture Distribution in a Thick Sheet (Study of Han and Ulmanen)

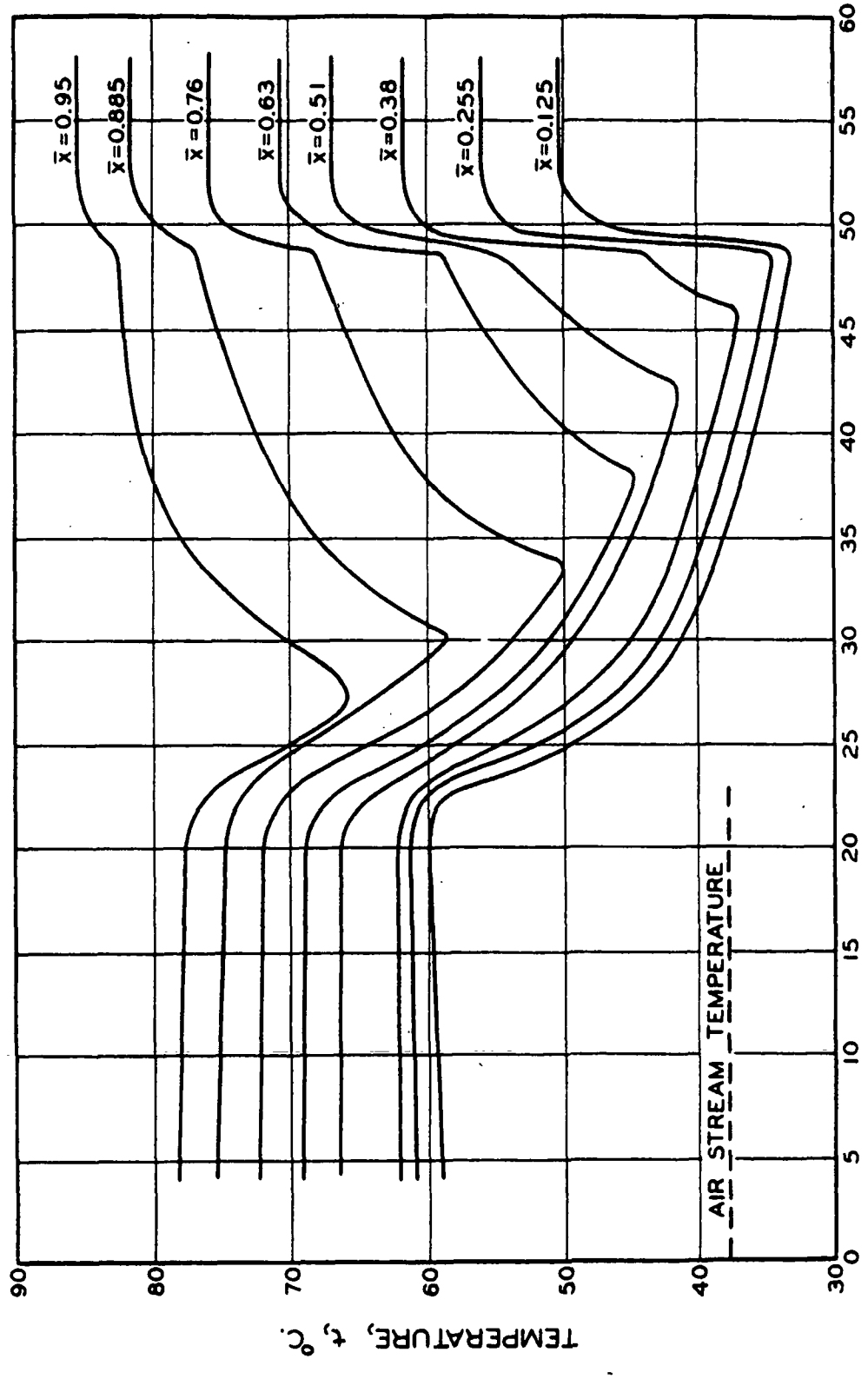

Figure 27. Temperature Curves

given in Fig. 16. It can be seen that after an initial rapid rise, the temperature at any position in the bed remains relatively constant for about 22 1/2 minutes of drying. However, it is not absolutely constant. A tendency can be noted for the temperature to decrease slightly over this period at positions nearer the hot surface, and to increase slightly at positions nearer the open face.

After 22 1/2 minutes, the temperatures at all levels in the bed decrease rapidly from the relatively constant values prevalent during the earlier period of drying. From Fig. 24 it can be seen that this temperature transition point corresponds to the point where the approximately constant-rate period is superceded by the so-called falling-rate period. In addition, from Fig. 25 it is apparent that this transition point coincides with the point where liquid water completely disappears from the hot surface-glass fiber bed interface.

At a given level in the bed, the temperature continues to fall until after a certain period of drying when the temperature rises sharply and continues to increase. This point corresponds (see Fig. 25) with the point where liquid water recedes from the hot surface past the particular level under consideration.

The temperature then continues to increase but at a continually decreasing rate until a second sharp rise is experienced after which the temperature reaches a constant value. This second rapid increase in temperature has been found to correspond to the end of the drying period, i.e., the time when all liquid water has been evaporated from the bed. A short period follows during which equilibrium conditions of heat transfer through the fiber bed are established.

This picture of the temperature conditions in a glass fiber bed during a hot surface drying operation is in many ways similar to that presented by Ulmanen (see Fig. 28). Notable differences are that (1) the clear association of temperature transition points with the reduction of local saturation (water content) to zero, apparent for the glass fiber system, is not in fact true for the pulp system where local saturation presumably never falls to zero; and (2) the decrease in the temperature within the glass fiber bed after the initial drying period is much greater than the similar decrease shown for a pulp bed, e.g., the temperature near the surface of the glass fiber bed falls below the temperature of the air stream while for the pulp bed the temperature near the surface remains substantially above this value.

The significance of these observations and particularly of the similarities and discrepancies between data for the glass fiber system of this study and the pulp system of Ulmanen's investigation will become apparent as this analysis continues..

On the basis of the above observations, two distinct periods of drying can be distinguished for the glass fiber system. During the first period, liquid water is present at the hot surface interface. This period appears to correspond to the classic "constant rate" period. The second period is characterized by the complete absence of liquid water from the hot surface interface and apparently corresponds to the so-called "falling rate" period. Although the implied distinction between the terms constant- and falling-rate periods of drying is somewhat misleading when applied to the glass fiber system of this study, these terms will be used in subsequent discussion to distinguish the two periods of drying defined above.

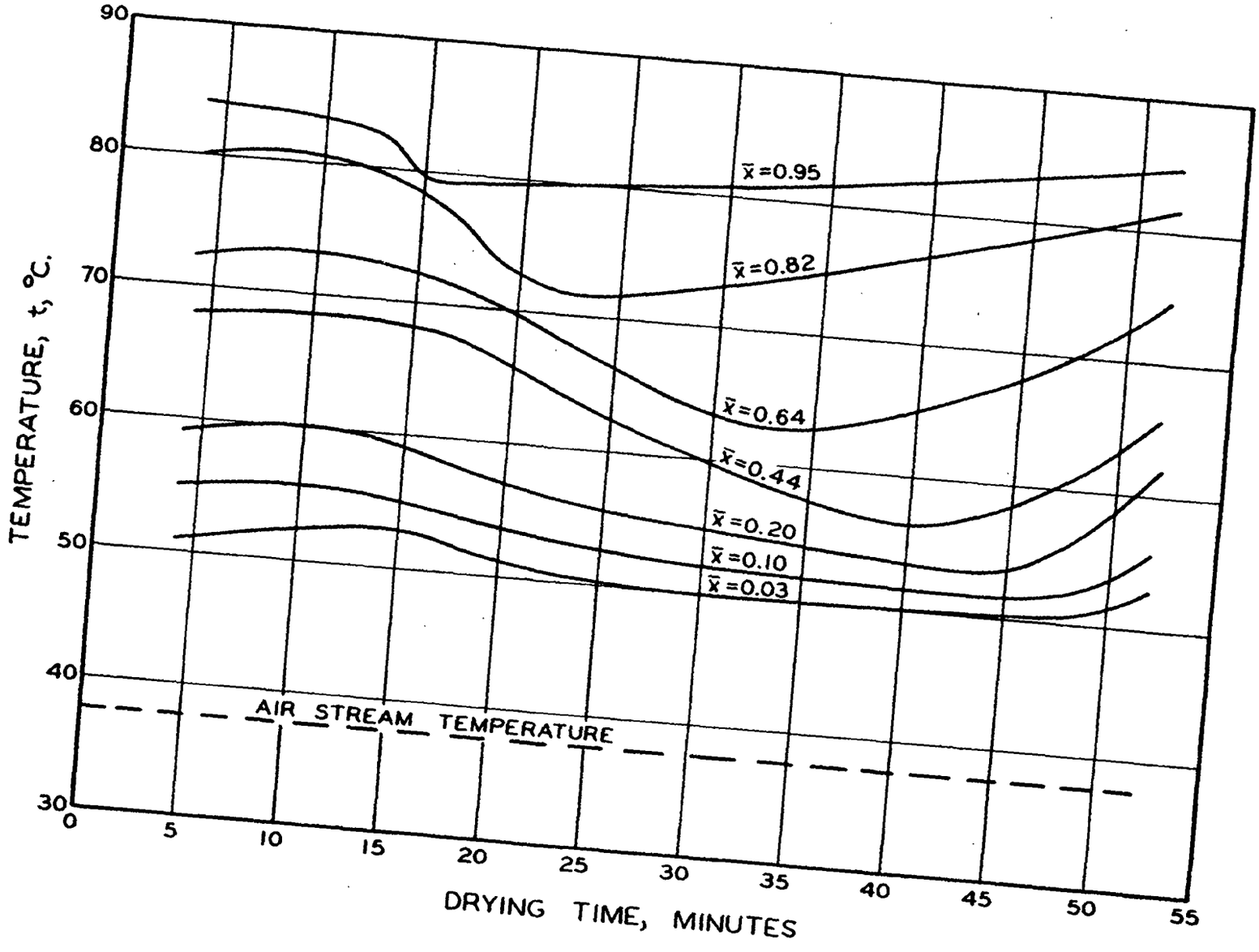

Figure 28. Temperature Curves for Pulp Bed
Ulmanen's Study

MATHEMATICAL MODEL

The interpretation of experimental data is greatly aided if the data can be handled through analogy with a realistic mathematical model. This is particularly true where a complex interaction of factors makes accurate qualitative interpretation extremely difficult. It is the purpose of the following section to introduce a mathematical model which can be realistically used to define the mass and energy interchanges that can occur during the hot surface drying of a glass fiber bed.

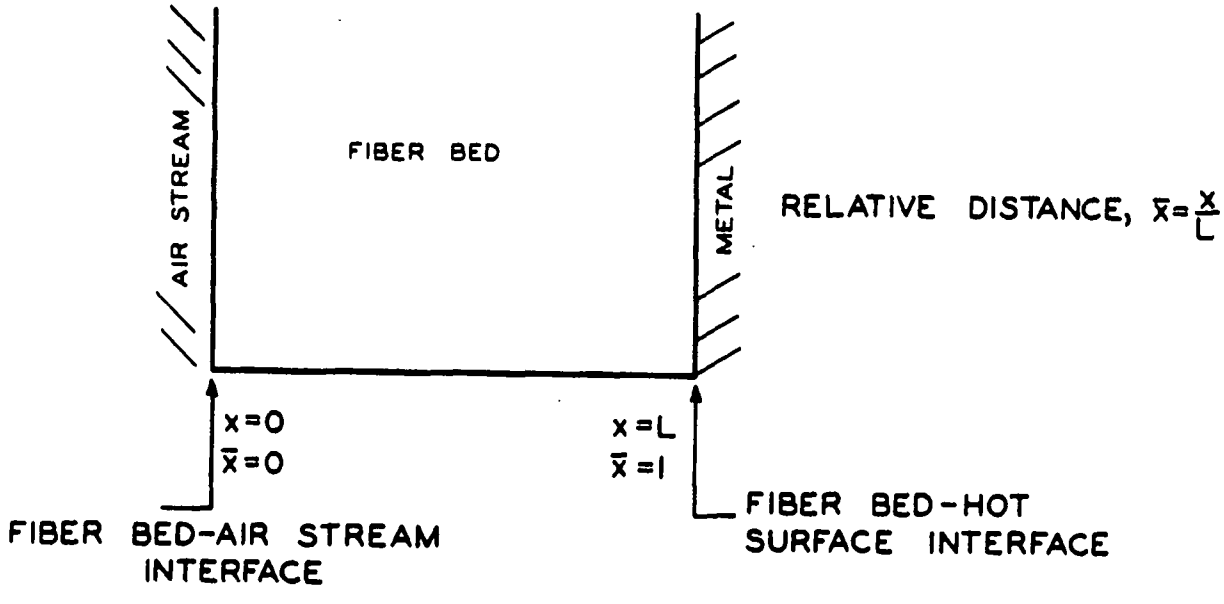

The above sketch describes the system which is to be considered. From this sketch it is apparent that the over-all system can be thought of as a combination of three separate and essentially homogeneous systems and two boundary layers; viz. homogeneous metal, a boundary layer which is described as the fiber bed-hot surface interface or simply the hot surface interface, the fiber bed itself which can be thought of as a homogeneous system even though point to point variation will occur in moisture content,

a boundary layer which is described as the fiber bed-air stream interface or simply the air interface, and finally the air stream itself.

For the metal system we are only concerned with energy flow or more specifically heat flux. This heat flux will be equal to the product of the thermal conductivity of the metal and the temperature gradient in the metal at any point. The heat flow to the hot surface interface can be defined as the heat flux in the metal at a point infinitely close to the interface and is hence the product of the thermal conductivity of the metal and the temperature gradient in the metal immediately adjacent to the hot surface interface.

As discussed earlier in this thesis it is a well-documented fact that liquid water flows to the hot surface interface and that evaporation of water occurs at this interface. Therefore, it is proper to consider not only energy but also mass interchanges at the hot surface interface. A material and energy balance for the hot surface interface will yield boundary equations which define heat and mass transfer at the hot surface interface.

A consideration of what occurs at any point within the fiber bed during hot surface drying must account for both liquid and vapor flow, a local interchange between the liquid and gaseous state, and a heat flow. A material and energy balance at any internal point in the fiber bed which accounts in a generalized way for the above items can be used to define heat and mass transfer at any point within the fiber bed. It is important to recognize that such an equation will apply to a point within the fiber bed infinitely close to either the hot surface or air interface but it cannot be applied to describe heat and mass transfer at these interfaces.

A material and energy balance for the air interface will produce additional boundary equations which define heat and mass transfer at this interface.

Therefore, it can be seen that the proper mathematical definition of heat and mass transfer for a fiber bed during hot surface drying requires the derivation of boundary equations to account for interchanges at the two interfaces, and a generalized equation to apply to all points between but not including the interfaces.

GENERALIZED EQUATION

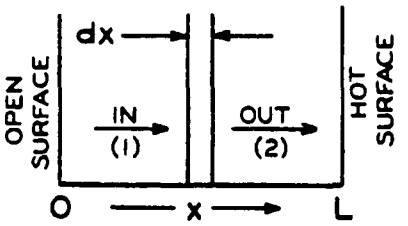

The above diagram illustrates the sign convention which has been adopted, i.e., distance, x, increases in the positive direction.

At any particular time the element, dx, will contain the solid substance of the porous media (fiber), liquid water, and a gaseous mixture of air and water vapor. In terms of the previously defined concepts of porosity, e, and saturation, s, we can write:

$$a_F = (1-e) \tag{5}$$

$$a_L = se \tag{6}$$

$$a_G = (1-s)_e \tag{7}$$

where a_F, a_L, and a_G are the respective fractions of the total geometric cross-sectional area occupied by fiber, liquid water, and the gaseous mixture of water vapor and air.

Material Balance

The basis for the material balance is unit time and unit area. Unless liquid water is entirely absent from the element dx, the contribution of water vapor and air to a material balance are negligible. Assuming no shrinkage of the fiber bed, the solid fraction in the element, dx, remains constant. Thus, the material balance can be qualitatively described by:

> accumulation = water into element - water out of element - water evaporated from element.

Liquid flow in a porous media during drying is in response to a capillary pressure gradient. Experience indicates that the flow in the system will be laminar. Therefore, the d'Arcy equation can be realistically applied to define the flow rate into and from the element dx.

Flow rate in:

$$dM_1/d\theta = - \frac{K_c \rho_L}{\mu} \frac{\partial P_c}{\partial x} \qquad (8)$$

where $dM_1/d\theta$ is the mass flow rate of liquid water into the element dx per unit geometric area; K_c is the permeability; μ is the viscosity of water; $\partial P_c/\partial x$ is the capillary pressure gradient.

Flow rate out:

$$\frac{dM_2}{d\theta} = - \frac{\rho_L}{\mu} \left[\left(K_c + \frac{\partial K_c}{\partial x} dx \right) \left(\frac{\partial P_c}{\partial x} + \frac{\partial \left(\frac{\partial P_c}{\partial x} \right)}{\partial x} dx \right) \right] \qquad (9)$$

where the porosity is defined as a constant, and the viscosity and density are assumed to remain essentially constant across the element dx.

The accumulation of water in the element dx is given by Equation (10):

$$\frac{dM}{d\theta} = e\,\rho_L \frac{\partial s}{\partial \theta}\,dx \qquad (10)$$

where $dM/d\theta$ is the rate of accumulation, and $\partial s/\partial\theta$ is the rate of change of saturation in element dx.

By defining $\partial s_w/\partial\theta$ as the rate of change of saturation in the element, dx, produced by evaporation:

$$\frac{dW}{d\theta} = e\,\rho_L \frac{\partial s_w}{\partial \theta}\,dx \qquad (11)$$

where $dW/d\theta$ is the rate of evaporation from the element, dx.

In terms of the material balance:

$$\frac{dM}{d\theta} = \left(\frac{dM_1}{d\theta} - \frac{dM_2}{d\theta}\right) - \frac{dW}{d\theta}$$

Applying Equations (8) to (11) to the above expression, neglecting terms in which the derivative appears to a higher power, and simplifying, gives:

$$e\,\frac{\partial s}{\partial \theta} = \frac{1}{\mu}\left[\frac{\partial P_c}{\partial x}\,\frac{\partial K_c}{\partial x} + K_c \frac{\partial^2 P_c}{\partial x^2}\right] - e\,\frac{\partial s_w}{\partial \theta} \qquad (12)$$

In handling the experimental data it is more convenient to refer to some position in the bed as a fraction of the distance from the open to the closed face,

$$\text{i.e.,} \quad \bar{x} = x/L \qquad (13)$$

where $\bar{x}$ is the fraction represented by distance x from the open face divided by total thickness L.

It follows that:

$$dx = L d\bar{x} \qquad (14)$$

$$\text{and} \quad d^2x = L^2 d\bar{x}^2 \tag{15}$$

Substituting (14) and (15) into Equation (12) gives:

$$e\frac{\partial s}{\partial \theta} = \frac{1}{\mu L^2}\left[\frac{\partial P_c}{\partial \bar{x}}\frac{\partial K_c}{\partial \bar{x}} + K_c\frac{\partial^2 P_c}{\partial \bar{x}^2}\right] - e\frac{\partial s_w}{\partial \theta} \tag{16}$$

Energy Balance

For the purposes of this analysis the energy or heat content (enthalpy) of the system is defined as zero at 0°C. The energy balance across the element, dx, can be qualitatively depicted as:

Heat in:

1) Heat transferred into the element via conduction, convection, radiation.

2) Heat content of water which flows into the element.

3) Heat content of air/water vapor which flows into the element.

Heat out:

1) Heat transferred out of the element via conduction, convection, radiation.

2) Heat content of water which flows out of the element.

3) Heat content of air/water vapor which flows out of the element.

Accumulation of heat:

1) Heat absorbed by solid fiber in the element.

2) Heat absorbed by liquid water in the element.

3) Heat absorbed by air/water vapor in the element.

Heat in - Heat out = Accumulation

The basis for the energy balance is unit time and unit area.

The rate of heat transfer by conduction, convection and radiation into the element,

$$\frac{dq_1}{d\theta} = -k_a \frac{\partial t}{\partial x} \tag{17}$$

where $dq_1/d\theta$ is the rate of heat transfer into the element; k_a is the apparent thermal conductivity; and $\partial t/\partial x$ is the temperature gradient.

Heat transfer from the element,

$$\frac{dq_2}{d\theta} = -\left(k_a + \frac{\partial k_a}{\partial x} dx\right)\left(\frac{\partial t}{\partial x} + \frac{\partial\left(\frac{\partial t}{\partial x}\right)}{\partial x} dx\right) \tag{18}$$

The heat content of an incremental mass of liquid water is by definition:

$$dh_L = dMC_L t \tag{19}$$

where dh_L is the heat content of an incremental mass of liquid water, dM; C_L is the specific heat of water; and t is the temperature of the water above 0°C. (i.e., numerically equivalent to the actual temperature).

Combining (19) with Equation (8) gives the heat content of the water flowing into the element.

$$\frac{dh_{L1}}{d\theta} = -\frac{K_c \rho_L C_L}{\mu} t \frac{\partial P_c}{\partial x} \tag{20}$$

The heat content of the water flowing out of the element is

$$\frac{dh_{L2}}{d\theta} = -\frac{\rho_L C_L}{\mu}\left(K_c + \frac{\partial K_c}{\partial x} dx\right)\left(t + \frac{\partial t}{\partial x} dx\right)\left(\frac{\partial P_c}{\partial x} + \frac{\partial\left[\frac{\partial P_c}{\partial x}\right]}{\partial x} dx\right) \tag{21}$$

where the specific heat, C_{L2} and the density, ρ_L, are assumed to remain constant across the element, dx.

The water vapor which diffuses out of the element, dx, is approximately equal to the water vapor which diffuses into the element plus the water vapor produced by evaporation from the element. This assumes that the accumulation or depletion of water vapor in the element is not great.

Since the specific heat of water vapor is small (compared to water) it is a reasonable approximation to assume that the difference between the heat content of the water vapor which diffuses into the element and that which diffuses out is the heat content of the water vapor which is produced by evaporation from the element dx. This can be written:

$$\frac{dh_v}{d\theta} = e\rho_L \frac{\partial s_w}{\partial \theta} (\lambda + C_L t)\, dx \qquad (22)$$

where dh_v is the heat content associated with the water vapor produced by evaporation from the element, dx; $\partial s_w/\partial\theta$ is the rate of change of saturation in element, dx, which can be attributed to evaporation from the element; and λ is the latent heat of vaporization at the temperature, t, existing in the element, dx.

The initial heat content of the element, dx,

$$h_i = \left[(1-e)\rho_F C_F + es\rho_L C_L\right] t\, dx \qquad (23)$$

where the heat content of the air and water vapor has been neglected.

The final heat content,

$$h_F = \left[(1-e)\rho_F C_F + e(s + \frac{\partial s}{\partial \theta} d\theta)\rho_L C_L\right]\left[t + \frac{\partial t}{\partial \theta} d\theta\right] dx \qquad (24)$$

Hence, the rate of charge of sensible heat,

$$\frac{dh}{d\theta} = \frac{h_F - h_i}{d\theta} = et\rho_L C_L \frac{\partial s}{\partial \theta} dx + \frac{\partial t}{\partial \theta}\left[(1-e)\rho_F C_F + es\rho_L C_L\right] dx \qquad (25)$$

In terms of the energy balance:

$$\frac{dh}{d\theta} = \left(\frac{dq_1}{d\theta} - \frac{dq_2}{d\theta}\right) + \left(\frac{dh_{L1}}{d\theta} - \frac{dh_{L2}}{d\theta}\right) - \frac{dh_v}{d\theta}$$

Substituting into the above expression from Equations (17), (18), (20), (21), (22), and (23), discarding terms in which the derivative appears to a higher power, and simplifying:

$$\left[k_a \frac{\partial^2 t}{\partial x^2} + \frac{\partial k_a}{\partial x}\frac{\partial t}{\partial x}\right] + \frac{\rho_L C_L t}{\mu}\left[\frac{\partial P_c}{\partial x}\frac{\partial K_c}{\partial x} + K_c \frac{\partial^2 P_c}{\partial x^2}\right]$$

$$+ \frac{K_c \rho_L C_L}{\mu}\frac{\partial t}{\partial x}\frac{\partial P_c}{\partial x} - e\rho_L \frac{\partial s_w}{\partial \theta}(\lambda + C_L t)$$

$$= et\rho_L C_L \frac{\partial s}{\partial \theta} + \frac{\partial t}{\partial \theta}\left[(1-e)\rho_F C_F + es\rho_L C_L\right] \qquad (26)$$

Substituting from Equation (12) for the terms in the underscored bracket of Equation (26) and simplifying:

$$k_a \frac{\partial^2 t}{\partial x^2} + \frac{\partial k_a}{\partial x}\frac{\partial t}{\partial x} + \frac{K_c \rho_L C_L}{\mu}\frac{\partial t}{\partial x}\frac{\partial P_c}{\partial x}$$

$$- e\rho_L \lambda \frac{\partial s_w}{\partial \theta} = \frac{\partial t}{\partial \theta}\left[(1-e)\rho_F C_F + es\rho_L C_L\right] \qquad (27)$$

Substituting from Equations (14) and (15) gives the final form:

$$\frac{1}{L^2}\left[k_a \frac{\partial^2 t}{\partial \bar{x}^2} + \frac{\partial k_a}{\partial \bar{x}}\frac{\partial t}{\partial \bar{x}}\right] + \frac{K_c \rho_L C_L}{\mu L^2}\frac{\partial t}{\partial \bar{x}}\frac{\partial P_c}{\partial \bar{x}}$$

$$- e\rho_L \lambda \frac{\partial s_w}{\partial \theta} = \frac{\partial t}{\partial \theta}\left[(1-e)\rho_F C_F + es\rho_L C_L\right] \qquad (28)$$

This mathematical relation has been derived to apply to a glass fiber bed. It is of interest to consider the possible application of this relation to the paper system.

The first difficulty encountered is that paper shrinks during drying. This means that the porosity is no longer a constant. However, this objection can be overcome by introducing the porosity as a variable into the derivation of the above equation.

The second and more formidable difficulty is that the liquid saturation at any point is defined not only by the water present in interfiber spaces, but also by water present in the fiber lumen and by water physically bound to the fiber. These different components will respond in a different manner to capillary forces and so the definition of liquid flow utilized in the above derivation cannot be directly applied to the paper system.

A better understanding of capillary flow in a paper network appears necessary before a reasonable modification can be made to allow the above equation to be applied to the drying of paper.

HOT SURFACE INTERFACE BOUNDARY EQUATIONS

Conditions at the hot surface interface can be described according to the accompanying sketch:

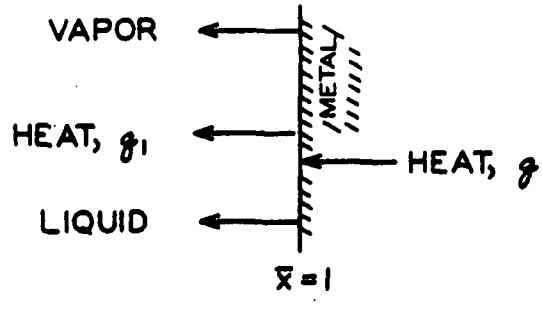

Since we are interested in the interchanges that occur at an interface which can be regarded as infinitely thin, the volume and heat capacities at the interface must be negligible. It is therefore correct to state that the difference between the heat supplied to the interface from the hot surface and the heat transferred into the fiber bed from the interface is used to cause evaporation at the interface. Further, the rate of flow of liquid water to the interface must equal the evaporation.

In terms of the nomenclature previously adopted, these statements can be expressed as:

$$Q = \frac{k_m}{L}\left(\frac{\partial t}{\partial \bar{x}}\right)_{m,\bar{x}=1.0} = \left(\frac{k_a}{L}\frac{\partial t}{\partial \bar{x}}\right)_{\bar{x}=1.0} + \lambda e \rho_L L \left(\frac{\partial S_w}{\partial \theta}\right)_{\bar{x}=1.0} \qquad (29)$$

$$\frac{K_c \rho_L}{L\mu}\left(\frac{\partial P_c}{\partial \bar{x}}\right)_{\bar{x}=1.0} = e\rho_L L \left(\frac{\partial S_w}{\partial \theta}\right)_{\bar{x}=1.0} \qquad (30)$$

where $\underline{Q}$ is the total heat flow delivered to the hot surface interface; $\underline{k}_m$ is the conductivity of the metal; $(\partial \underline{t}/\partial \bar{\underline{x}})_{\underline{m},\bar{\underline{x}}=1.0}$ is the temperature gradient in the metal at the interface; $(\partial \underline{S}_w/\partial\theta)_{\bar{\underline{x}}=1.0}$ is the rate of change of total saturation due to evaporation at the hot surface interface; and all other terms are as defined earlier.

AIR INTERFACE BOUNDARY EQUATIONS

Conditions at the air interface can be described according to the accompanying sketch:

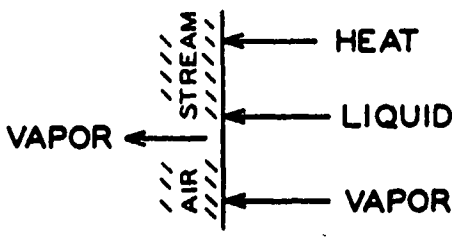

Since we are again concerned with an interface it is proper to neglect volume and heat capacities. If the heat losses to the air stream other than by vapor transport are neglected, then the heat transferred to the air interface is used to cause evaporation at the interface and the rate of liquid flow to the interface equals the rate of evaporation. Mathematically this can be expressed as:

$$\left(\frac{k_a}{L}\frac{\partial t}{\partial \bar{x}}\right)_{\bar{x}=0} = \lambda e c_L L \left(\frac{\partial S_w}{\partial \theta}\right)_{\bar{x}=0} \tag{31}$$

$$\frac{K_c \rho_L}{L\mu}\left(\frac{\partial P_c}{\partial \bar{x}}\right)_{\bar{x}=0} = e\rho_L L \left(\frac{\partial S_w}{\partial \theta}\right)_{\bar{x}=0} \tag{32}$$

where $(\partial \underline{S}_w/\partial \theta)_{\underline{x}=0}$ is the rate of change of total saturation due to evaporation at the air interface; and other terms are as previously defined.

QUALITATIVE TREATMENT

It is one goal of this thesis to demonstrate a quantitative approach to the elucidation of heat and mass transfer during hot surface drying. However, it is felt that a qualitative picture should be developed first since such a picture will be independent of any assumptions which it may be necessary to incorporate into a quantitative treatment. Hence, it is the purpose of this section to elucidate on the basis of the experimental data and the mathematical model an advanced qualitative picture of the hot surface drying mechanism.

Early work on hot surface drying of porous media has confirmed the intuitive concept that the open surface is a site for evaporation of water.

This has led to the descriptive concepts of Sherwood which have been discussed earlier of saturated and unsaturated surface drying supplied by a liquid flow from the interior. Then Dreshfield's study of the hot surface drying operation clearly indicated that evaporation occurs both at the open surface and at the hot surface and that the flow of liquid water in the region of each surface is toward that surface. This evidence is confirmed by several other studies and the moisture distribution data for the glass fiber system is entirely in accord with this concept. It is therefore from this point that the qualitative analysis will proceed.

The manner in which heat and mass transfer interactions occur within the glass fiber bed can be visualized by considering a rearranged form of Equation (28).

$$\frac{\partial s_w}{\partial \theta}(e\rho_L\lambda) = \frac{1}{L^2}\left[k_a \frac{\partial^2 t}{\partial \bar{x}^2} + \frac{\partial k_a}{\partial \bar{x}}\frac{\partial t}{\partial \bar{x}}\right] + \frac{K_c \rho_L C_L}{\mu L^2}\frac{\partial t}{\partial \bar{x}}\frac{\partial P_c}{\partial \bar{x}} - \frac{\partial t}{\partial \theta}\left[(1-e)\rho_F C_F + es\rho_L C_L\right] \tag{28a}$$

Here we can see that the evaporation or condensation at any point in the bed (represented by $\partial s_w/\partial\theta$) is related to a summation of three terms. The first is a heat transfer term, the second a liquid flow term, and the third a heat capacity term. The significance of this equation will be considered for two positions in the bed during the constant rate period; viz. (1) where the liquid flow is toward the air interface, and (2) where the liquid flow is toward the hot surface interface.

In Fig. 29 the temperature distribution and temperature gradient curve for the glass fiber bed at 10 minutes of drying are presented. It is apparent that for any position in the bed both the temperature and the

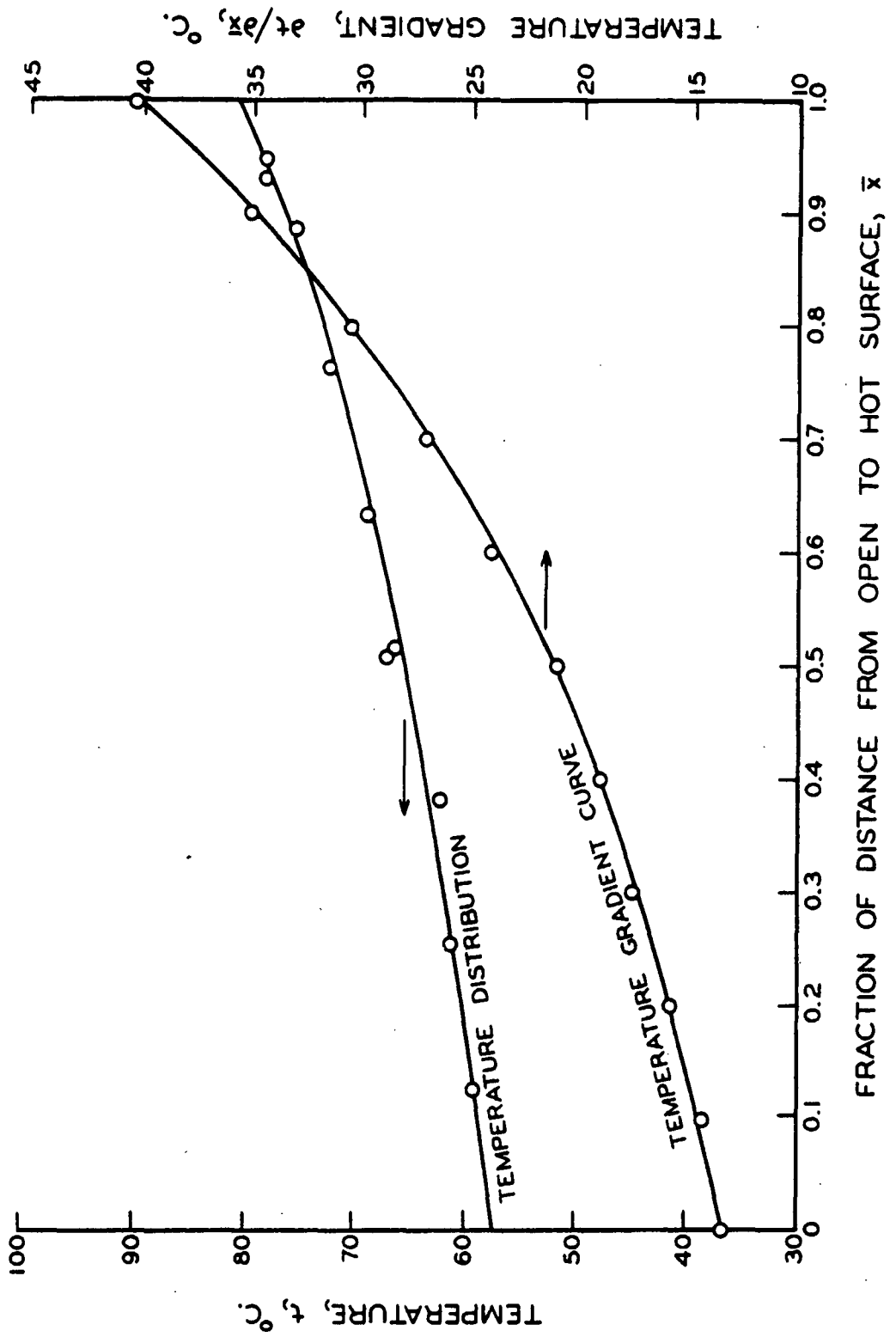

Figure 29. Temperature Distribution and Gradient Curves - Drying Time 10 Min.

temperature gradient increase as $\bar{x}$ increases. Thus, the derivatives $\partial t/\partial \bar{x}$, and $\partial^2 t/\partial \bar{x}^2$ will everywhere have a positive value.

It is generally believed that the apparent thermal conductivity of a porous bed increases as the moisture content increases. Although this has not been rigorously demonstrated experimentally, all available evidence suggests that this is the case and certainly no known evidence contradicts such a view. From Fig. 25 the moisture content can be seen to increase as $\bar{x}$ increases in the region of the open surface and to decrease as $\bar{x}$ increases in the region of the hot surface. Therefore, according to the above reasoning $\partial k_a/\partial \bar{x}$ will be positive near the open surface and negative near the hot surface.

The temperature at any point in the bed remains relatively constant over the constant rate period. Therefore $\partial t/\partial \theta$ will have a value very close to zero.

Thus, it can be seen from the experimental evidence for the constant rate period that in the region near the open surface all the terms on the right hand side of Equation (28a) with the exception of the negligible heat capacity term will be positive. Hence, $\partial s_w/\partial \theta$ will be positive which means that evaporation must be occurring internally in the region near the open surface.

In the region near the hot surface both the liquid flow term and the second part of the heat transfer term become negative. It is a reasonable possibility, therefore, that in this region of the bed, $\partial s_w/\partial \theta$ will become negative indicating that internal condensation is occurring.

Dreshfield on the basis of dye dilution measurements concluded that net condensation occurred at all internal positions during the constant-rate period of the hot surface drying of thin pulp mats. However, his experimental evidence refers only to the two central laminates of a four laminate system, and therefore does not preclude the possibility that internal evaporation was occurring in the air interface laminate. Therefore, although the data clearly support the existence of internal condensation in the central regions and hence by implication the region next to the hot surface, they do not deny the existence of internal evaporation at points near the open surface.

The concept supported by the experimental evidence for a glass fiber bed that internal evaporation occurs near the open surface is thus quite compatible with the evidence supplied by Dreshfield. However, the possibility that no internal condensation occurs at any point in the fiber bed would require the introduction of some fundamental distinction between the two systems which cannot be acknowledged on the basis of the similarity between systems of the moisture distribution and drying rate data. Hence, although the experimental data for the glass fiber bed cannot rigorously demonstrate the existence of internal condensation near the hot surface a consideration of this data relative to that of Dreshfield can be seen to supply a very strong case for the existence of such a phenomenon.

The above analysis indicates that for the constant rate period water which is evaporated at the hot surface interface tends to condense in regions of the glass fiber bed adjacent to the hot surface. In this region, which will be referred to as the zone of condensation, the partial

pressure of the water vapor in the available air spaces must be equal to the saturation partial pressure. However, at some level in the fiber bed the partial pressure of the water vapor must fall below saturation and net evaporation occurs at all subsequent positions to the open face. This region of the bed will be called the zone of evaporation.

Because of the moisture gradient, liquid water tends to flow toward the region adjacent to the hot surface. Since internal condensation occurs in this region during the constant rate period, the decrease in the moisture content of this region must occur by virtue of evaporation at the hot surface interface and transport of the water vapor back through and out of this region.

The transport mechanism suggested by Dreshfield involves the water vapor produced at the hot surface interface in a series of condensation-evaporation cycles. Although the validity of this concept can be neither established nor disputed on the basis of existing data, it appears more reasonable to consider that water vapor produced at the hot surface diffuses away from this surface by virtue of the partial pressure gradient impressed by the temperature gradient, and that a portion of this water vapor condenses in all regions where saturation conditions are exceeded.

At the outset of the falling rate period it has been shown that liquid water disappears from the hot surface interface. Since water vapor can then be no longer supplied by evaporation at the hot surface, internal condensation must cease and the zone of evaporation will expand to include the former zone of condensation.

From this general picture it is clear that for the drying of a glass fiber bed during the constant rate period water vapor produced by evaporation at the hot surface interface diffuses through the zone of condensation to the accompaniment of condensation until it reaches the zone of evaporation. Thereafter, this vapor is supplemented continually by internal evaporation. The vapor which diffuses to the air interface is thus a combination of vapor produced at the hot surface interface and vapor produced by internal evaporation. Evaporation from the air interface then adds a further increment of vapor which together with the vapor from the two other sources diffuses into the air stream. It is the sum of these three effects which result in the over-all drying rate.

In the falling rate period evaporation at the hot surface ceases and so the over-all drying rate is a summation from only two sources; viz. internal evaporation which occurs at all points within the bed, and evaporation from the air interface.

In the quantitative treatment which is to follow, an attempt is made to secure some indication of the relative importance of the three contributions to over-all drying rate. In addition, the importance of various factors on liquid, vapor, and heat flow is estimated. However, before proceeding to this treatment it is of interest in the light of the above qualitative analysis to discuss the mechanism of hot surface drying and the effect of internal structure upon hot surface drying phenomena as implied by a comparison of the data of this study with that of Ulmanen for a pulp bed.

THE MECHANISM OF HOT SURFACE DRYING

The distinctive feature of hot surface drying as a drying operation is that while heat is supplied to one surface of the material water vapor can leave only from the opposite face. This provides a fascinating problem in counter- and concurrent heat, liquid water, and water vapor transfer, the net result of which is a characteristic drying rate curve which for many systems has implied veritable simplicity. The number of studies and body of opinion which support the concept of a truly constant initial hot surface drying rate have already been mentioned. It would appear that this facade masks a considerably more complex process than has hitherto been generally realized.

The over-all drying rates for a pulp bed (Ulmanen's study) and for a glass fiber bed (this study) are compared in Fig. 30. Both curves show that a slowly decreasing drying rate exists during the constant rate period. This has also been noted by King and Newitt (8) for the hot surface drying of glass beads. Since the moisture content at all positions (including both faces) of the fiber beds changes markedly during the constant rate period, and even the temperature changes slightly, it is not surprising that the drying rate also changes. What is of interest is that the changes in rate are sufficiently small to have established the myth of the constant rate period. On the basis of the triple contribution to over-all drying rate a logical explanation can be given for this apparent constancy of drying rate.

Evaporation from the open surface during the constant rate period, assuming relatively constant surface temperature and temperature gradient

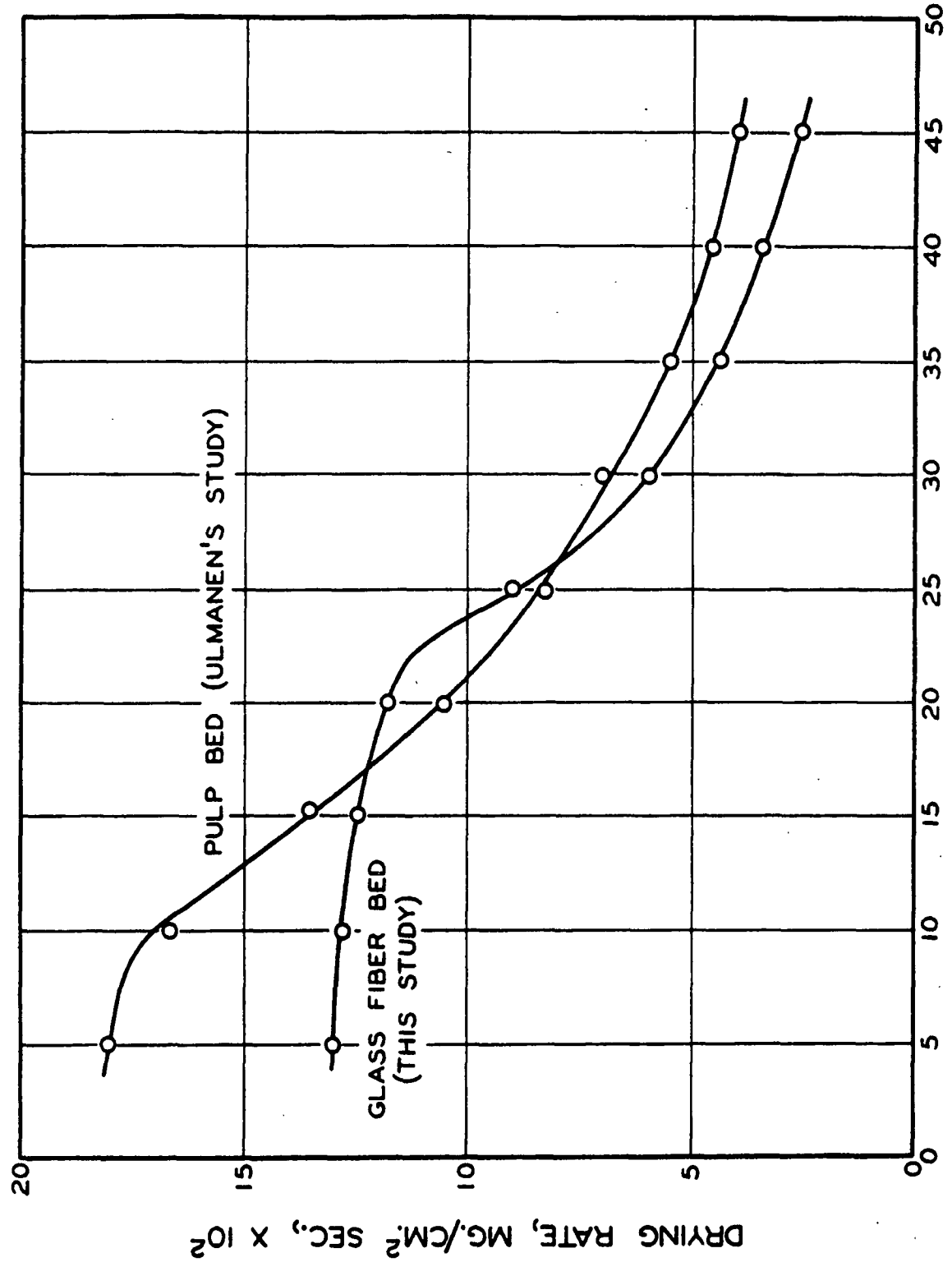

Figure 30. Comparative Drying Rate Glass Fiber - Pulp Bed

(which appears to be generally true for all systems) must logically decrease as the moisture content decreases; i.e., the heat supply to the surface should decrease and the area available for evaporation should decrease. During this period of drying the moisture content at the open surface falls substantially. This suggests that the open surface evaporation rate must also decrease. This natural decrease must therefore be compensated for by an increase in the rate at which water vapor diffuses from the interior.

The rate of diffusion of water vapor from the interior of the bed will be some function of the partial pressure gradient, the area available for diffusion and the diffusion coefficient. Since the actual temperature at any point in the bed changes only slightly during the constant rate period, the diffusion coefficient at any point in the bed would not be expected to change significantly. The partial pressure gradient will depend upon partial pressure conditions (1) at the hot surface, and (2) at the open face. Saturation partial pressure exists near the hot surface and will not change much since the temperature changes only slightly. The partial pressure at the boundary layer between fiber system and air stream will depend upon air stream conditions (which are constant) and presumably the rate at which vapor is introduced to the boundary layer by surface evaporation. As surface evaporation decreases the conditions of partial pressure in this boundary layer would, by this argument, favor increasing diffusion from the interior. Finally, the decreasing moisture content increases the area available for diffusion and hence increases the potential for water vapor diffusion.

In short, as drying proceeds the expectation is that diffusion of water vapor from the interior will increase. This supplies the compensating

factor which offsets a decrease in surface evaporation rate and maintains the relatively constant rate observed for the constant rate period.

Attempts have been made to summon evidence by which the so-called rate-controlling mechanism of the hot surface drying operation could be elucidated. This has led to a belief that such a mechanism exists, whether it be heat transfer to or through the fiber bed, or resistance to water vapor diffusion through or from the bed. In fact, the existence of such a mechanism is doubtful.

Evaporation from any system requires heat. Therefore, the heat transfer rate is important. However, it is impossible to isolate the rate of heat transfer to the bed as an independent variable. It is governed by apparent conductivity and temperature gradient which themselves depend on a combination of almost every conceivable factor which can logically be associated with a drying operation.

The apparent conductivity at the hot surface interface is a strong function of the local moisture content. The local moisture content depends upon the degree of balance which exists between liquid water flow to the hot surface and evaporation from the hot surface. Liquid flow to the hot surface is a function of the basic pore structure of the porous material and the moisture gradient. The temperature gradient existing at the hot surface is dependent upon the temperature of the bed adjacent to the hot surface. If heat transferred to the bed increases the temperature of the bed in distinction to causing evaporation, the temperature gradient will become smaller. Hence, the rate of evaporation from the bed is a deciding factor. This is dependent upon heat transfer through the bed to

promote surface evaporation and internal diffusion of water vapor to prevent total condensation of water vapor produced by hot surface evaporation as well as to allow internal evaporation. The rate of internal diffusion is, among other things, a function of the pore structure and moisture content. Final diffusion of water vapor from the bed across the boundary layer is affected by air stream conditions.

The interdependence of heat and mass transfer, boundary conditions of drying, internal pore structure, and drying rate apparently has not been adequately realized. There is little doubt, however, that a proper understanding of these interrelationships is the key to a more complete knowledge of the drying operation. The outward effect of some of these interrelationships can be observed by a comparison of the hot surface drying of a glass fiber bed and a pulp bed.

The boundary conditions established for the hot surface drying of the glass fiber beds of this study were almost identical to those imposed by Ulmanen in his similar study of pulp beds. The differences observed between these two studies cannot, therefore, be attributed to boundary conditions. Hence, the comparison represents a valid means of high-lighting the effect of the physical and chemical characteristics which differentiate pulp and glass fiber systems on the interrelationships mentioned above.

Figure 31 represents a summary of a number of important drying characteristics comparing the pulp and glass fiber systems.

The initial drying rate for the pulp bed is greater than for the glass fiber bed. At the same time, the pulp bed has a higher moisture content

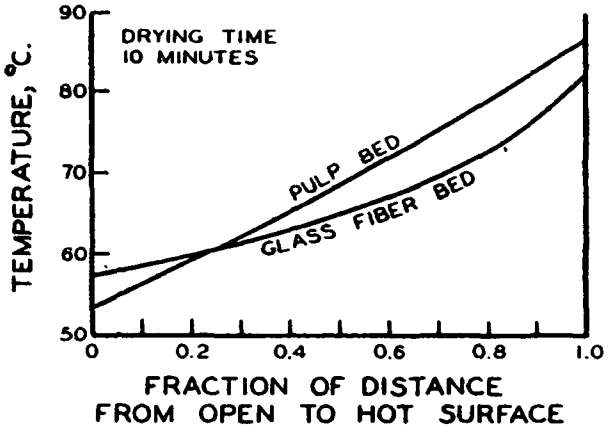

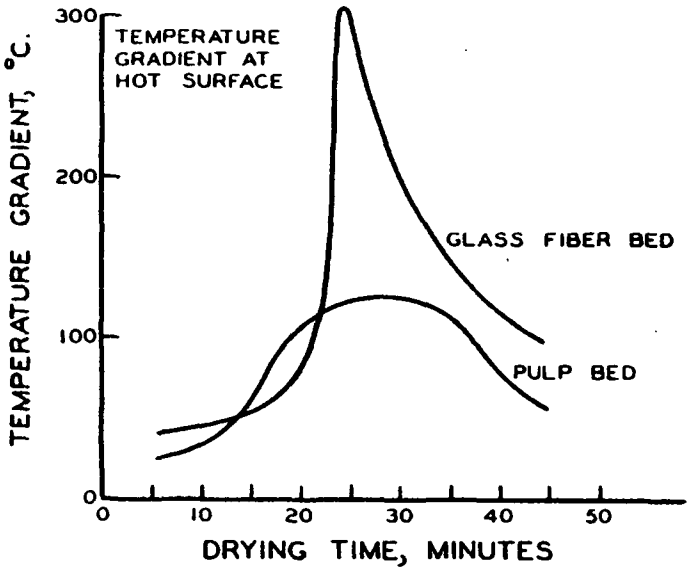

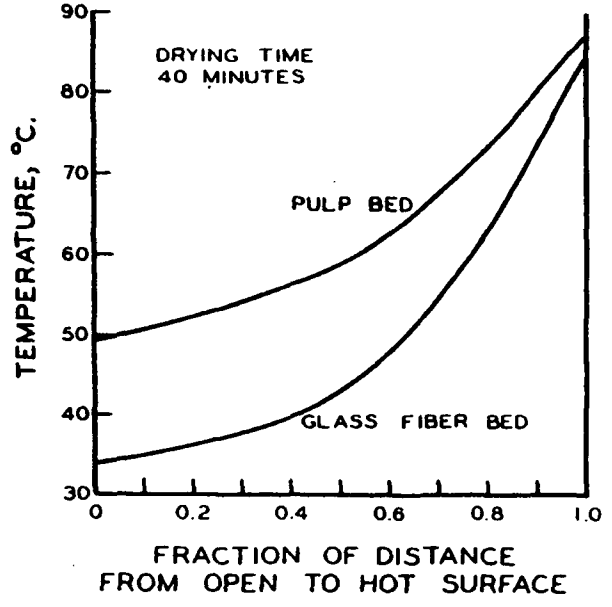

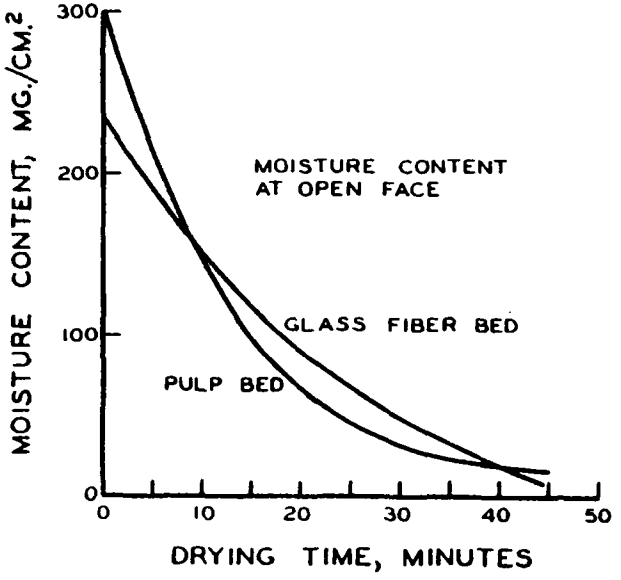

Figure 31 Comparative Properties Glass Fiber vs. Pulp Bed

at the hot surface and hence presumably a higher apparent conductivity. The higher moisture content at the hot surface is in part due to the slightly higher initial moisture content of the pulp bed but more significantly to the fact that the moisture content falls more rapidly at the hot surface for the glass fiber bed. This is a direct result of the capillary nature of the glass fiber bed. It has a considerably more uniform pore structure than does a pulp bed and so the capillary driving force for a particular moisture gradient will be much less. This is illustrated in Fig. 32 where the capillary pressure-saturation relationship for the glass fiber bed of this study is compared with a typical result for a pulp bed. The permeability to flow, although presumably greater for the glass fiber bed, is not sufficiently so to offset the particularly large difference in capillary driving force. Under these circumstances it is inevitable that liquid flow to the surface will compete less favorably with hot surface evaporation resulting in a lower moisture content at the hot surface for the glass fiber bed. Thus, one can expect the heat flow to the glass fiber bed to be less than for the pulp bed. The consequence of this lower heat flow is a lower drying rate.

The constant rate period ends at an earlier drying time for the pulp bed than for the glass fiber bed. In addition, a substantial moisture content still exists at the hot surface. This is in distinction to the glass fiber system where the end of the constant rate period is characterized by the disappearance of liquid water from the hot surface. For the explanation of these events it is necessary to turn once more to the concept of the three contributions to over-all drying rate.

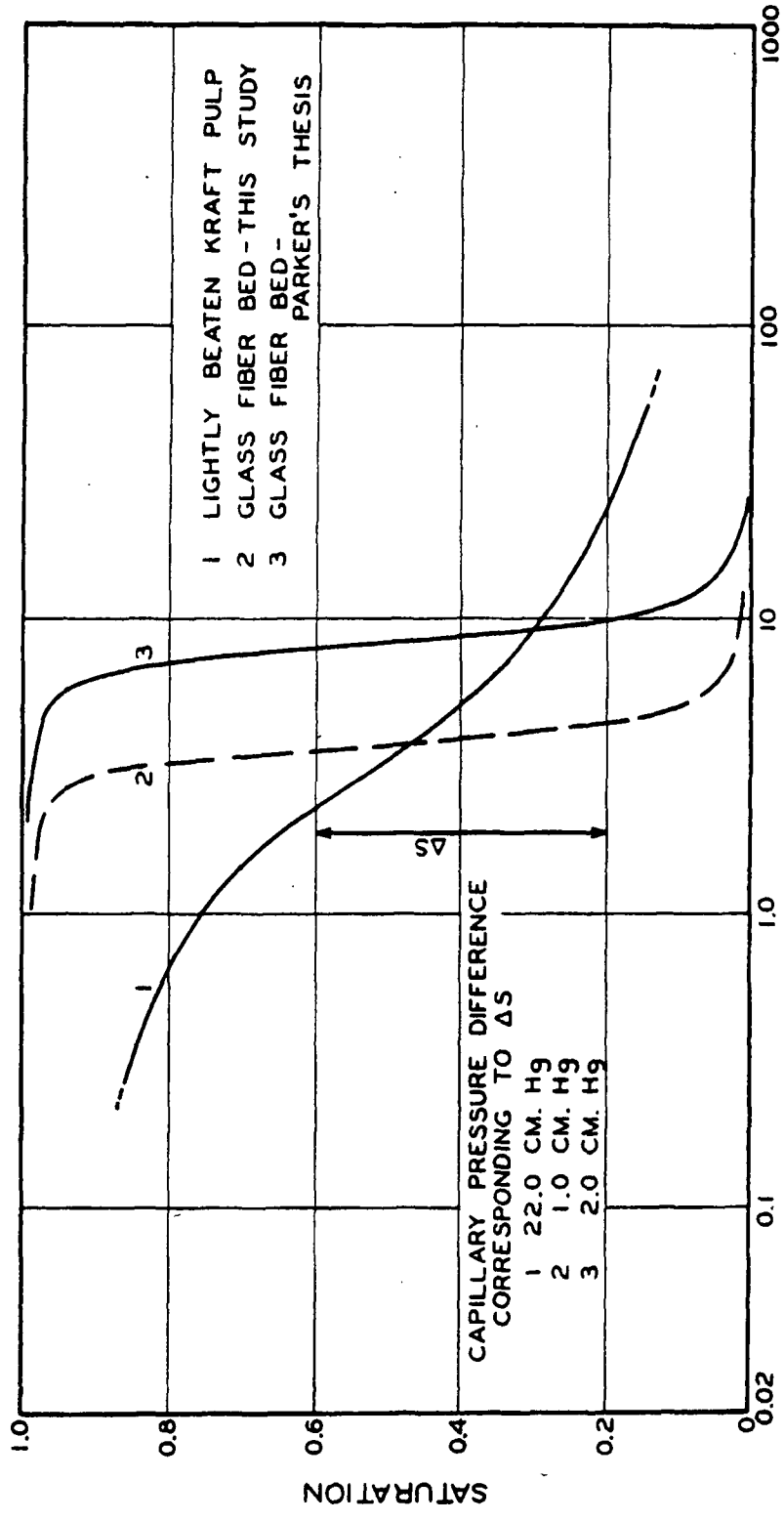

Figure 32. Capillary Pressure Studies

It can be noted from Fig. 31 that the temperature gradient at and near the open surface is substantially higher for the pulp bed than for the glass fiber bed. A good explanation for this difference is the possibility that for a pulp bed heat must be transferred nearer to the open face while for a glass fiber bed the heat is to a considerable extent absorbed as latent heat of vaporization at positions closer to the hot surface. In other words, this is an indication that the zone of condensation may be more extensive in the pulp bed and that therefore evaporation from the air interface contributes a larger proportion toward the over-all drying rate than is the case for the glass fiber bed.

In addition, the pulp bed is less porous than is the glass fiber bed and so less space is available for vapor diffusion. This higher resistance will tend to reduce the contribution to over-all drying rate from interior diffusion of water vapor and donate the heat supply to surface evaporation. This postulated higher surface evaporation rate could also account for the steeper moisture gradient at the open face which has been mentioned for the pulp system.

The constant rate period must end when the diffusion of water vapor from the interior can no longer compensate for the decreasing surface evaporation rate. Since the initial surface evaporation rate is probably substantially greater for a pulp bed than a glass fiber bed the same percentage decrease in surface evaporation rate will represent a substantially greater loss in drying effect. In addition, the moisture content at the open face falls at a greater rate for the pulp bed so that the actual percentage decrease in surface evaporation rate should be greater

for the pulp bed. This argument suggests that a greater rate of increase of diffusion of water vapor from the interior of a pulp bed is necessary to compensate for the decreasing surface evaporation rate than is the case for a glass fiber system. The rate of increase of water vapor diffusion from the pulp bed is restricted by the fact that as water evaporates from the bed part of the space which should become available to diffusion is lost as a result of shrinkage of the pulp bed. A logical consequence of these effects is that diffusion of water vapor from the interior fails to compensate for loss of surface evaporation at an earlier period of drying for a pulp bed than is the case for the glass fiber system. Hence, the constant rate period terminates earlier.

It appears, therefore, that, for a pulp bed, resistance to internal water vapor diffusion is the prime-mover which calls to an end the constant rate period; for a glass fiber bed it is resistance to heat transfer.

In the later stages of the falling rate period the pulp bed drying rate is greater than the glass fiber bed drying rate. The continual presence of water at the hot surface presumably maintains a greater heat flow to the pulp bed than is the case for the glass fiber bed where a continually thickening layer of dry fiber separates the hot surface from the wet bed. This is evidenced by the large temperature decrease in the glass fiber bed which does not occur in the pulp bed. The presence of liquid water at the hot surface of a pulp bed can be explained by resorting to the physical and/or the chemical nature of this fiber system. The fine pore structure of the pulp bed which pre-exists and/or is produced by shrinkage may maintain liquid water at the interface by virtue of the large

capillary driving forces which potentially exist. Water trapped within the lumen of fibers near the interface would act as a natural reservoir for this flow.

The chemical nature of the cellulosic pulp fiber allows substantial amounts of water to be adsorbed on its surfaces. Water at the interface must, therefore, be at least partially chemically bound and may be totally so.

The mechanism of hot surface drying can thus be seen as a complex of interrelationships. The drying rate is governed by the interdependent internal heat and mass transfer processes. These internal processes are in turn governed by the internal structure of the porous material and the boundary conditions of drying. Although the effect of the latter factor has been well documented, it does not appear that the importance of internal structure (as evidenced by the contrasting results for pulp and glass fiber beds) has been properly recognized.

QUANTITATIVE TREATMENT

A natural phenomenon can never be reasonably understood until physical observation can be fitted to an embracing mathematical model and thus related to underlying fundamental concepts. The history of the study of hot surface drying clearly illustrates the difficulty introduced by the lack of any such quantitative treatment. The conclusions that have been drawn from experimental observation have in many cases been reasonable, in some cases shrewd, but in all cases incomplete. This will necessarily continue until a consistent mathematical description of the drying operation can be successfully evolved.

The qualitative treatment of the experimental data obtained for glass fibers emphasizes that hot surface drying and internal heat and mass transfer are essentially synonymous terms. Therefore, the understanding of the former can only come about through a diligent study of the latter. It is the purpose of this section to introduce a quantitative treatment of the mass and energy interchanges that occur during the drying of a glass fiber bed. The development which evolves is in many ways crude. Some of the assumptions upon which it builds must be recognized as questionable. Many of the calculations involved require the extraction of first and second derivatives from experimental data, a task which can be described as laboriously imprecise. However, it is hoped that this development will highlight profitable areas for new research and suggest a route toward a far more advanced mathematical concept of the drying process.

HEAT TRANSFER

Heat transfer through the glass fiber system during hot surface drying can be qualitatively discussed in terms of the equations derived in an earlier section. From the hot surface interface boundary equation (29) the total heat flow to the hot surface interface and hence to the fiber system is given by $(\underline{k}_{\underline{m}}/\underline{L})(\partial \underline{t}/\partial \bar{\underline{x}})_{\underline{m},\bar{\underline{x}}=1.0}$, the product of the thermal conductivity of the metal and the temperature gradient in the metal adjacent to the interface. From Equation (29) it can be seen that only a portion of the total heat supplied to the interface is transferred from the interface. The remainder is absorbed as latent heat by evaporation at the hot surface interface.

Heat transfer from the hot surface interface internally toward the air interface occurs, empirically at least, in response to the product of the internal temperature gradient and the local apparent thermal conductivity.

Finally, according to the air interface boundary equation (31), heat is transferred to the air interface and, neglecting heat loss to the air stream, is consumed by evaporation at the open surface.

The investigation and evaluation of the apparent thermal conductivity within the fiber bed during hot surface drying is the primary goal of this section of the thesis. The analysis of Han and Ulmanen (14) to describe the apparent thermal conductivity of a pulp bed as a function of the moisture content of the bed has been mentioned earlier. This appears to be a good starting point for a similar analysis of the glass fiber system.

In essence, Han and Ulmanen made a material and energy balance for their system as a whole. They assumed that heat losses by conduction or radiation to the air stream were negligible and were therefore able to equate the total heat flow to the bed to the changes in sensible heat of the components of the system plus the heat absorbed in causing evaporation from the bed. By making the same derivation in terms of the nomenclature introduced in the last section, it can be shown that:

$$Q = \lambda e \rho_L L \frac{\partial S}{\partial \theta} + \int_{\bar{x}=0}^{1.0} L(1-e)\rho_F C_F \frac{\partial t}{\partial \theta} d\bar{x} + \int_{\bar{x}=0}^{1.0} es L \rho_L C_L \frac{\partial t}{\partial \theta} d\bar{x} \qquad (33)$$

where $\partial S/\partial \theta$ is the rate of change of total saturation for the bed as a whole (the drying rate); and other terms are as defined earlier.

Combining Equations (29) and (33) it is apparent that:

$$\left(\frac{k_a}{L}\frac{\partial t}{\partial \bar{x}}\right)_{\bar{x}=1} + \lambda e \rho_L L \left(\frac{\partial S_w}{\partial \theta}\right)_{\bar{x}=1.0} = \lambda e \rho_L L \frac{\partial S}{\partial \theta} + \int_{\bar{x}=0}^{1.0} L(1-e)\rho_F C_F \frac{\partial t}{\partial \theta}\, d\bar{x} + \int_{\bar{x}=0}^{1.0} es L \rho_L C_L \frac{\partial t}{\partial \theta}\, d\bar{x} \qquad (34)$$

Since there is no method of evaluating the evaporation rate at the hot surface, $(\partial S_w/\partial \theta)_{\bar{x}=1.0}$, Equation (34) cannot be used to determine k_e as defined by the original mathematical model as long as the hot surface evaporation term is significant. Han and Ulmanen by their treatment ignore the hot surface evaporation term and thus essentially define a somewhat artificial apparent thermal conductivity which in terms of this analysis can be formulated as:

$$\left(\frac{k'_a}{L}\frac{\partial t}{\partial \bar{x}}\right)_{\bar{x}=1.0} = \left(\frac{k_a}{L}\frac{\partial t}{\partial \bar{x}}\right)_{\bar{x}=1.0} + \lambda e \rho_L L \left(\frac{\partial S_w}{\partial \theta}\right)_{\bar{x}=1.0}$$

Their analysis evaluates this artificial apparent thermal conductivity, k'_e, as a function of moisture content. This value will approach the apparent thermal conductivity concept of this study as the hot surface evaporation rate becomes small.

Earlier discussion indicated that for the glass fiber system liquid water completely disappeared from the hot surface interface after about 22-1/2 minutes of drying. Under these circumstances no hot surface evaporation can occur and so Equation (34) can be used to evaluate the apparent thermal conductivity of the dry fiber bed.

In addition Equation (34) can be integrated by introducing $d\theta$ to each term and integrating from θ_1 to θ_2.

$$\int_{\theta_1}^{\theta_2} \frac{k_a}{L}\left(\frac{\partial t}{\partial \bar{x}}\right)_{\bar{x}=1.0} d\theta = \int_{\theta_1}^{\theta_2} \lambda e o_L L \frac{\partial S}{\partial \theta} + \int_{\bar{x}=0}^{1.0} C_F \rho_F (1-e) L (t\theta_2 - t\theta_1) d\bar{x} + \int_{\bar{x}=0}^{1.0} e s L \rho_L C_L (t\theta_2 - t\theta_1) d\bar{x} \qquad (35)$$

and this integral form evaluated over the period when no liquid water exists at the hot surface interface. This gives a further determination of the apparent conductivity of the dry bed. The integral form can be expected to give a value for k_a which is less susceptible to error due to errors in the measurement of temperature gradient, etc. This is significant since these calculations rely on data obtained during the falling rate period of drying where measurements were recognized to be less precise than for the constant rate period.

The apparent thermal conductivity values calculated at different times for dry bed conditions at the interface together with an evaluation using the integral form of the equation over the drying period from 30 to 45 minutes, are presented in Table VI.

These apparent thermal conductivity values indicate a satisfactory degree of internal consistency. The actual average value of 1.00×10^{-4} compares favorably with the value specified by the glass fiber manufacturer for their microfiber felt (porosity approximately 0.975) of 0.952×10^{-4} cal./cm.^{2} sec. (°C./cm.).

It is of interest to consider the significance of this value in terms of the actual conductivity of the components of the system. In the most

TABLE VI

DRY BED APPARENT THERMAL CONDUCTIVITIES

Drying Time, min.	Saturation At Hot Surface	Apparent Thermal Conductivity,[a] cal./cm.^{2} sec. (°C./cm.) x 10^4
25	0	0.98
30	0	0.95
35	0	1.07
40	0	1.01
45	0	0.97
[a]Evaluation using integral form		1.04

general case, for instance, three paths can be considered to exist for conduction of heat in the fiber bed; viz. solid fiber, liquid water, and a gaseous mixture of air and water vapor. Assuming (1) that conduction of heat occurs along three parallel paths in a direction perpendicular to the plane of the hot surface, (2) that all points in a given plane in the fiber bed are at the same temperature, and (3) that the volume concepts of porosity and saturation can be applied to any cross-sectional area, we can write:

$$k = (1-e)k_F + esk_L + e(1-s)k_V \qquad (36)$$

where k is the actual pure conductivity of the fiber system; k_F is the conductivity of the glass fibers; k_L is the conductivity of liquid water; k_V is the conductivity of the gaseous mixture of air and water vapor; and $(1-e)$, es, and $e(1-s)$ are the respective fractions of these components present in the cross section.

For the dry fiber bed the saturation is zero and Equation (36) reduces to:

$$k = (1-e)k_F + ek_v \qquad (37)$$

Handbook data indicates that the thermal conductivity of both air and water vapor is in the neighborhood of 0.6×10^{-4} cal./cm.^{2} sec. (°C./cm.). Using this value for k_v and assuming that the calculated value for k_e of 1.00×10^{-4} is a valid measure of the actual conductivity, k, the conductivity of the glass fibers is found to be 7.5×10^{-4} cal./cm.^{2} sec. (°C./cm.).

Various sources quote the thermal conductivity of solid glass at about 30×10^{-4} cal./cm.^{2} sec. (°C./cm.). One would expect the thermal conductivity of glass fibers to be substantially less than the conductivity of solid glass by virtue of the fact that the fibers are not fused together. The values quoted indicate an apparent "contact coefficient" of 0.25. Although a number of possible mechanisms such as tortuosity of conducting path, contact resistance, etc., can be cited as contributing to this contact coefficient, a value of 0.25 seems entirely possible.

By this analysis the apparent thermal conductivity as measured for the dry fiber bed can possibly be accounted for in terms of pure conduction only. This agrees with Finck's assertion (18) that natural convection is not an important heat transfer mechanism in dry porous beds unless very loosely packed.

It is now necessary to consider the problem of evaluating the apparent thermal conductivity of a partially saturated glass fiber bed. The following analysis offers this possibility.

It has been established experimentally (2) that liquid flow during hot surface drying is toward the air interface in the region of that interface and toward the hot surface interface in the region of that interface. Therefore, at some internal and intermediate position a plane of zero flow must occur. Heat supplied to the section of the bed between the hot surface and this plane where liquid flow is zero, minus the heat transferred from this section must equal the heat absorbed (1) by evaporation from this section, and (2) as sensible heat by the fiber and water present in this section. The heat supplied to the bed is given by Equation (33). A derivation similar to that required for Equation (33) yields:

$$Q - \left(\frac{k_a}{L}\frac{\partial t}{\partial \bar{x}}\right)_{\bar{x}=\bar{x}_1} = e\rho_L L\lambda \int_{\bar{x}=\bar{x}_1}^{1.0} \frac{\partial s}{\partial \theta}\, d\bar{x} + \int_{\bar{x}=\bar{x}_1}^{1.0} L(1-e)\rho_F C_F \frac{\partial t}{\partial \theta}\, d\bar{x} + \int_{\bar{x}=\bar{x}_1}^{1.0} es L\rho_L C_L \frac{\partial t}{\partial \theta}\, d\bar{x} \quad (38)$$

where $\bar{x}_1$ signifies the position in the bed where liquid flow is zero; $\partial s/\partial\theta$ is the rate of change of local saturation; $\int \partial s/\partial\theta$ is, therefore, the rate of change of cumulative saturation for the section of the bed between $\bar{x} = \bar{x}_1$ and $\bar{x} = 1.0$; and all other terms are as defined earlier.

Before Equation (38) can be used to evaluate k_a, it is necessary to establish the location of the plane $\bar{x}_1$. At this location the driving force for liquid flow, $\partial P_c/\partial \bar{x}$, will be zero. The capillary pressure at any point in a porous bed will be affected by the saturation at that point and also by the temperature. Thus, the capillary driving force will be some function of the moisture gradient and the temperature gradient. Since the temperature gradient in the central regions of the bed is not very great it is a fairly good assumption that the plane of zero liquid

flow will be close to the plane where the moisture gradient is zero--somewhere between $\bar{x} = 0.4$ and $\bar{x} = 0.6$ for the constant rate period.

Once the location of this plane has been established, all terms with the exception of k_a are calculable from experimental data. Thus, according to Equation (38) the apparent thermal conductivity can be estimated for various drying times. It is found that at a particular drying time this value is relatively independent of the precise location of the plane of zero liquid flow. The location of the plane was therefore established at the point where the moisture gradient is zero and k_a calculated for various drying times in the constant rate period. These values correspond to a definite saturation at $\bar{x} = \bar{x}_1$, and so a relationship between apparent thermal conductivity and saturation can be construed. This data is plotted in Fig. 33. The previously calculated apparent thermal conductivity at zero saturation is included and the dotted section represents a very arbitrary interpolation. The significance of this relationship will now be considered.

Equation (36) has been introduced as a model to define conduction in the fiber bed. The thermal conductivity of water is about 15.0×10^{-4} cal./cm.^{2} sec. (°C./cm.). Using this value for k_L and the previously proposed numerical values for k_F and k_v allows the conductivity of the fiber bed as a function of moisture content to be determined. This relationship is compared with the previously calculated apparent thermal conductivity relationship in Fig. 34.

It is obvious that the calculated conductivity as defined by Equation (36) cannot account for the apparent thermal conductivity calculated from experimental data. This suggests the following possibilities:

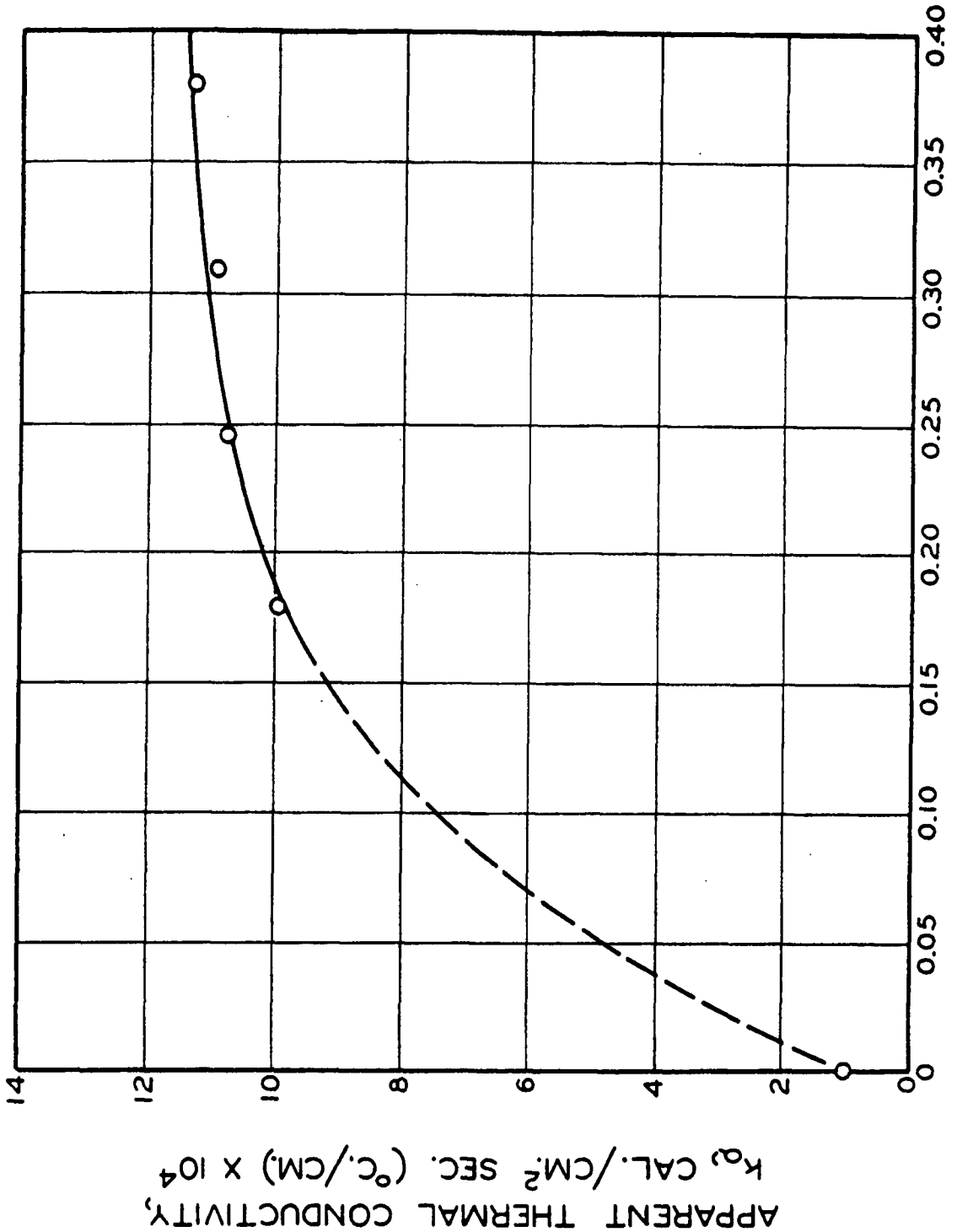

Figure 33. Apparent Conductivity

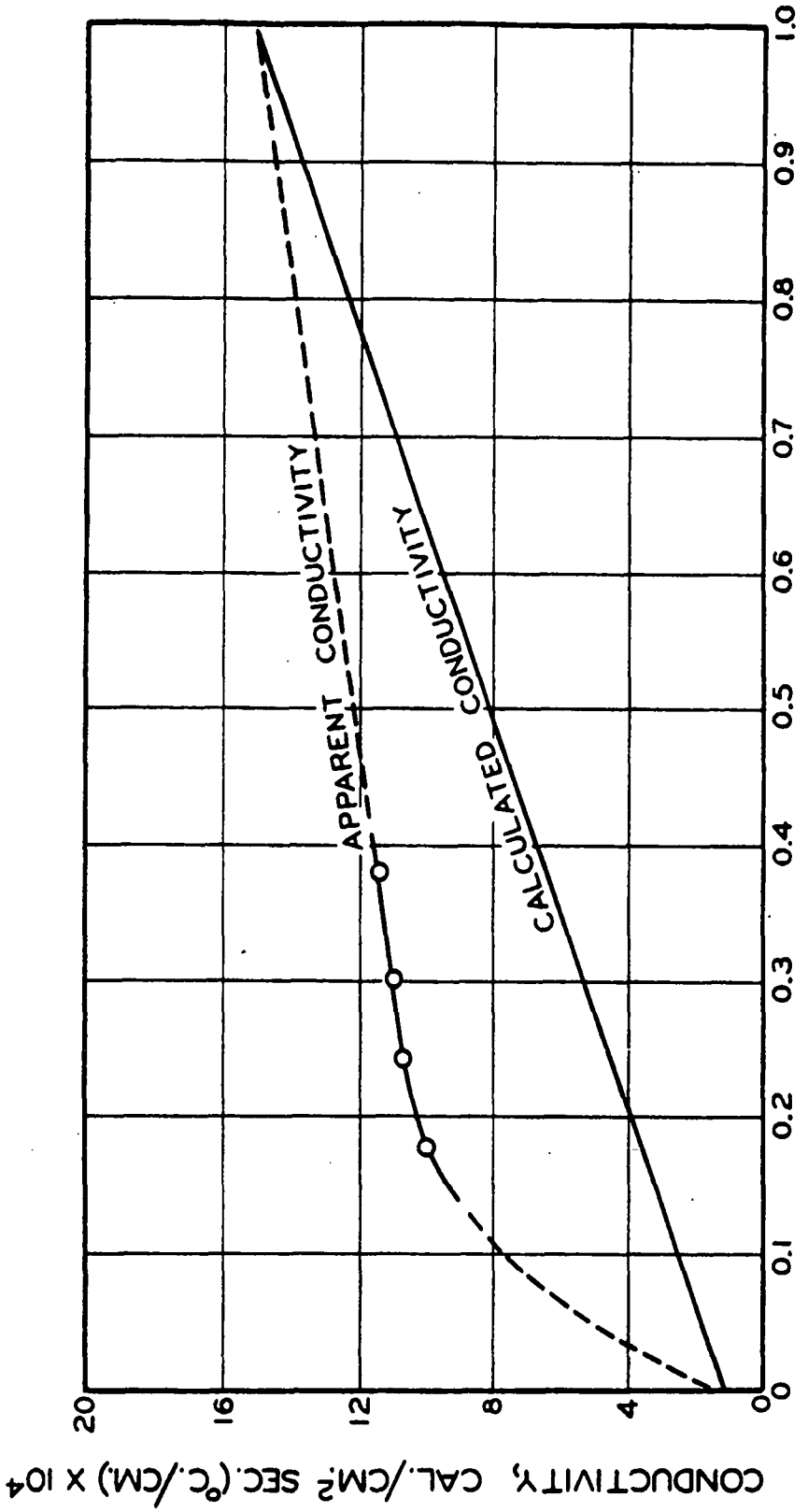

Figure 34. Apparent and Calculated Conductivity

(1) Conduction contributes as little as 50% toward the over-all heat transfer and hence convection and/or radiation must account for the remainder.

(2) The physical model implied by the assumptions defining the conductivity, k, does not correspond to what actually occurs in the fiber bed. That is, the actual conductivity is greater than that calculated on the basis of the defined model.

Although the physical model suggested for conduction in a porous material can be severely criticized, it is difficult to accept that it is so far from reality as to underestimate the actual conduction by a factor of more than two. The consequences of assuming that the calculated conduction is in fact a fair estimate of the actual conduction is, of course, that the combination of radiation and convection must contribute significantly to over-all heat transfer.

Finck (18) suggests that, for very loosely packed kapok, up to 15% of the total heat transfer may occur by radiation. For the more closely packed glass fiber bed with liquid water as well as water vapor present, it is probable that radiation will contribute substantially less than this to over-all heat transfer. It does not appear, therefore, that radiation can account for much of the discrepancy between calculated conductivity and the apparent thermal conductivity of the glass fiber bed. Therefore, the existence of a significant convection heat transfer mechanism must be seriously considered.

A number of consequences follow the acceptance of convection as an important factor in determining the value of the apparent thermal conductivity.

First, the definition of heat flow as the product of an apparent conductivity and a temperature gradient must be recognized as highly empirical since convective heat transfer is not fundamentally associated with a temperature gradient. Second, and possibly more important, no unique relationship can be expected to exist between apparent thermal conductivity and moisture content. Such factors as local evaporation or condensation rate, direction and rate of liquid flow, etc., in addition to local saturation might well affect convective heat transfer. In other words, the apparent conductivity will be affected not only by the degree of liquid saturation but also by factors which are associated with the actual rate at which drying is effected.

In the light of these comments, it is necessary to reconsider the significance of the apparent conductivity relationship shown in Fig. 33 and 34. The data points shown represent the apparent conductivity for different saturations in essentially the same section of the bed (central portion) during the constant rate period. Under these circumstances it is possible that if we divide the factors which affect the apparent conductivity into (1) saturation, and (2) nonsaturation factors, that the nonsaturation factors are reasonably constant and that the relationship shown does illustrate essentially a saturation-apparent conductivity relationship. On this basis, it is of interest to note the general shape of the extrapolated curve. It can be seen that at a saturation of 1.0 (void volume totally occupied by water) the apparent conductivity and actual conductivity curves meet. This implies that convective heat transfer under such conditions is nonexistent. Since there is no void space

available, neither internal evaporation nor condensation can occur and it is quite reasonable to suppose that convection will not be important. As the saturation decreases, two opposing "saturation" factors can be considered operative. First, the available space into which vapor can be introduced increases thus potentially increasing the evaporation rate. Second, the decreasing quantity of water available for evaporation potentially reduces the evaporation rate. At a saturation level of about 0.15 the latter factor is apparently predominant and convective heat transfer diminishes rapidly until for a dry fiber bed it becomes once more negligible.

This explanation for the curves of Fig. 34 does give a realistically consistent picture of the general relationships that one might anticipate between convection and conductive heat transfer in relation to saturation. However, this does not mean that the relationship shown in Fig. 33 can be used to evaluate $\underline{k}_{\underline{a}}$ anywhere in the bed at any time from only a knowledge of the local saturation. In fact, the only reasonable application of Fig. 33 is to evaluate $\underline{k}_{\underline{a}}$ from a knowledge of the local saturation for the central portion of the bed and only for the constant rate period of drying.

This can be illustrated by evaluating $\underline{k}_{\underline{a}}$ according to Equation (38) for the falling rate period of drying. It should be remembered, however, that the experimental data used to make this calculation lacks the precision obtained during the constant rate period. Table VII compares these values of $\underline{k}_{\underline{a}}$ with the predicted values according to the extrapolated curve of Fig. 33, and with the calculated true conductivity values.

TABLE VII

COMPARISON OF VARIOUS CONDUCTIVITY VALUES

Saturation	k_a from Falling Rate Period determination, cal./cm.^{2}sec.(°C./cm.) x 10^4	k_a Estimated from Fig. 33, cal./cm.^{2}sec.(°C./cm.) x 10^4	k Calculated from Equation (36), cal./cm.^{2}sec.(°C./cm.) x 10^4
0.128	4.1	8.5	2.8
0.096	3.4	7.3	2.3
0.071	3.0	6.1	2.0
0.050	2.8	5.0	1.7

It is reasonable to suppose that convective heat transfer will be more important during the constant rate than the falling rate period since the drying rate is significantly greater in the former. This view is supported by the data presented in Table VII. This clearly illustrates the disconcerting and discouraging fact that the evaluation of the apparent conductivity at one point in the fiber bed and at one particular drying time is of questionable value in predicting the apparent conductivity under any other conditions or circumstances.

Brief consideration can now be given to the apparent thermal conductivity relationship defined by Han and Ulmanen and presented in Fig. 4. The theoretical significance of the apparent thermal conductivity implied in the derivation by Han and Ulmanen has already been mentioned. It is improbable in view of the previous discussion that convective heat transfer is not significant in the pulp system. Hence, it must be inferred that the shape of the curve obtained by Han and Ulmanen is a result not only of the decrease in the moisture content but also of the decrease in drying rate

which from their basic data demonstrably accompanies the decrease in moisture content. In other words, the depicted relationship between apparent thermal conductivity and moisture content is not unique and cannot realistically be used to imply the existence of certain mechanistic phenomena.

The most satisfactory analysis of heat transfer that can be supplied by the data of this study suggest that in the hot surface drying of a glass fiber bed both conduction and convection contribute significantly to over-all heat transfer. Radiation is probably not significant. The convective heat transfer is the result of fluid movement associated with the drying process and hence is some function of the rate at which drying is proceeding.

Future investigation should consider the validity of the suggested model for evaluating the conductivity of a porous material. A glass fiber system in which the pore space is totally filled with a solid such as wax would seem amenable to conductivity measurement and hence a test of the suggested model. A verification of the importance of convective heat transfer during hot surface drying by some direct experiment would offer support for the analysis presented above.

EVAPORATION

During the constant rate period of the hot surface drying of a glass fiber bed it has been shown that evaporation of water occurs (1) at the hot surface interface, (2) internally from the zone of condensation, and (3) at the air interface. It is possible on the basis of certain assumptions to evaluate each of these quantities from the experimental data.

The rate of evaporation from the air interface is given by the air interface boundary equation (31). Its evaluation requires a knowledge of the apparent conductivity, $\underline{k_a}$, at the interface. It is assumed that for the constant rate period the apparent conductivity at the air interface can be determined from a knowledge of the local saturation according to Fig. 33. The validity of such an assumption is dependent upon whether conditions at the interface and in the central region of the bed are sufficiently similar that convective heat transfer is essentially the same.

In order to complete the picture it is assumed that for the falling rate period the data supplied in Table VII can be used as a valid estimate of the apparent conductivity in this period. Here again this implies the similarity of convective heat transfer at the air interface to that in the central region of the bed.

On the basis of these assumptions the open surface evaporation rate, $(\partial \underline{S_w}/\partial\theta)_{\underline{\bar{x}=0}}$, can be evaluated from Equation (31). The result of this evaluation is presented in Fig. 35. The similarity between this curve and the over-all drying rate curve is apparent.

The water vapor which is produced at the hot surface interface and diffuses out of the zone of condensation can be evaluated from a material and energy balance for the zone of condensation. The derivation of such a material and energy balance yields Equation (39).

$$Q - \left(\frac{k_a}{L}\frac{\partial t}{\partial \bar{x}}\right)_{\bar{x}=\bar{x}_2} - e\rho_L L\lambda\left(\frac{\partial S_w}{\partial\theta}\right)_{\bar{x}=\bar{x}_2} = eL\rho_L C_L \int_{\bar{x}=\bar{x}_2}^{1.0} t\,\frac{\partial s}{\partial\theta}\,d\bar{x}$$

$$- eL\rho_L C_L (t)_{\bar{x}=\bar{x}_2} \int_{\bar{x}=\bar{x}_2}^{1.0} \frac{\partial s}{\partial\theta}\,d\bar{x} + L(1-e)\rho_F C_F \int_{\bar{x}=\bar{x}_2}^{1.0} \frac{\partial t}{\partial\theta}\,d\bar{x} + Le\rho_L C_L \int_{\bar{x}=\bar{x}_2}^{1.0} s\,\frac{\partial t}{\partial\theta}\,d\bar{x} \quad (39)$$

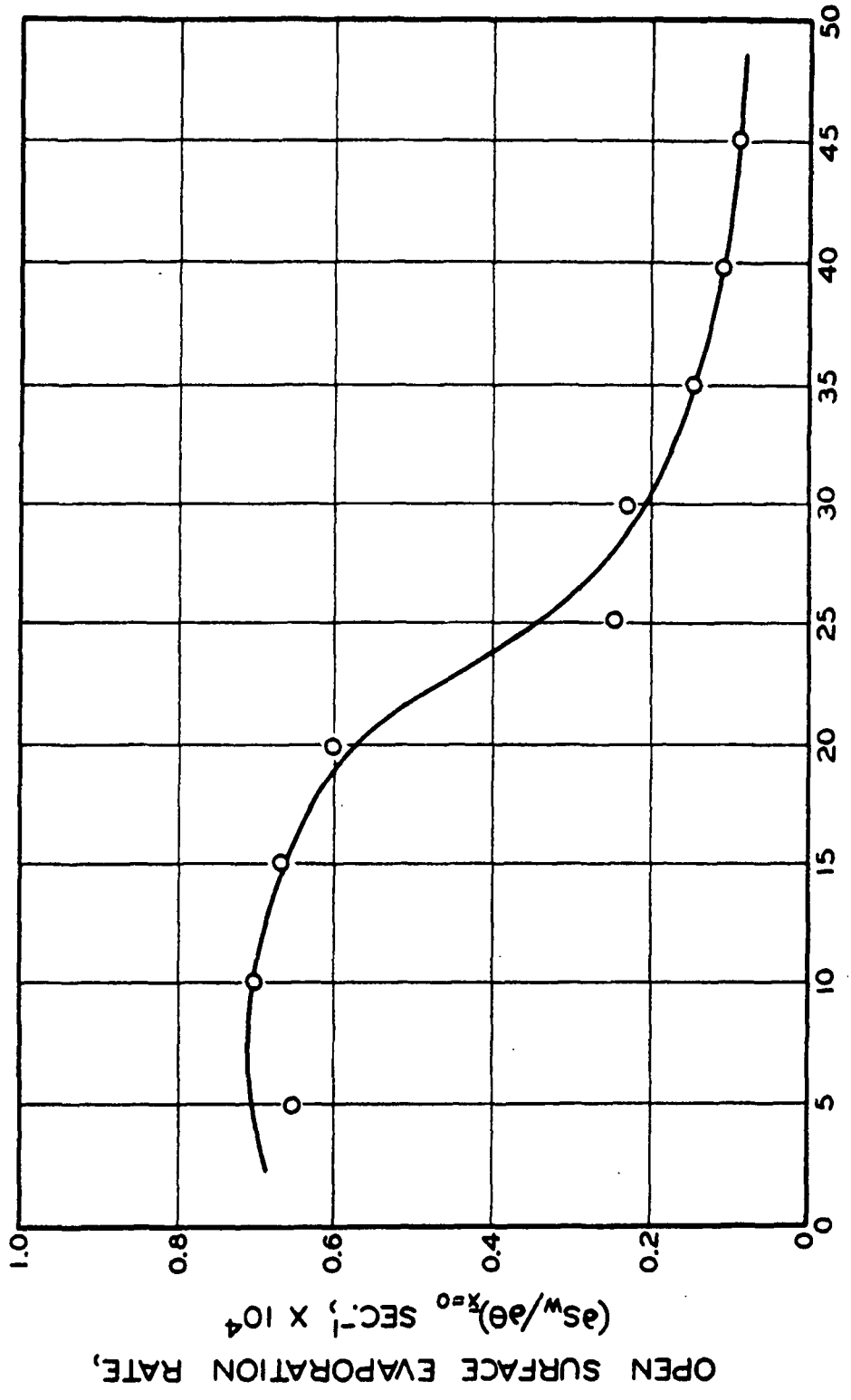

Figure 35. Open Surface Evaporation Rate

where $\underline{Q}$ is the heat supplied from the hot surface according to Equation (33); $(\partial \underline{S}_w/\partial\theta)_{\underline{\bar{x}}=\underline{\bar{x}}_2}$ is the rate of change of total saturation resulting from water vapor produced at the hot surface interface which diffuses from the bed; $\partial \underline{s}/\partial\theta$ is the rate of change of local saturation; $\bar{x}_2$ represents the location of the plane which separates the zone of condensation from the zone of evaporation; and all other terms are as defined previously.

Two assumptions are necessary before Equation (39) can be used to evaluate $(\partial \underline{S}_w/\partial\theta)_{\underline{\bar{x}}=\underline{\bar{x}}_2}$ from experimental data. First, the location of the plane $\bar{x}_2$ must be determined. It seems reasonable that the junction between the zones of condensation and evaporation will occur somewhere near the point where the moisture gradient begins to increase sharply. From Fig. 25 this can be seen to occur in the region $\bar{x} = 0.7$ to $\bar{x} = 0.8$. The assumption is made that $\bar{x}_2 = 0.7$. Second, it is necessary to make the same assumption with regard to the estimation of $\underline{k}_a$ that was made in order to evaluate the open surface evaporation rate; namely, that conditions at $\bar{x} = 0.7$ and in the central region of the bed are sufficiently similar during the constant rate period that the data from the central region can be considered to apply at $\bar{x} = 0.7$.

On the basis of these assumptions, Equation (39) can be used to evaluate $(\partial \underline{S}_w/\partial\theta)_{\underline{\bar{x}}=\underline{\bar{x}}_2}$ from the experimental data. The result is shown graphically in Fig. 36.

The over-all drying rate (Fig. 24) represents the summation of the data presented in Fig. 35, the data presented in Fig. 36 and the vapor which is produced by evaporation from the zone of evaporation. By difference, then, the internal evaporation rate can be evaluated. This is presented

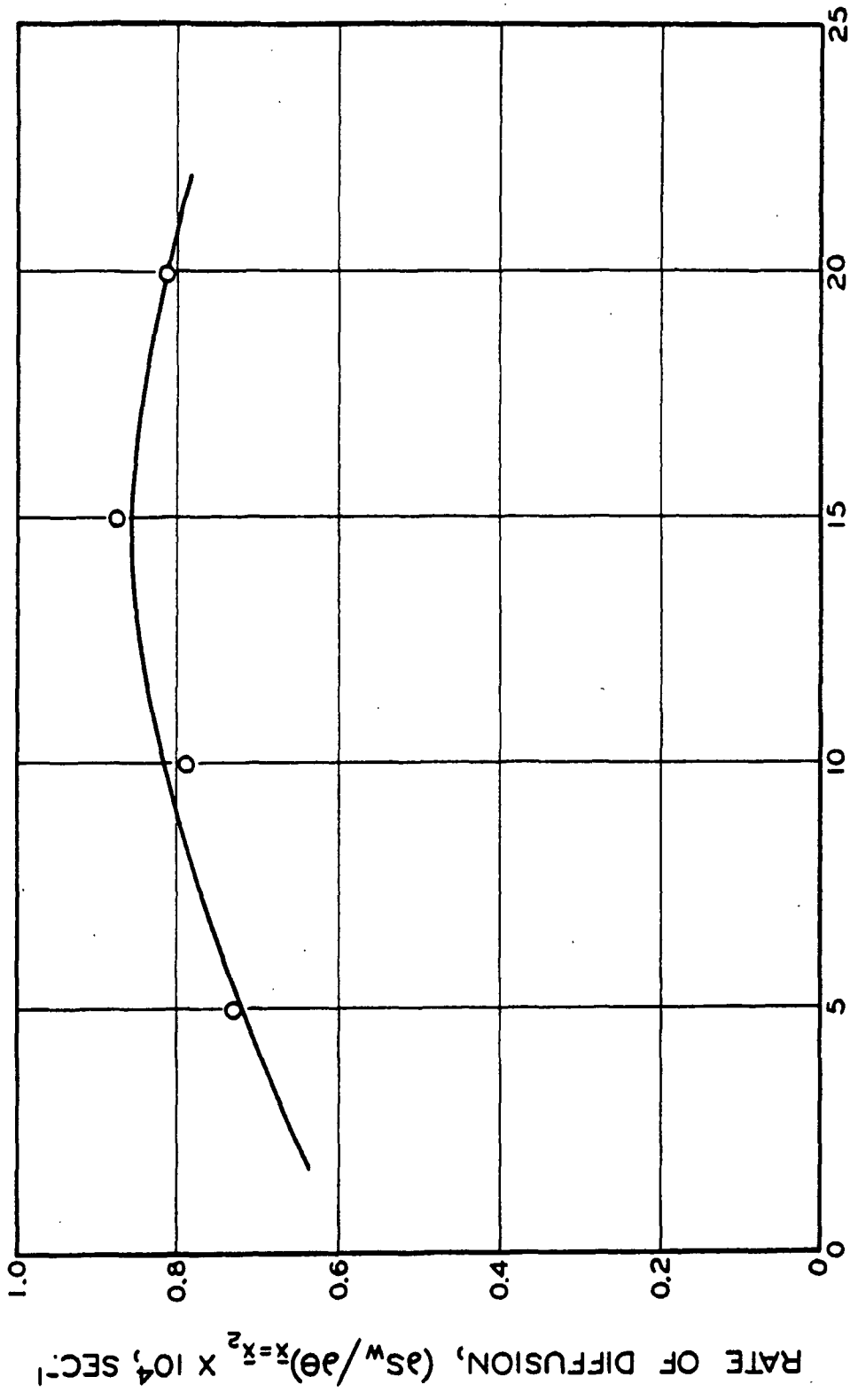

Figure 36. Rate of Diffusion of Water Vapor Produced at the Hot Surface from the Zone of Condensation

as the rate of change of cumulative saturation due to internal evaporation from the zone of evaporation in Fig. 37. The contributions of the various components to the over-all drying rate are shown in Fig. 38.

In view of the assumptions involved in its construction, Fig. 38 cannot be confirmed as an accurate quantitative picture of the relative importance of the various contributors to the over-all drying rate. However, it is a good qualitative picture and illustrates the type of balance one should expect in achieving a particular over-all drying rate.

In the constant rate period, it appears that roughly equal contributions are made (1) by water vapor which diffuses from the hot surface interface through the zone of condensation, (2) by water vapor which is produced by internal evaporation from the zone of evaporation, and (3) by water produced by open surface evaporation. An increasing rate of diffusion from the zone of condensation is offset by decreasing internal and open surface evaporation rate to give the over-all drying effect measured experimentally.. The constant rate period ends when liquid water disappears from the hot surface and hence evaporation at the hot surface ceases. The zone of evaporation broadens to eliminate the zone of condensation and, therefore, the rate of internal evaporation increases sharply. In the falling rate period, internal evaporation appears to account for 70-80% of the over-all drying rate.

It is now worth considering at least qualitatively on the basis of the above analysis the manner in which evaporation and condensation occur locally in the interior of the bed during the constant rate period. Conditions at a drying time of 10 minutes are typical of the constant rate period and so subsequent evaluation will be restricted to that drying time.

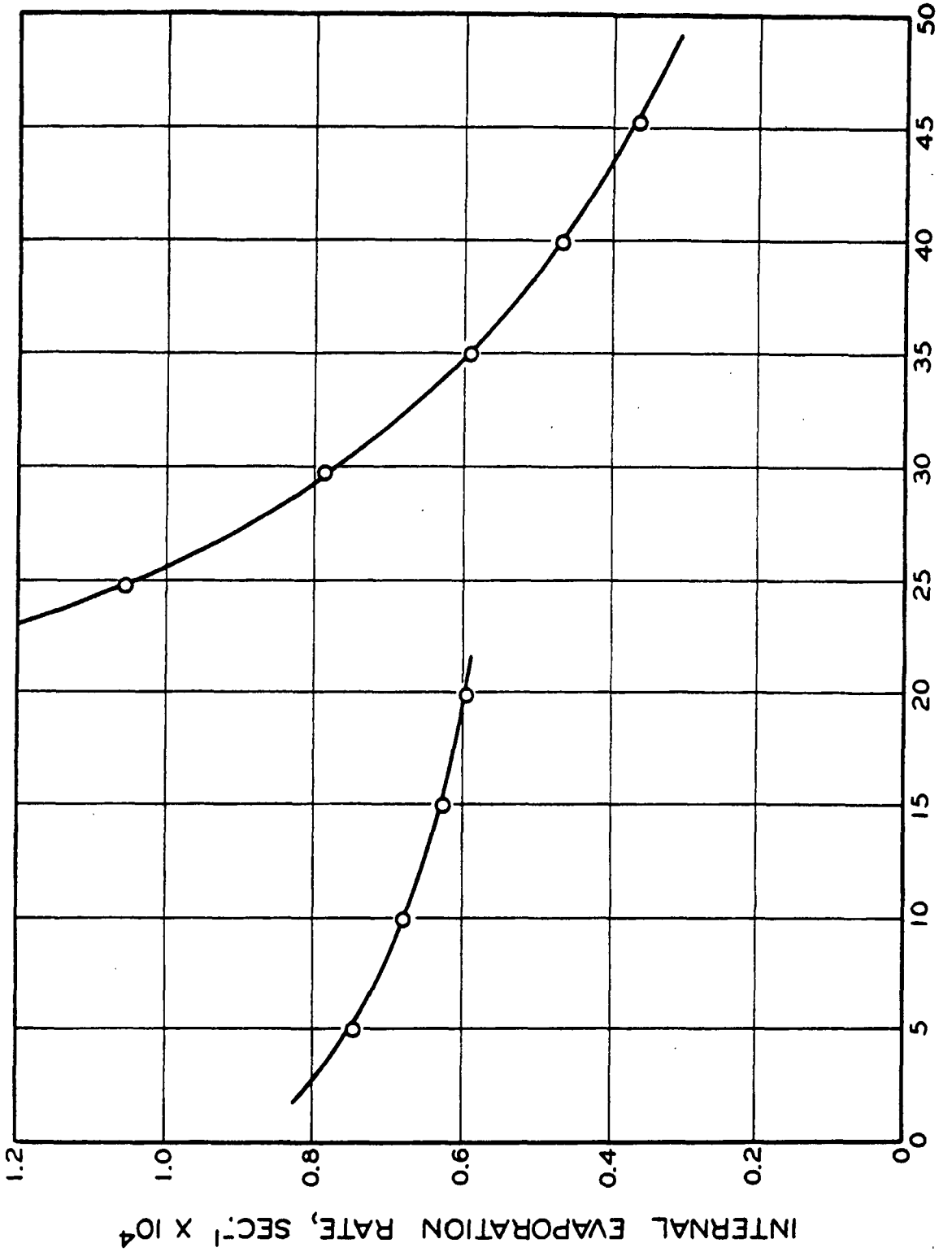

Figure 57. Total Internal Evaporation Rate

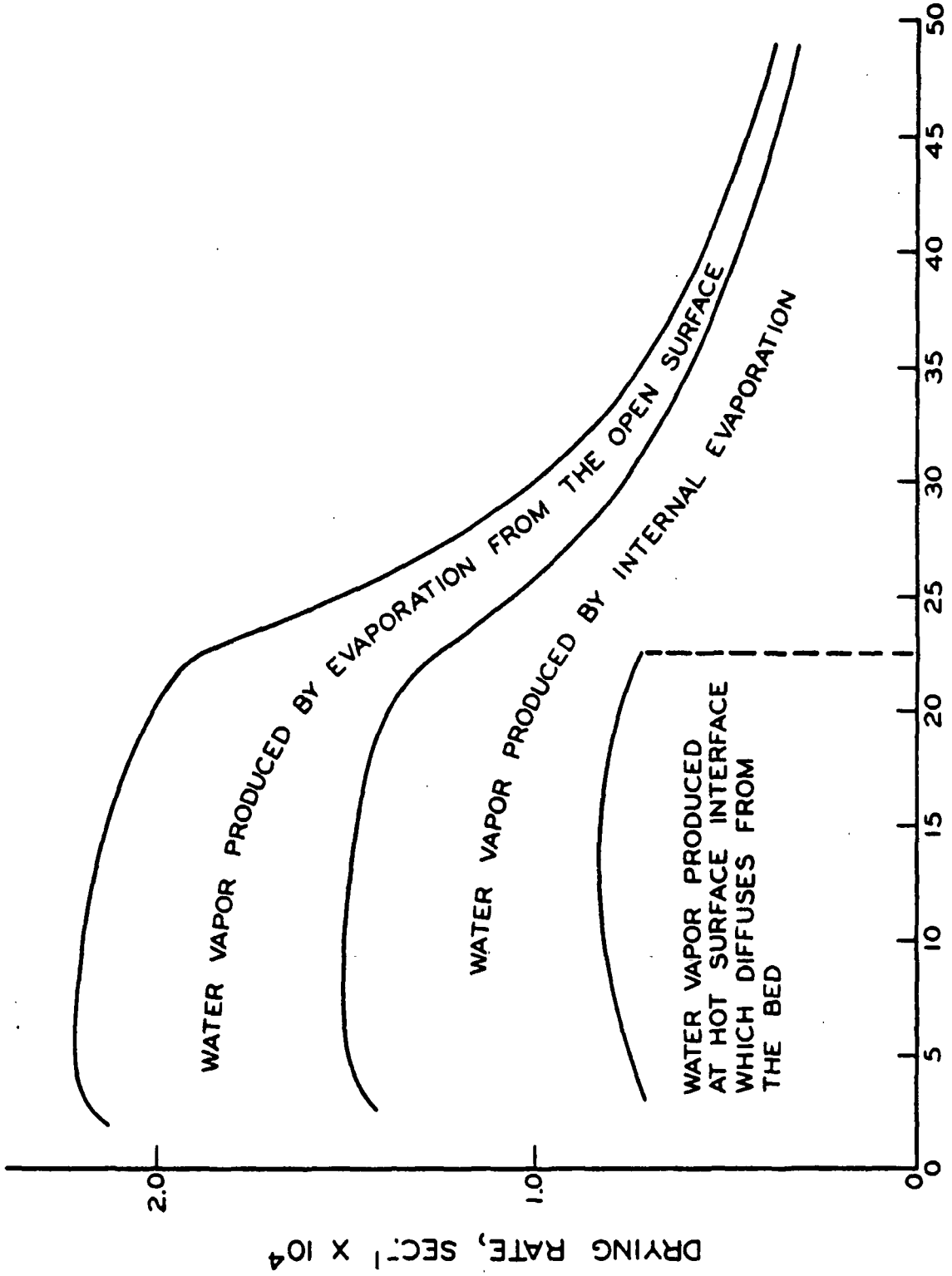

Figure 38. Combined Drying Rate Curve

The total contribution to the drying rate from internal evaporation at 10 minutes drying time has been evaluated and is given in Fig. 37 as 0.63×10^{-4} sec.$^{-1}$.

The total condensation rate is equal to the difference between the evaporation rate at the hot surface interface and the rate at which vapor diffuses from the zone of condensation. This latter value has been calculated and is recorded in Fig. 36 as 0.81×10^{-4}. The hot surface evaporation rate can be evaluated according to hot surface interface boundary equation (29). However, this evaluation requires a numerical definition of the apparent thermal conductivity at the hot surface interface. To assume that the conditions near the hot surface interface are similar to those in the central region of the bed is obviously untrue. If one uses a value of $\underline{k}_{\underline{a}}$ obtained on the basis of such an assumption (i.e., from Fig. 33) one can estimate the hot surface evaporation rate, $(\partial \underline{S}_{\underline{w}}/\partial\theta)_{\underline{x}=1.0}$, from Equation (29) to be 0.65×10^{-4}. This value is less than the quantity of vapor which diffuses from the zone of condensation and therefore indicates that the assumed value for $\underline{k}_{\underline{a}}$ must be too large. The smallest value for $\underline{k}_{\underline{a}}$ that can logically be assumed is that to be expected for pure conduction only. Using such a value for $\underline{k}_{\underline{a}}$ obtained from the lower curve of Fig. 34 gives a hot surface evaporation rate of 1.92×10^{-4}. It follows therefore that the probable value lies between this value and the diffusion rate from the zone of condensation, 0.81×10^{-4}. Hence, the total condensation rate lies between zero and 1.11×10^{-4}.

By way of interjection, it is of interest to note the possible implication of the above calculations that the influence of convective heat transfer

on over-all heat transfer is less pronounced where condensation is occurring than where evaporation is occurring.

From the above estimates and assuming that the transition point between the zone of condensation and evaporation occurs at $\bar{x} = 0.7$, any number of curves can be drawn to represent the appropriate distribution of internal condensation and evaporation. However, the most probable distribution is shown in Fig. 39. The following reasons are cited to support this view.

(1) The maximum change in saturation in the zone of evaporation occurs between the air interface and $\bar{x} = 0.2$. It appears reasonable to attribute to this section the maximum evaporation rate. Since the available space increases continuously in this region the increase in evaporation rate should be continuously increasing. The changes in saturation between $\bar{x} = 0.2$ and $\bar{x} = 0.7$ are not great. This suggests that the evaporation rate which near $\bar{x} = 0.7$ must be small will not increase greatly over this region. The area under the curve from $\bar{x} = 0.7$ to $\bar{x} = 0$ should be 0.81×10^{-4}.

(2) The maximum rate of change of saturation in the zone of condensation occurs between $\bar{x} = 0.7$ and $\bar{x} = 0.8$. It seems reasonable, therefore, to attribute to this region the maximum change in condensation rate. In the zone $\bar{x} = 0.8$ to $\bar{x} = 1.0$ two opposing factors would appear to be operative. The quantity of vapor available for condensation is a maximum near $\bar{x} = 1.0$. Also the space available for vapor is a maximum. On this basis it would seem that the condensation potential as far as space is concerned increases in the direction away from the hot surface while the condensation potential

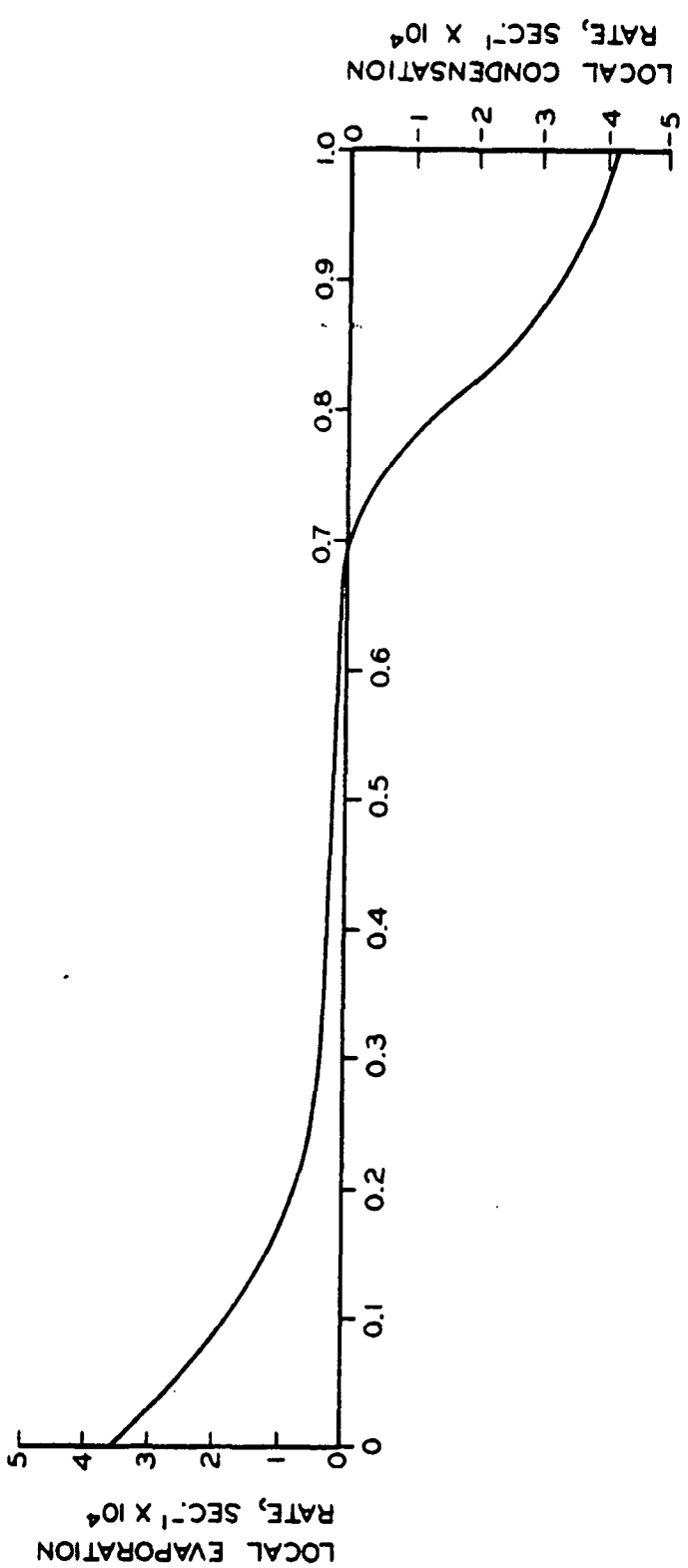

Figure 39. Local Internal Evaporation and Condensation Rates
Drying Time, 10 Min.

in terms of availability of vapor decreases. The balance of these factors should result in the type of curvature indicated. The area under the curve from $\bar{X} = 0.7$ to $\bar{X} = 1.0$ should be less than 1.11×10^{-4} sec.$^{-1}$.

WATER VAPOR DIFFUSION

The analysis for the glass fiber bed indicates that during the constant rate period of a hot surface drying operation water vapor produced at the hot surface interface diffuses through the zone of condensation to the accompaniment of continual condensation and then through the zone of evaporation to the accompaniment of continual evaporation. It is of interest to consider, therefore, the quantitative aspects of such diffusion.

The rate of water vapor diffusion is dependent upon the partial pressure gradient, the cross-sectional area available for diffusion, and an empirical diffusion coefficient. For unit geometric area this can be expressed as:

$$\frac{dW}{d\theta} = \frac{D(1-s)e}{L} \frac{\partial p}{\partial \bar{x}} \qquad (40)$$

where $dW/d\theta$ is the mass rate of diffusion of water vapor; D is an empirical diffusion coefficient; $(1-s)e$ is the fraction of the geometric area available to water vapor diffusion; and $\partial p/\partial \bar{x}$ is the partial pressure gradient.

In terms of the cumulative saturation concept used throughout this thesis:

$$\frac{dW}{\partial\theta} = \rho_L e L \frac{\partial S_w}{\partial\theta} \qquad (41)$$

whence

$$\frac{\partial S_w}{\partial\theta} = \frac{D(1-s)}{\rho_L L^2} \frac{\partial p}{\partial \bar{x}} \qquad (42)$$

where $\partial S_w/\partial\theta$ is the water vapor diffusion rate expressed as a rate change of cumulative saturation.

The rate of diffusion of water vapor across the boundary between the zones of condensation and evaporation has been calculated according to Equation (39) and presented as $(\partial S_w/\partial\theta)_{\bar{x}=\bar{x}_2}$ in Fig. 36. It is apparent that at this particular location $\partial S_w/\partial\theta$ must equal $(\partial S_w/\partial\theta)_{\bar{x}=\bar{x}_2}$.

In the zone of condensation, water vapor saturation must be exceeded for condensation to occur. The assumption can, therefore, be made that the partial pressure existing at any point in the zone of condensation is the partial pressure required to saturate at the existing local temperature.

Hence:

$$\frac{\partial p}{\partial \bar{x}} = \frac{\partial p_s}{\partial t}\,\frac{\partial t}{\partial \bar{x}} \qquad (43)$$

where $\partial p_s/\partial t$ is the rate of change of the saturation partial pressure of water vapor with temperature and can be calculated from the steam tables.

On the basis of the above assumption, the empirical diffusion coefficient, D, can be evaluated from experimental data according to Equation (42) for the conditions existing at the boundary between condensation and evaporation zones at various intervals during the constant rate period.

These values are presented in Table VIII.

The value of the diffusion coefficient can be seen to remain relatively constant over the constant rate period for the conditions prevalent at the boundary position. A diffusion coefficient is generally a strong function

TABLE VIII

VALUES OF DIFFUSION COEFFICIENT

Drying Time, min.	Diffusion Coefficient, g./cm. sec.
5	1.30×10^{-4}
10	1.29×10^{-4}
15	1.29×10^{-4}
20	1.15×10^{-4}
Average value	1.26×10^{-4}

of temperature. Since the temperature at the boundary position changes only slightly it is reasonable to expect this constancy.

Classical mass transfer (20) gives the steady state diffusion of one gas through a second stagnant gas as:

$$\frac{U_v c_v}{M_v} = \frac{D_v P}{RT\,(1-p)} \frac{\partial p}{\partial x} \qquad (44)$$

where U_v is the velocity of the diffusing gas; ρ_v is its density; M_v is its molecular weight; D_v is the molecular diffusion coefficient of the gas; P is the total pressure; R is the universal gas constant; T is the absolute temperature; p is the partial pressure of the gas; and $\partial p/\partial x$ is the partial pressure gradient.

Reducing Equation (44) to a form analagous with Equation (42) gives:

$$\frac{\partial S_w}{\partial \theta} = \frac{M_v(1-s)D_v P}{RT\rho_L(1-p)L^2} \frac{\partial p}{\partial x} \qquad (45)$$

Therefore, it is apparent that for water vapor:

$$D = \frac{18\ D_v P}{RT(1-p)} \qquad (46)$$

An empirical correlation for the molecular diffusion of water vapor in air attributed to Spalding (20) gives:

$$D_v = \frac{1.46 \times 10^{-4}}{P} \quad \frac{T^{5/2}}{T + 441} \qquad (47)$$

where D_v is expressed as ft.^{2}/hr.; P is in atmospheres; and T is in °R. This relation is used to express the molecular diffusion coefficient, D_v, as cm.^{2}/sec. as a function of t(°C.) in Fig. 40.

The temperature at the boundary between condensation and evaporation zones is approximately constant for the constant rate period at 70°C. Evaluating D_v for this temperature from Fig. 40 and substituting into Equation (46) gives a measure of the empirical diffusion coefficient in terms of the assumed relation to molecular diffusion. This value is 3.12×10^{-4} g./cm. sec. compared with the average value of 1.26×10^{-4} from Table VIII.

Assuming for the moment that water vapor diffusion in a glass fiber bed during drying is in fact molecular diffusion, it is to be expected that the apparent molecular diffusion coefficient would be less than the normal molecular diffusion coefficient by virtue of the fact that in a porous bed the path of the diffusing vapor will be tortuous.

The tortuosity factor for liquid-saturated porous beds is generally considered to have the value 1.41 ($\sqrt{2}$). Basing an evaluation on Parker's

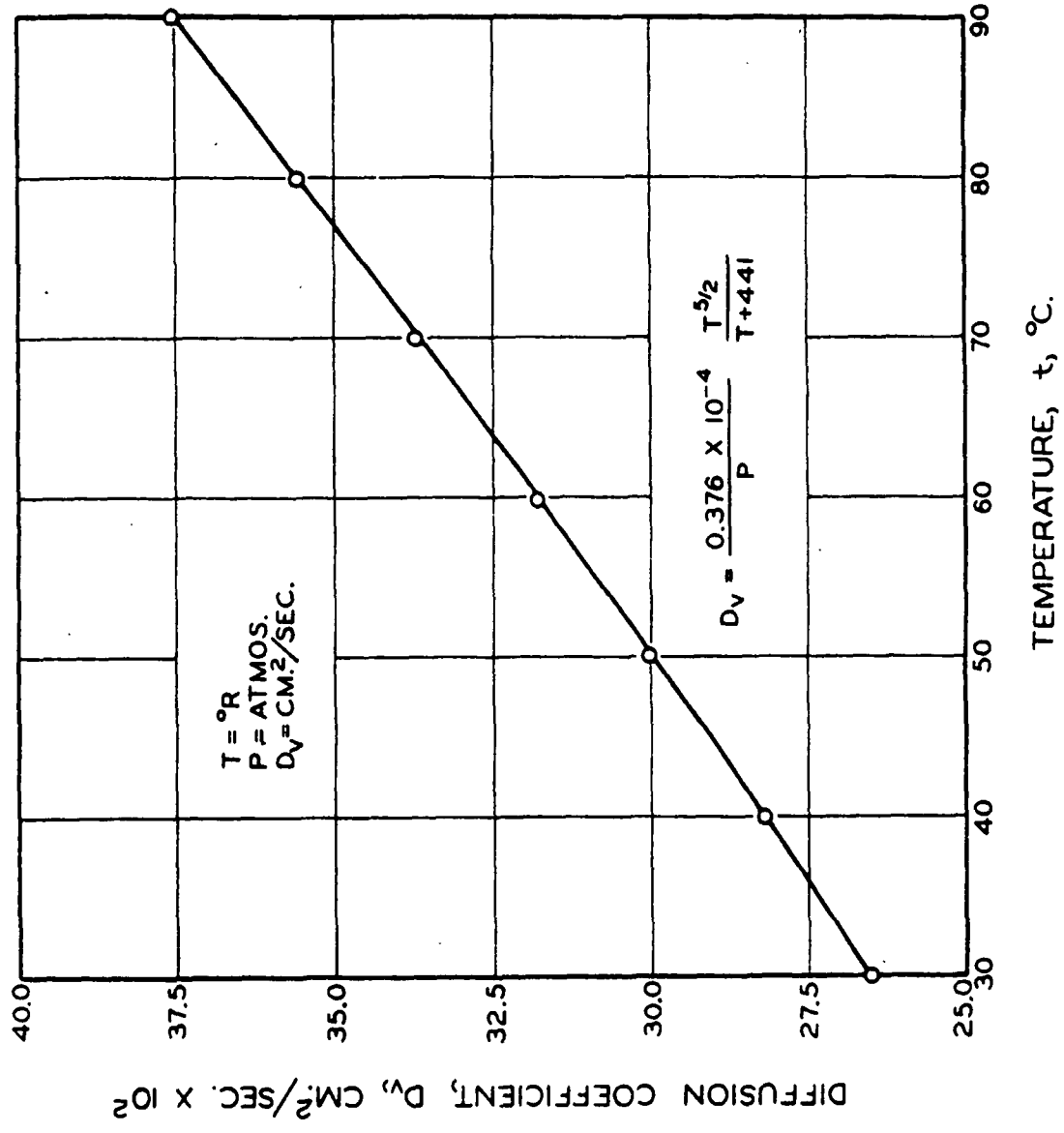

Figure 40. Diffusion Coefficient as a Function of Temperature

analysis of tortuosity variations in partially saturated beds of glass fibers gives values of tortuosity for beds of water saturation 0.5 to 0.9 as 3.7 to 2.7. Assuming the equivalence of tortuosity for liquid and vapor paths at the same fluid saturation suggests a tortuosity factor for the diffusing vapor under conditions at the boundary at about 3.2. The apparent tortuosity factor obtained by comparing the true molecular diffusion coefficient with the calculated empirical coefficient (3.12/1.26) is 2.5.

This rather tenuous argument lends support to a conclusion that water vapor diffusion within a glass fiber bed can be reasonably handled by the laws governing molecular diffusion.

On the basis of this analysis of water vapor diffusion and with the help of the qualitative picture of distribution of local internal evaporation given in Fig. 39, it is possible to establish a qualitative picture of the partial pressure gradient in the glass fiber bed.

The rate of diffusion of water vapor from the zone of condensation is given by Fig. 36. From the cumulative area under the curve shown in Fig. 39, the diffusion rate at any point can be reconstructed at 10 minutes of drying. Using the diffusion coefficient concepts developed by the above analysis allows the partial pressure gradient, $\partial \underline{p}/\partial \underline{\bar{x}}$, to be evaluated at any point according to Equation (42).

The curve shown in Fig. 41 describing the partial pressure as a function of $\underline{\bar{x}}$ gives partial pressure gradients in agreement with the above calculations and therefore is consistent with the general analysis established to date.

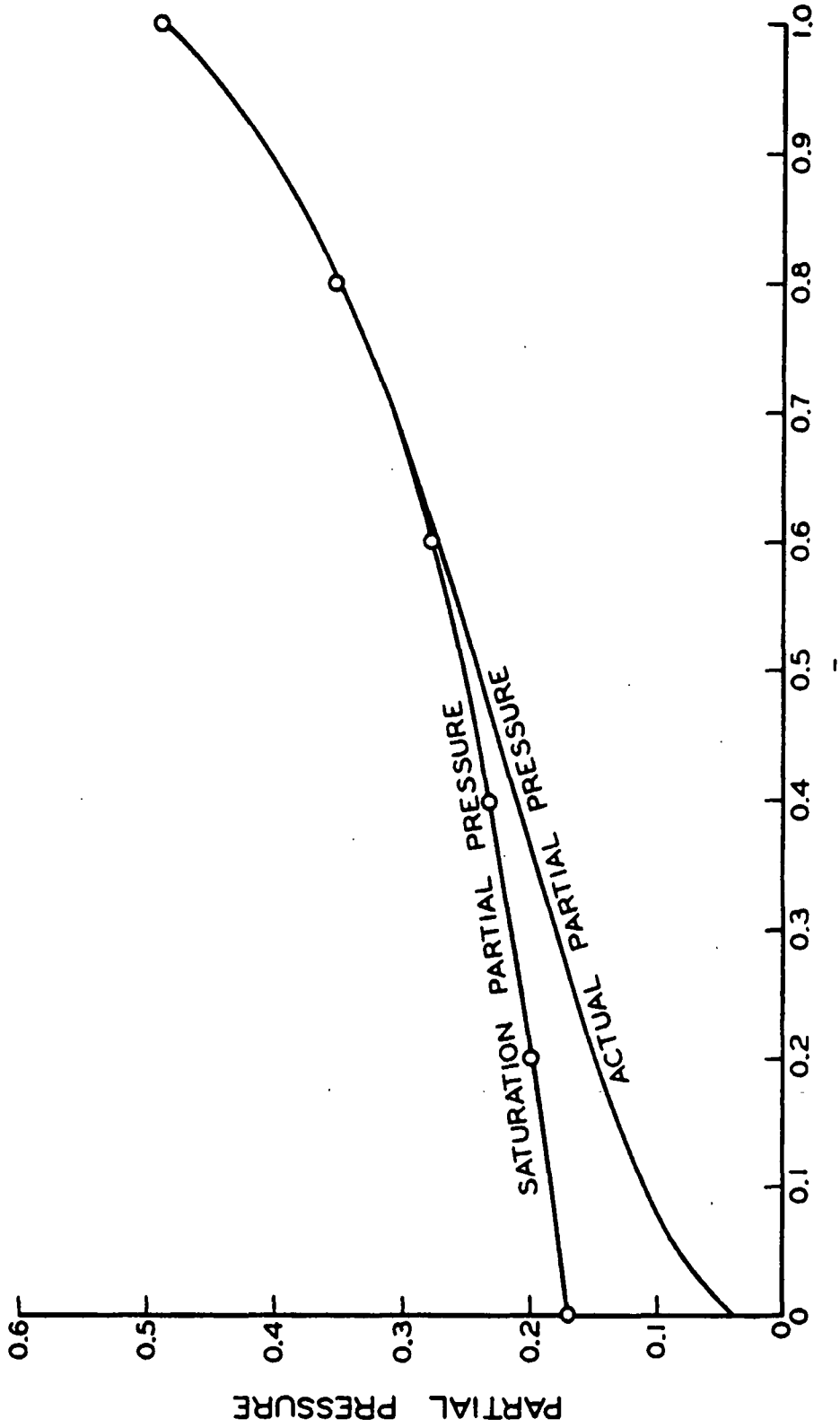

Figure 41. Partial Pressure Curve
10 Minutes of Drying

It will be seen that the partial pressure at the open surface of the bed is substantially below the saturation partial pressure but significantly above the partial pressure of the air stream. The partial pressure in the fiber bed falls below the saturation partial pressure at the end of the zone of condensation. Thereafter, the discrepancy between saturated and actual partial pressure increases, increasing the driving force for evaporation. The maximum increase in this driving force occurs after $\bar{x} = 0.2$ and thus corresponds to the region of maximum evaporation as defined by Fig. 39. The partial pressure at the surface remains sufficiently above the partial pressure in the air stream to yield a substantial partial pressure gradient across the boundary layer to allow final diffusion from the bed of the total vapor produced.

Future investigation of water vapor diffusion during drying could study the steady state diffusion rate through dry porous beds as well as porous beds partially saturated with a water-immiscible liquid. This should allow a more comprehensive analysis of the factors such as tortuosity which presumably affect the diffusion rate and how they are affected by the degree of liquid saturation of the bed.

LIQUID WATER FLOW

The flow of liquid water during the hot surface drying operation is in response to a capillary pressure gradient. The definition of liquid flow requires the elucidation of this driving force together with the resistance to flow. In the development of Equation (28) these two flow-defining factors were introduced through the d'Arcy equation and appear as the capillary driving force, $\partial \underline{P}_c / \partial \bar{x}$, and the unsaturated permeability, $\underline{K}_c$.

The capillary pressure of a liquid existing in a porous system at equilibrium is dependent upon (1) the effective pore radius, (2) the surface tension of the liquid, and (3) the temperature of the system.

(1) The capillary pressure of a liquid in a porous bed as a function of the degree of liquid saturation of the bed gives an empirical measure of the effective pore size. Such a capillary pressure-saturation relationship under equilibrium conditions has been assessed for the glass fiber bed and is presented in Fig. 42. This data can be transformed into a cumulative effective pore-size distribution function according to Equation (4). This transformation is shown in Fig. 43. This relationship defines the radius of curvature at capillary equilibrium of all water-air interfaces present in the glass fiber system at any particular degree of water saturation. The local degree of water saturation at any point in the glass fiber bed at any drying time has been evaluated experimentally. The assumption can be arbitrarily made that the curvature of the local air-water interfaces under the nonequilibrium conditions existing within the fiber bed during the drying operation is the same as for equilibrium conditions at the same saturation. By this assumption the effective pore radius at any point in the fiber bed at any drying time can be assessed from a knowledge of the local saturation by consulting Fig. 43.

(2) The surface tension of a liquid is a strong function of temperature. Since the temperature in the glass fiber bed during drying varies it is apparent that the surface tension will also vary. Hence, the point-to-point variation in capillary pressure will not only be a function of local saturation but also of the local surface tension.

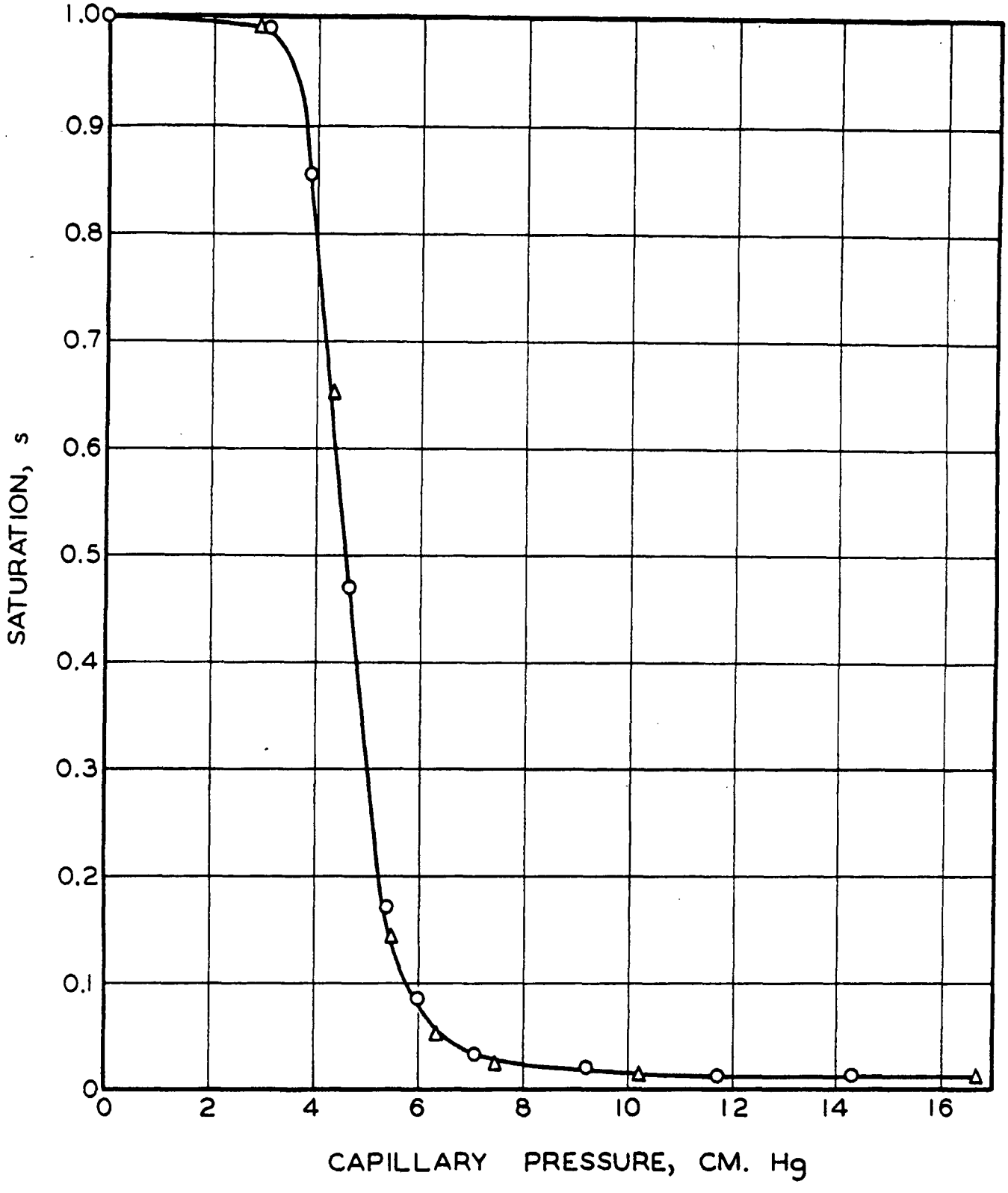

Figure 42. Capillary Pressure Curve

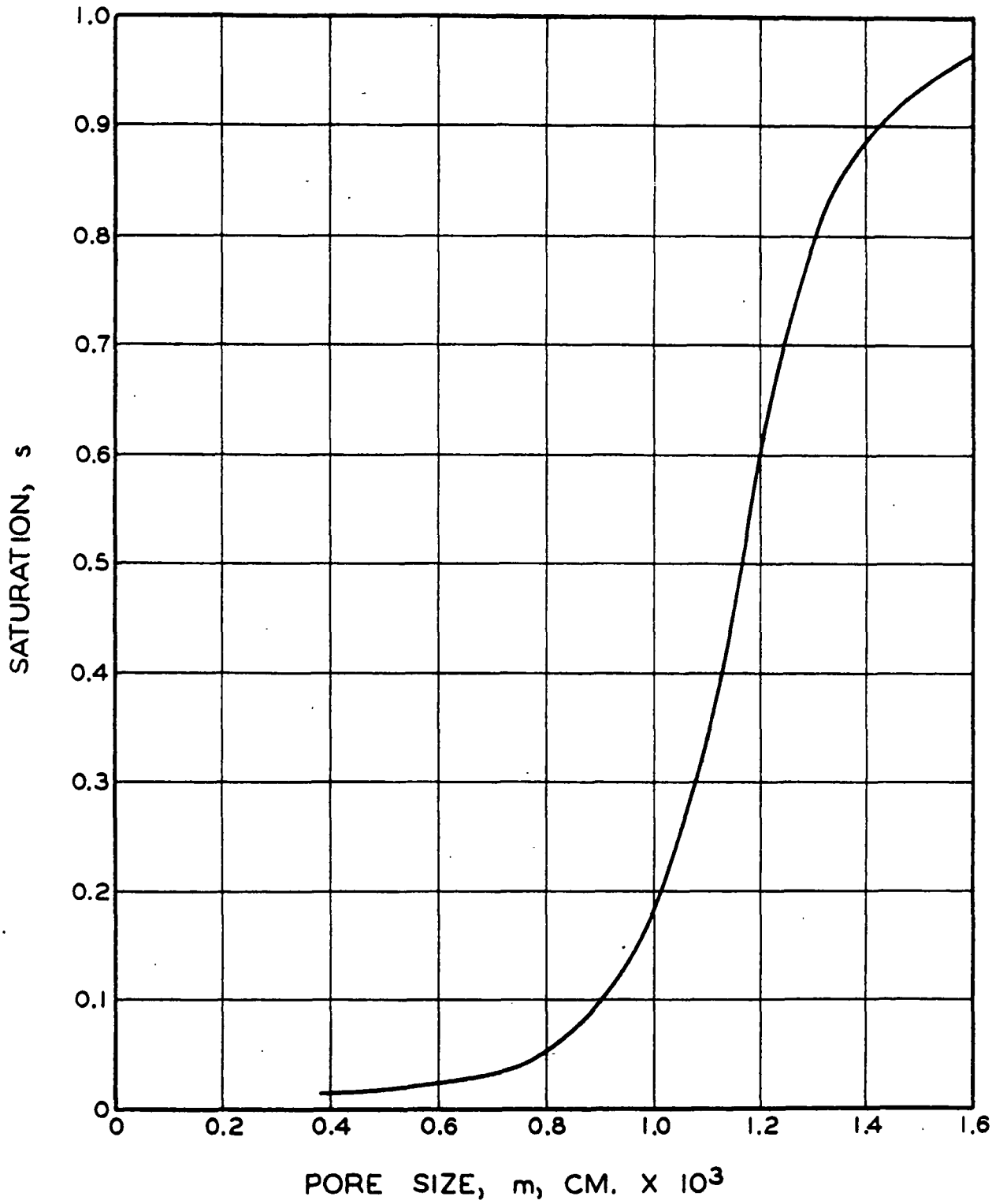

Figure 43. Cumulative Pore Size Distribution

(3) Over the temperature range which is being considered in relation to the drying of the glass fiber bed it is a good assumption that the primary effect of the temperature on capillary pressure is a result of its influence on surface tension. In other words, the capillary pressure will be the same function of temperature as is surface tension.

On the basis of this preamble it is reasonable to accept that the capillary pressure is a function of saturation and temperature only; i.e., $\underline{P_c} = \underline{f}(\underline{s},\underline{t})$. From this it follows that:

$$\frac{\partial P_c}{\partial \bar{x}} = \left(\frac{\partial P_c}{\partial s}\right)\left(\frac{\partial s}{\partial \bar{x}}\right) + \left(\frac{\partial P_c}{\partial t}\right)\left(\frac{\partial t}{\partial \bar{x}}\right) \qquad (48)$$

According to the assumptions of the above analysis, $\partial \underline{P_c}/\partial \underline{s}$ can be evaluated from Fig. 42; $\partial \underline{P_c}/\partial \underline{t}$ can be evaluated from a knowledge of the variation of surface tension with temperature obtainable from any handbook; and the other factors can be evaluated from the experimental data. Hence, the capillary driving force can be evaluated at any drying time for any point in the glass fiber bed.

A similar analysis allows an estimate of the value of the permeability, $\underline{K_c}$, to be made using concepts developed by Parker (15). In his work, Parker studied the equilibrium water permeability of glass fiber beds as a function of the degree of water saturation of the fiber bed. A necessary assumption in applying his concepts to a drying study is that the point permeability in the glass fiber bed during drying is the same as the equilibrium permeability for the bed at the same saturation.

Parker derived and demonstrated the utility of the following relationship:

$$K_r = \frac{K_c}{K} = \frac{k_o T^2 C^2 \int_0^s m^2 ds}{k_{oc} T_c^2 C_c^2 \int_0^1 m^2 ds} \qquad (49)$$

where K_r is the relative permeability, K_c is the unsaturated permeability, K is the saturated permeability, the term $k_o T^2 C^2$ represents shape and tortuosity characteristics of a saturated bed, the term $k_{oc} T_c^2 C_c^2$ represents these characteristics of an unsaturated bed, and m is the effective cumulative pore size at saturation s.

Parker showed that at least as a first approximation, the ratio $k_o T^2 C^2 / k_{oc} T_c^2 C_c^2$ is independent of fiber diameter; that is, glass fiber beds of different average fiber diameter gave the same value for this ratio. Hence, this value should also apply to the glass fiber beds used in the drying study.

The saturated permeability of the glass fibers of this study was measured as a function of porosity. This data is shown in Fig. 44. From this curve, the saturated permeability, K, at the porosity value of the beds used in the drying study is obtained.

The effective pore size distribution function, m, obtained from capillary pressure measurements has been presented in Fig. 43. Using the data represented by this figure, m^2 can be plotted against s and the term $\int_0^s m^2 \, ds$ and $\int_0^1 m^2 \, ds$ evaluated from the area beneath this curve.

Hence, using Parker's data to evaluate $k_o T^2 C^2 / k_{oc} T_c^2 C_c^2$ and evaluating the other terms experimentally, K_c can be calculated as a function of saturation. This relationship is shown in Fig. 45. Hence, according to

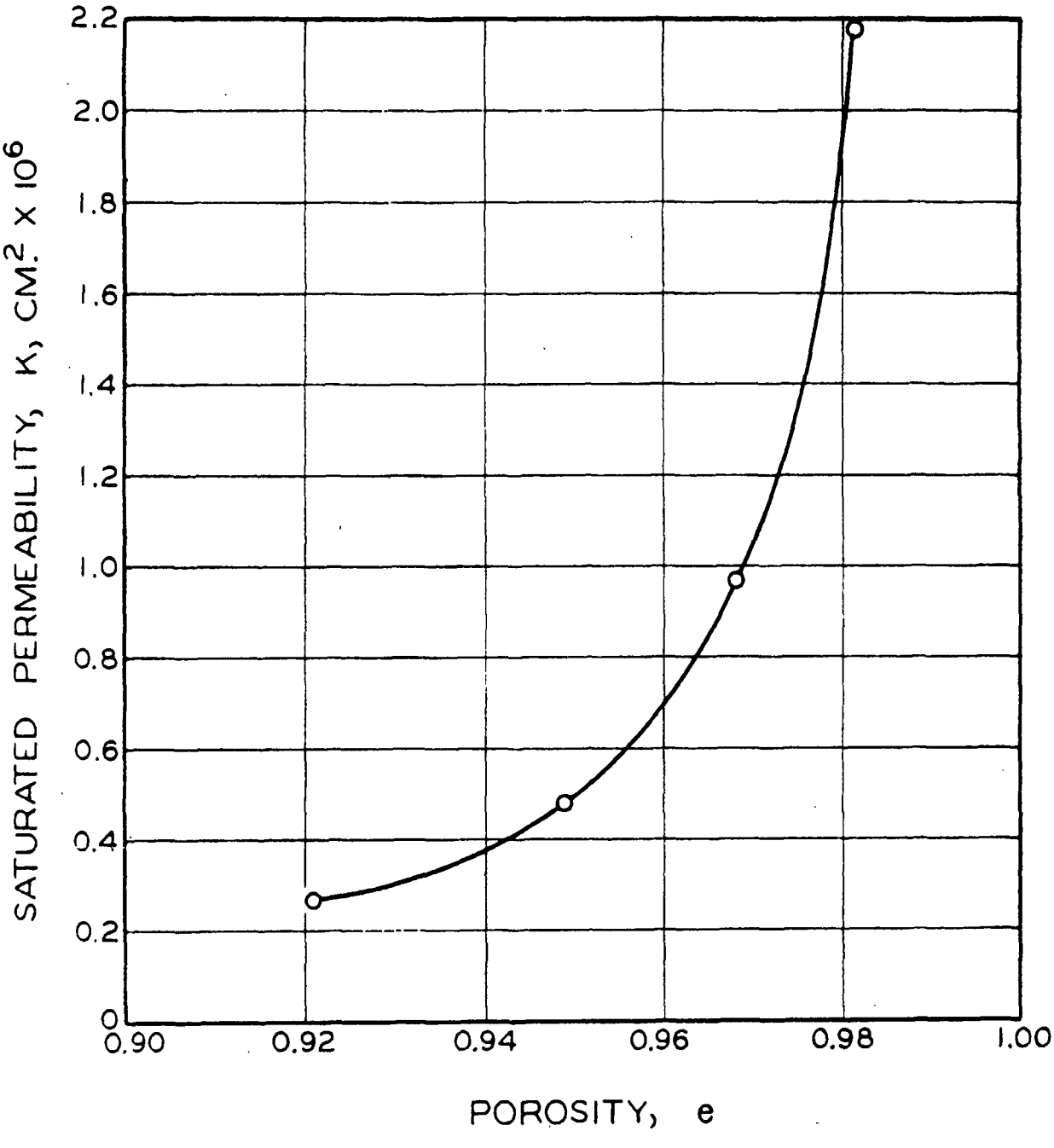

Figure 44. Saturated Permeability Data

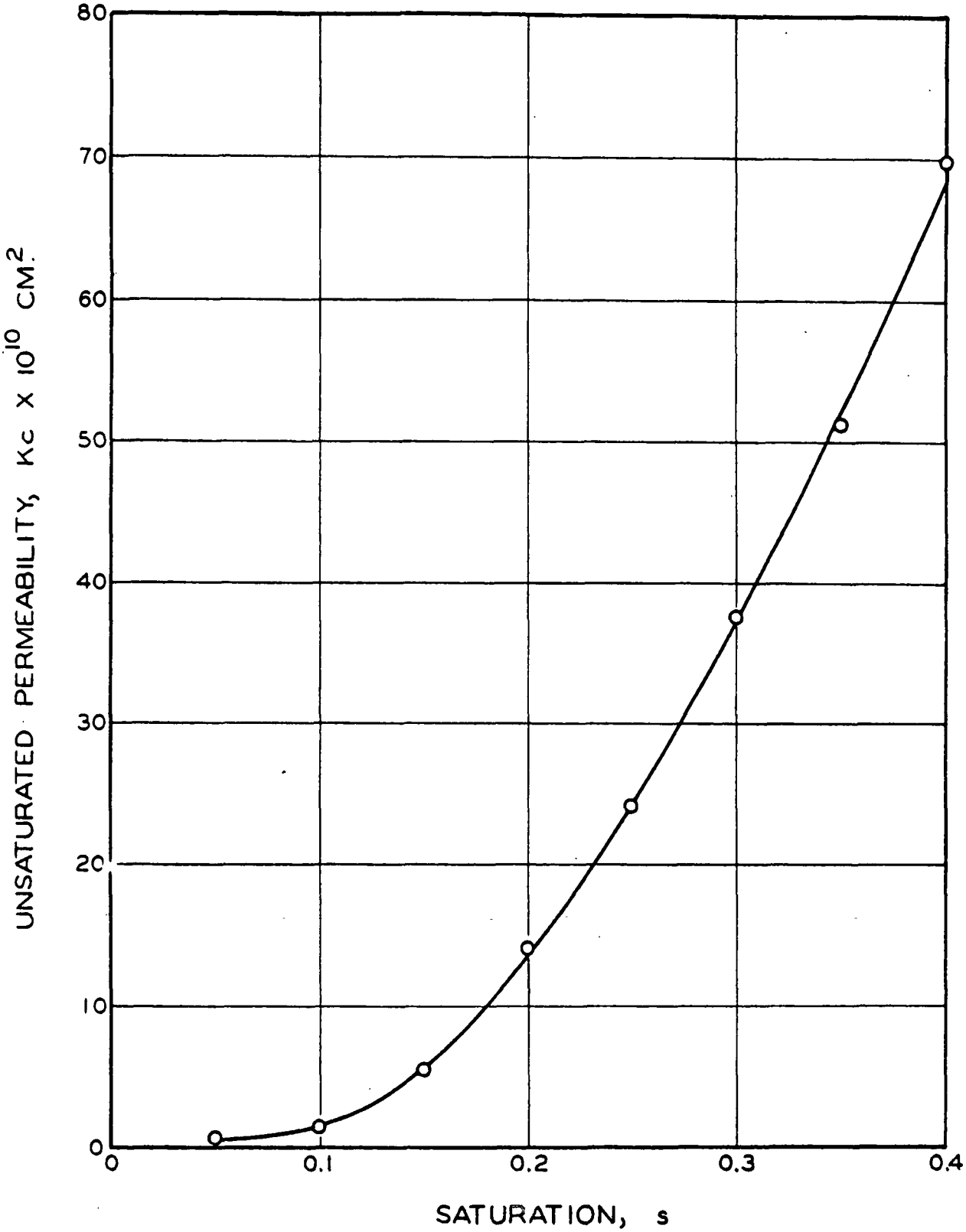

Figure 45. Unsaturated Permeability as a Function of Saturation

this analysis a knowledge of the local saturation in the glass fiber bed at any point and drying time allows the evaluation of the unsaturated permeability at that point and drying time.

We are now in a position to test the validity of the assumptions used to define the capillary driving force and permeability which in turn define liquid flow during drying. Boundary equation (32) defines the rate at which liquid water flows to the air interface. Using this equation together with Equation (48) to define $\partial \underline{P}_c / \partial \underline{x}$, and Fig. 45 to define $\underline{K}_c$ allows the calculation of the open surface evaporation rate, $(\partial \underline{S}_w / \partial \theta)_{\underline{x}=0}$. This value can be compared with that calculated from heat transfer considerations defined by Equation (31). This comparison is made in Table IX.

TABLE IX

COMPARISON OF RATE DATA

Drying Time, min.	$(\partial \underline{S}_w / \partial \theta)_{\underline{x}=0}$ According to Heat Transfer Considerations, $sec.^{-1} \times 10^{-4}$	$(\partial \underline{S}_w / \partial \theta)_{\underline{x}=0}$ According to Liquid Flow Considerations, $sec.^{-1} \times 10^{-4}$	Ratio
5	0.70	157	224
10	0.70	137	196
15	0.66	72	110
20	0.59	50	85

Assuming that the surface evaporation rate defined by heat transfer considerations is reasonable, it is apparent that the estimate according to the assumptions involved in defining liquid flow is one to two hundred times too high. Since the temperature effect turns out to be negligible in terms of the saturation effect as far as capillary pressure is concerned,

it is evident that this discrepancy must be attributed to the factor $(\partial \underline{P}_c/\partial \underline{s})(\partial \underline{s}/\partial \underline{\bar{x}})\underline{K}_c$. The moisture gradient cannot be expected to account for any significant portion of this error and so the product $\underline{K}_c\ \partial \underline{P}_c/\partial \underline{s}$ must be considered responsible.

Since the two factors have been evaluated according to equilibrium concepts it must be concluded that the dynamic conditions existing in the fiber bed during drying introduce additional considerations which significantly affect these factors. More specifically, either both or one of these two factors is significantly smaller for the unsteady state conditions prevalent during drying than would be the case at capillary equilibrium.

Considering these factors separately it is somewhat difficult to conceive that the liquid permeability, $\underline{K}_c$, would be substantially less at a given saturation for unsteady state relative to steady state conditions. However, the capillary-pressure saturation relationship will depend on the effective radius of curvature of air-water interfaces. It is readily conceived that in addition to being a function of the pore structure of the porous media, this curvature will also be some function of the local evaporation or condensation rate, liquid flow rate, etc. Hence, it seems most probable that the discrepancy noted is primarily due to the improper assumption that the equilibrium capillary pressure-saturation relationship remains valid under unsteady state conditions.

The results of this analysis of liquid flow during the drying of a glass fiber bed suggest a number of interesting experimental approaches to a further elucidation of this phenomenon. A study of the effect of

steady state evaporation or condensation on the radius of curvature of the air-water interface in actual capillary tubes of varying size would be of significance. Also, studies of unsteady state unsaturated permeability in glass fiber systems, and of steady state unsaturated permeability in the presence of steady state evaporation or condensation would also contribute manifestly to a further elucidation of liquid flow during drying for a model system.

SUMMARY AND CONCLUSION

The hot surface drying operation has previously been investigated with regard to the effect of boundary conditions such as hot surface temperature or air stream conditions upon the over-all drying rate. These studies have resulted in empirical observation and the classification of the drying cycle into the constant rate and falling rate periods. Various hypotheses have been advanced to explain local observations.

A more penetrating study by Dreshfield of the hot surface drying of pulp beds elucidated the moisture distribution and demonstrated the existence of a plane of evaporation at the hot surface interface. These results were supported by a similar study conducted by Ulmanen. These two studies indicated the need for a basic investigation of internal heat and mass transfer during the hot surface drying of a porous material. This investigation was designed with the aim of adding to the understanding of hot surface drying through a study of these transfer processes.

A glass fiber system was selected for study because of its following ideal properties:

1) During drying no changes occur in the internal geometry of the fiber bed (in distinction to pulp beds where shrinkage occurs).

2) All water in the bed is simply capillary-held and hence free to flow (in distinction to pulp beds where chemically bound water and water trapped within the fiber lumen are also present).

The experimental method developed by Dreshfield was used with minor but improving modifications to obtain a measure of the hot surface drying rate and moisture distribution for the glass fiber system.

Fine-wire thermocouples were employed to secure a measure of the temperature distribution within the glass fiber system during hot surface drying.

Capillary pressure measurements were made according to the method adopted by Parker, to evaluate the internal pore structure of the glass fiber bed.

A high precision of measurement was obtained for the hot surface drying characteristics of any one particular glass fiber bed. However, a between-bed variation in measurement was detected which could not be eliminated. This was attributed to variation in the quantity and distribution of fine material in different glass fiber beds. This variation was found to have no effect on the results for the constant rate period but had an accumulating effect upon the later drying period. A rational adjustment of the data was made to correct for this variation in the later drying period in order to allow a reasonable qualitative picture to be presented. Primary analysis of data was restricted to the constant rate period where measurement was quite precise.

A mathematical description of heat and mass transfer during the hot surface drying of a glass fiber bed was derived. These derivations resulted in boundary equations to account for mass and energy interchanges at the hot surface and air interfaces, and a generalized differential equation to apply to any internal point in the fiber bed.

Hot surface interface boundaries equations:

$$Q = \frac{k_m}{L}\left(\frac{\partial t}{\partial \bar{x}}\right)_m \bar{x}=1.0 = \frac{k_a}{L}\left(\frac{\partial t}{\partial \bar{x}}\right)\bar{x}=1.0 + \lambda e \rho_L L \left(\frac{\partial S_w}{\partial \theta}\right)\bar{x}=1.0$$

$$\frac{K_c \rho_L}{L\mu}\left(\frac{\partial P_c}{\partial \bar{x}}\right)\bar{x}=1.0 = e\rho_L L\left(\frac{\partial S_w}{\partial \theta}\right)\bar{x}=1.0$$

Air interface boundary equations:

$$\left(\frac{k_a}{L}\frac{\partial t}{\partial \bar{x}}\right)\bar{x}=0 = \lambda e \rho_L L\left(\frac{\partial S_w}{\partial \theta}\right)\bar{x}=0$$

$$\frac{K_c \rho_L}{L\mu}\left(\frac{\partial P_c}{\partial \bar{x}}\right)\bar{x}=0 = e\rho_L L\left(\frac{\partial S_w}{\partial \theta}\right)\bar{x}=0$$

Generalized differential equation:

$$\frac{\partial s_w}{\partial \theta}(e\rho_L\lambda) = \frac{1}{L^2}\left[k_a \frac{\partial^2 t}{\partial \bar{x}^2} + \frac{\partial k_a}{\partial \bar{x}}\frac{\partial t}{\partial \bar{x}}\right] + \frac{\rho_L C_L K_c}{\mu L^2}\frac{\partial t}{\partial \bar{x}}\frac{\partial P_c}{\partial \bar{x}} - \frac{\partial t}{\partial \theta}\left[(1-e)\rho_F C_F + es\rho_L C_L\right]$$

An examination of the experimental data in relation to the mathematical model supports the concept of the existence during the constant rate period of a zone of condensation within the fiber bed adjacent to the hot surface, and a zone of evaporation near the open or air interface. The description of drying which is most consistent with this concept is that water which evaporates at the hot surface interface diffuses back through the bed under the influence of the partial pressure gradient. In the zone of condensation the diffusion is accompanied by continual condensation. However, at some point in the fiber bed the partial pressure falls below that required to saturate the available pore space and at all

subsequent positions to the air interface the diffusing vapor is supplemented by internal evaporation.

The over-all drying rate is thus the result of evaporation of water from three sources; viz. (1) water which evaporates at the hot surface interface and diffuses back through the zone of condensation, (2) water which evaporates internally from the zone of evaporation, and (3) water which evaporates from the air interface.

The falling rate period for the glass fiber bed commences when liquid water disappears from the hot surface interface. Evaporation at the interface therefore ceases and the zone of evaporation expands to eliminate the zone of condensation. Thereafter, the over-all drying rate is the result of internal evaporation and open surface evaporation.

A consideration of the experimental evidence of this study together with that from the very similar study with pulp beds by Ulmanen on the basis of the above picture of the hot surface drying operation allows the following general conclusions.

1) The apparent constancy of the drying rate during the constant rate period of a hot surface drying operation can be attributed to a compensating balance between surface evaporation and water vapor diffusion from the interior of the bed.

2) The constant rate period is not necessarily characterized by any particular drying mechanism for all porous materials, nor is it necessarily distinguished from the falling rate period by a significant change in mechanism.

3) The over-all drying rate of a porous material is a function of the interrelated internal heat and mass transfer processes. The concept of rate controlling mechanism is therefore misleading when applied to the hot surface drying operation.

4) The interrelated internal heat and mass transfer processes of the hot surface drying operation are affected by the boundary conditions of drying and by the physical and chemical characteristics of the particular porous material.

5) The importance of the effect of internal structure upon hot surface drying phenomena is illustrated by a comparison of the significant differences between the drying characteristics of a glass fiber and a pulp bed. These can be attributed solely to the differences in internal pore structure and chemical nature between the two systems.

A quantitative treatment of the drying data for the glass fiber bed was introduced in order to obtain some idea of the significance of the various factors which affect heat, vapor, and liquid flow.

Heat transfer was analyzed by an evaluation of dry and wet bed apparent thermal conductivity according to derived material and energy balance equations for different regions of the fiber bed. Several conclusions evolve from the subsequent analysis.

1) It is possible that pure conduction can account for the heat transfer in the dry fiber bed.

2) It is improbable that pure conduction can account for the heat transfer in the partially saturated fiber bed.

3) It is unlikely that radiation is of any significance to heat transfer in the glass fiber bed.

4) It is highly probable that convection contributes significantly to heat transfer in the partially saturated fiber bed. Convective heat transfer appears to be some function of the local fluid movement including local evaporation and condensation. It is possible that local evaporation contributes more significantly to convective heat transfer than does local condensation.

A quantitative evaluation was made of evaporation which occurs at the hot surface interface, internally in the fiber bed, and from the air interface. On the basis of certain assumptions it was found that:

1) For a glass fiber bed during the constant rate period approximately equal contributions are made to the over-all drying rate by water vapor produced (a) by evaporation at the hot surface interface, (b) by internal evaporation, and (c) by evaporation from the air interface.

2) In the falling rate period internal evaporation accounts for 70-80% of the over-all drying rate; evaporation from the air interface accounts for the remainder.

Water vapor diffusion was investigated quantitatively through an evaluation of diffusion coefficients which govern the diffusion of water vapor from the zone of condensation. The calculated coefficients were compared with values predicted according to reported empirical studies of molecular diffusion of water vapor through air. It was concluded that discrepancies between calculated and predicted diffusion coefficients could be accounted for by a tortuosity factor such as is commonly associated with fluid flow through materials.

Liquid flow during drying was quantitatively investigated by an evaluation of the capillary driving force and the unsaturated permeability according to existing equilibrium concepts. The introduction of such an evaluation into the equation describing liquid flow to the air interface gave a flow rate a hundred times greater than could possibly be expected. From this it was concluded that:

1) Equilibrium concepts cannot be used to adequately define capillary driving force and permeability during the unsteady state conditions existing during drying.

2) It is probable that the major discrepancy is associated with the evaluation of the capillary pressure gradient according to equilibrium capillary pressure-saturation measurements.

SIGNIFICANCE OF THIS STUDY AND THOUGHTS FOR FUTURE WORK

This investigation represents the first published study which has been able to analyze the internal heat and mass transfer phenomena associated with a hot surface drying operation to any satisfactory extent. The result has been a significant clarification of hot surface drying as a chemical engineering process. The importance of internal heat and mass transfer as the heart of the drying operation has been emphasized. In addition, a consistent mathematical interpretation has been introduced which should give impetus to more detailed studies of the drying phenomenon. Finally, the significance of internal pore structure as an important drying variable has been demonstrated.

Specific research work to clarify heat transfer, liquid flow, and vapor diffusion in a porous material has already been suggested. In addition, empirical drying studies similar to this one, using different ideal and nonideal systems would contribute information of great value in extending the concepts suggested by this study to apply to the paper system. In particular, a detailed study of an ideal porous system in which experimental perfection would allow a precise definition of all stages of drying (in distinction to this study where experimental error was encountered for measurements during the falling rate period) would be a significant contribution.

In view of the results of this thesis, the air drying operation should be re-examined with a view to clarifying existing concepts of "constant drying rate" and "surface evaporation" as expressed in the comprehensive work of Higgins (1).

The general aim of all such research work is to reduce the drying operation to a well-documented phenomenon. It should then be possible to establish experimentally one or two parameters for a particular material (a particular pulp) which could be substituted into empirical relationships to predict drying time under any boundary conditions.

NOMENCLATURE

a_F Fraction of the cross-sectional area occupied by fiber, dimensionless.

a_G Fraction of the cross-sectional area occupied by the gaseous mixture of air and water vapor, dimensionless.

a_L Fraction of the cross-sectional area occupied by liquid water, dimensionless.

C_F Specific heat of fiber, cal./g.°C.

C_L Specific heat of liquid water, cal./g.°C.

D Empirical diffusion coefficient, g./sec.

D_v Molecular diffusion coefficient, $cm.^2/cm.$ sec.

e Porosity, dimensionless.

h_L Heat content (enthalpy) of liquid water, cal./g.

h_v Heat content of water vapor, cal./g.

k Actual conductivity of glass fiber bed, $cal./cm.^2$ sec. (°C./cm.).

k_a Apparent thermal conductivity of glass fiber bed, $cal./cm.^2$ sec. (°C./cm.).

k_F Actual conductivity of glass fibers, $cal./cm.^2$ sec. (°C./cm.).

k_L Actual conductivity of liquid water, $cal./cm.^2$ sec. (°C./cm.).

k_v Actual conductivity of mixture air/water vapor, $cal./cm.^2$ sec. (°C./cm.).

K Liquid permeability of fiber bed at complete water saturation, $cm.^2$.

K_c Liquid permeability of partially saturated glass fiber beds, $cm.^2$.

K_r Relative permeability, K_c/K, dimensionless.

L Thickness of fiber bed, cm.

m Hydraulic radius, cm.

M Mass of liquid water, $g./cm.^2$.

P Total pressure, $dynes/cm.^2$.

P_c Capillary pressure, $dynes/cm.^2$.

p Partial pressure of water vapor, dimensionless.

p_s Saturation partial pressure of water vapor, dimensionless.

Q Heat flow, cal./cm.^{2} sec.

q Quantity of heat, cal./cm.^{2}.

R Universal gas constant.

r Radius of equivalent circular capillary, cm.

r_1, r_2 Principal radii of curvature of a surface, cm.

S Total saturation (referring to liquid water), dimensionless.

S_w Total saturation (referring to water vapor), dimensionless.

s Local saturation (referring to liquid water), dimensionless.

s_w Local saturation (referring to water vapor), dimensionless.

T Temperature, °K.

t Temperature, °C.

u_v Velocity of diffusing vapor, cm./sec.

W Mass of water vapor, g./cm.^{2}.

x Distance from open face to any position in fiber bed, cm.

$\bar{x}$ Fraction of the distance from the open to the hot surface, dimensionless.

γ Surface tension, dynes/cm.

λ Latent heat of vaporization of water, cal./g.

ϕ Contact angle between liquid and solid phase, degrees.

θ Time, sec.

ρ_F Density of glass fibers, g./cm.^{3}.

ρ_L Density of liquid water, g./cm.^{3}.

ρ_v Density of water vapor, g./cm.^{3}.

μ Viscosity, poise.

LITERATURE CITED

1. Higgins, James J. A study of air drying of paper. Doctor's Dissertation. Appleton, Wis., The Institute of Paper Chemistry, 1951. 122 p.

2. Dreshfield, Arthur C., Jr. A study of transverse moisture distribution and movement during hot-surface drying of paper. Doctor's Dissertation. Appleton, Wis., The Institute of Paper Chemistry, 1956. 175 p.

3. McCready, D. W., Paper Trade J. 101, no. 13:63-6(Sept. 26, 1935).

4. Sherwood, T. K., Ind. Eng. Chem. 25, no. 3:311-16(March, 1933).

5. Ceaglske, N. H., and Hougen, O. A., Ind. Eng. Chem. 29, no. 7:805-13(July, 1937).

6. Cowen, W., J. Soc. Dyers Colorists 55, no. 6:290-302(June, 1939).

7. McCready, D. W , Paper Trade J. 101, no. 13:66-71(Sept. 26, 1935).

8. King, A. R., and Newitt, D. M., Trans. Inst. Chem. Engrs. 33:64-9 (1955).

9. Preston, J. M., and Chen, J. C., J. Soc. Dyers Colorists 62, no. 12:361-4(Dec., 1946).

10. Sherwood, T. K., Gardner, H. S., and Whitney, R. P., Paper Trade J. 106, no. 24:29-35(June 16, 1938).

11. Sherwood, T. K., Ind. Eng. Chem. 21, no. 10:976-80(Oct., 1929).

12. Ulmanen, T. Unpublished work, 1957.

13. Barkas, W. W., and Hallan, R., World's Paper Trade Rev. 139, Tech. Convention no.:52, 57-8, 60(March, 1953).

14. Han, S. T., and Ulmanen, T., Tappi 41, no. 4:185-9(April, 1958).

15. Parker, Joseph D. An investigation of the permeability to water of partially saturated beds of glass fibers. Doctor's Dissertation. Appleton, Wis., The Institute of Paper Chemistry, 1958. 203 p.

16. Carman, P. C. Flow of gases through porous media. New York, Academic Press, 1956. 182 p.

17. Preston, J. M., and Bennett, A., J. Soc. Dyers Colorists 67, no. 3: 101-3(March, 1951).

18. Finck, J. L. Research Paper No. 243. Bur. Standards J. Research 5, no. 5:984(Nov., 1930).

19. Ott, E., and Spurlin, H. M. Cellulose and cellulose derivatives. Part I. p. 406. New York, Interscience Publishers, Inc., 1954.

20. Sherwood, T. K., and Pigford, R. L. Absorption and extraction. p. 5. New York, McGraw-Hill Book Co., 1952.

21. Sherwood, T. K., and Pigford, R. L. Absorption and extraction. p. 10. New York, McGraw-Hill Book Co., 1952.

22. Christensen, G. N., and Barkas, W. W., Trans. Faraday Soc. 51, no. 1:130-45(Jan., 1955).

APPENDIX I

PREPARATION OF THERMOCOUPLES

The thermocouple is made by silver soldering 0.002-inch diameter Hoskins chromel and alumel thermocouple wires to form a junction. The soldering technique is essentially the one reported by Higgins (1) and is represented in Fig. 46. Thermocouple wires (A) are clamped between

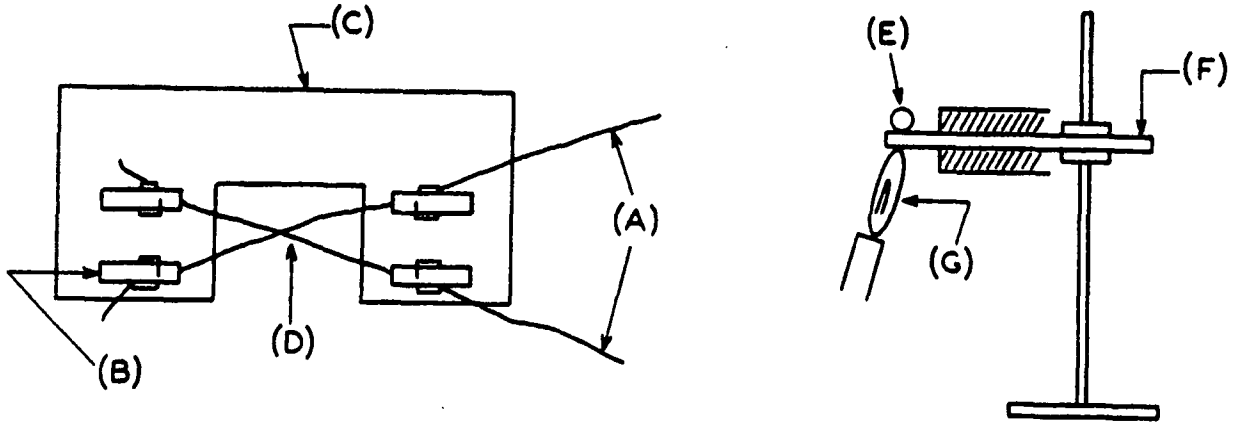

Figure 46. Thermocouple Preparation

clothes pegs (B) mounted on Frame (C). A double twist is made to form a junction (D). A bead of silver solder (E) supported on an insulated copper bar (F) is heated to melting by a hot oxygen-gas flame (G). The thermocouple junction is treated with a special flux and then dipped into the bead of liquid solder by manipulating frame (C). A very fine soldered joint can be obtained with practice and is desired in order to obtain rapid temperature response. The short lengths of wire above the junction are cut away leaving the lead wires joined at the junction.

APPENDIX II

PREPARATION OF RADIOACTIVE SOURCE

In this study, two radioactive isotopes were used, strontium^{90} and thallium^{204}. The strontium isotope being more energetic than the thallium was used for basis weight measurements beyond the range of thallium. For the lower basis weight measurements thallium^{204} was substituted in order to obtain better precision.

To be utilized, these isotopes must be incorporated into a source fulfilling two major requirements. The source must immobilize the radioactive isotope so that it can be located at a particular position within the test bed and remain fixed in that position throughout a series of drying runs. Second, the source itself must be of such configuration or dimensions that its physical presence in the test bed does not measurably affect the drying characteristics of the bed.

The method of source preparation utilized by Dreshfield (2) and by Ulmanen (12) was found to have several disadvantages. Chief among these was the fact that the radioactive isotope was not completely immobilized. A certain amount of leaching of the isotope invariably occurred during any drying run.

An alternative method of source preparation, intriguing because of its simplicity, was suggested by Mr. Dickey of the staff of The Institute of Paper Chemistry. This idea consisted of trapping radioactive material in glass and spinning the glass into fibers. The isotope encased by glass should be effectively immobilized while the presence of a few of these

fibers, albeit of larger diameter, in the test bed should not alter its drying characteristics. A minimum of development work soon established the validity of these assumptions and radioactive glass fiber sources were prepared accordingly. A detailed description of the method of preparing these fibers is presented below.

One end of a piece of 5-mm. soft glass tubing (about four inches long) is sealed using black construction glass. (The reason for using colored glass is to allow for the production of darker fibers which can be readily distinguished from the white fibers of the bed.) This sealed end is blown out to a bulb configuration with a diameter about twice that of the tube itself. The vessel then resembles a thin test tube with a black blister at the closed end.

Radioactive strontium^{90} (or thallium^{204}) is added from stock solution by micropipet to the prepared vessel. The equivalent of about 200 microcuries (mc.) of strontium^{90} or 800 mc. of thallium^{204} are thus transferred. The next step is to precipitate this radioactive material. Strontium sulfate and thallium sulfide are insoluble in water. Therefore, dilute sulfuric acid and a solution of ammonium sulfide are utilized as precipitants. Small amounts of these solutions are added to the radioactive solutions already contained in their respective vessels. The precipitates so formed are centrifuged into the bulb at the bottom of the vessel. A radioactive count indicated that the major part of the activity, which prior to centrifuging had been found uniformly along the length of the vessel, was now concentrated in the bulb. The supernatant liquid is removed from the vessel, and the moist precipitate at the bottom of the vessel is dried at a low temperature (50°C.) for twelve hours or so.

The bulb at the bottom end of the vessel is collapsed by flame heating, thus trapping the precipitate in the glass. Filaments are then pulled out from the bulb end and tested for radioactivity. Sections of the filament which give a substantial radioactive count are broken into fibers about one inch long and stored for use.

This method readily produced a supply of radioactive fibers containing either strontium^{90} or thallium^{204}. These were and can be used, recovered, and re-used for a period of time limited only by the decay rate of the radioactive material. The strontium source can be used for a century while the thallium source probably has an effective lifetime of about two to three years.

APPENDIX III

DENSITY MEASUREMENTS

The standard pycnometric density determination is too well known to warrant a description. However, when this technique is applied to the density measurement of fibers, a unique problem arises. Significant amounts of air are trapped or adsorbed by the fiber network. This contributes significantly to the volume of water that is displaced from the pycnometer. Therefore, the density value obtained is less than the true density. To avoid this defect the following procedure was developed.

A one-gram sample of glass fibers is deposited in a suction flask with boiling water and placed under a vacuum. This is the first deaeration treatment. After the slurry has cooled to room temperature, the fibers are transferred in a saturated condition to a pycnometer in a vacuum desiccator. Boiling water is poured into the pycnometer and desiccator until the pycnometer is completely submerged. The system is placed under a vacuum and the second deaeration treatment begins. When the water has cooled to the desired temperature, the pycnometer is stoppered, removed, dried, and weighed. The slurry contained in the pycnometer is filtered through a tared filter crucible, thus collecting the fiber sample. After drying, the weight of sample can be accurately determined.

This procedure as an adjunct to the normal pycnometric technique allows the density of the fibers to be accurately ascertained.

APPENDIX IV

LOCATION OF BASIC DATA

Data collected during the experimental stages of this thesis were recorded in The Institute of Paper Chemistry Note Book Nos. 1751 and 1825. This appendix locates in detail the primary data utilized for the analysis of this thesis report.

ITEM	Notebook	Pages
Calibration of uniform bore tube of capillary pressure apparatus	1751	8
Calibration of fine-wire thermocouple	1751	10-13
Beta gage "gain" and "voltage" settings	1751	20-23
Average fiber diameter	1751	50
Basic calibration, drying, and temperature data: D-124 to D-136	1825	109-129
Capillary pressure data:P105, P106	1825	130-131
Capillary pressure study:plate calibration	1825	130
Pycnometric density of glass fiber	1825	132-133